Fault Diagnosis in Induction Motor Using Soft Computing Techniques

Rudra Narayan Dash

Department Of Electrical Engineering
National Institute Of Technology, Rourkela-769008
India

Fault Diagnosis in Induction Motor Using Soft Computing Techniques

Thesis submitted in partial fulfillment
of the requirements for the degree of

Master of Technology (Research)

In

Electrical Engineering

By

Rudra Narayan Dash
Roll No. 608EE302

Under the guidance of

Dr. Susmita Das
Dr. Bidyadhar Subudhi

Department Of Electrical Engineering
National Institute Of Technology, Rourkela-769008
India

Department of Electrical Engineering
National Institute of Technology, Rourkela
Rourkela-769008, Orissa, India.

Certificate

This is to certify that the thesis entitled "Fault diagnosis in induction motor using soft computing techniques" by Mr. Rudra Narayan Dash submitted to the National Institute of Technology, Rourkela for the Degree of Master of Technology (Research) is a record of bona fide research work, carried out by him in the Department of Electrical Engineering under my supervision. I believe that the thesis fulfils part of the requirements for the award of master of Technology. The results embodied in the thesis have not been submitted for the award of any other degree.

Dr. Susmita Das
Department of Electrical Engineering
NIT Rourkela

Dr. Bidyadhar Subudhi
Department of Electrical Engineering
NIT Rourkela

Place: NIT, Rourkela
Date:

Acknowledgement

I take the opportunity to express my reverence to my supervisor Prof. Susmita Das and Co-Supervisor Prof. Bidyadhar Subudhi for their guidance, inspiration and innovative technical discussions during the course of this work. Their perpetual energy and enthusiasm in research had motivated others, including me. In addition, they were always accessible and willing to help their students with their research. As a result, research life became smooth and rewarding for me.

Prof. S. Ghosh, Prof. G.S. Rath and Prof. P. C. Panda deserve special thanks as my thesis committee members and Chairman.

I thank all my teachers Prof. J.K. Satapathy, Prof. A.K. Panda, Prof. D. Patra, Prof. S. R. Samantaray, Prof B. Chitti Babu and Prof. K. R. Subhashini for their contribution in my studies and research work. They have been great sources of inspiration to me and I thank them from the bottom of my heart.

I would like to express my thanks to Mr. S. Swain and Mr. B. N. Sahoo for helping me for conducting my experimental work.

I would like to thank all my friends and especially my classmates for all the thoughtful and mind stimulating discussions we had, which prompted us to think beyond the obvious.

Last but not least I would like to thank my parents, who taught me the value of hard work by their own example. They rendered me enormous support being apart during the whole tenure of my stay in NIT Rourkela.

Rudra Narayan Dash

CONTENTS

ABSTRACT

Induction motors are one of the commonly used electrical machines in industry because of various technical and economical reasons. These machines face various stresses during operating conditions. These stresses might lead to some modes of failures/faults. Hence condition monitoring becomes necessary in order to avoid catastrophic faults. Various fault monitoring techniques for induction motors can be broadly categorized as model based techniques, signal processing techniques, and soft computing techniques. In case of model based techniques, accurate models of the faulty machine are essentially required for achieving a good fault diagnosis. Sometimes it becomes difficult to obtain accurate models of the faulty machines and also to apply model based techniques.

Soft computing techniques provide good analysis of a faulty system even if accurate models are unavailable. Besides giving improved performance these techniques are easy to extend and modify. These can be made adaptive by the incorporation of new data or information. Multilayer perceptron neural network using back propagation algorithm have been extensively applied earlier for the detection of an inter-turn short circuit fault in the stator winding of an induction motor. This thesis extends applying other neuro-computing paradigms such as recurrent neural network (RNN), radial basis function neural network (RBFNN), and adaptive neural fuzzy inference system (ANFIS) for the detection and location of an inter-turn short circuit fault in the stator winding of an induction motor.

By using the neural networks, one can identify the particular phase of the induction motor where the inter-turn short circuit fault occurs. Subsequently, a discrete wavelet technique is exploited not only for the detection and location of an inter-turn short circuit fault but also to find out the quantification of degree of this fault in the stator winding of an induction motor. In this work, we have developed an experimental setup for the calculation of induction motor parameters under both healthy and inter-turn short circuit faulty conditions. These parameters are used to generate the phase shifts between the line currents and phase voltages under different load conditions. The

detection and location of an inter-turn short circuit fault in the stator winding is based on the monitoring of these three phase shifts. Extensive simulation results are presented in this thesis to demonstrate the effectiveness of the proposed methods.

LIST OF TABLES

LIST OF FIGURES

ACRONYMS

- MMF: Magneto Motive Force
- EPRI: Electric Power Research Institute
- BJT: Bipolar Junction Transistor
- IGBT: Insulated Gate Bipolar Transistor
- FDP: Fault Detection and Prediction
- MIMO : Multiple-Input- Multiple-Output
- FD: Fault Detection
- OLAD: Online Approximator in Discrete Time
- EMWFA: Extension in 2-D of the Modified Winding Function Approach
- OE: Output Error
- GMM: Gaussian Mixture Model
- RPS: Reconstructed Phase Space
- MCSA: Motor Current Signature Analysis
- MLPNN: Multilayer Perceptron Neural Network
- BP: Back Propagation
- RNN: Recurrent Neural Network
- RBFNN: Radial Basis Function Neural Network
- ANFIS : Adaptive Neural Fuzzy Inference System
- WT: Wavelet Technique
- FFNN: Feed-Forward Neural Network
- MSE: Mean Square Error
- MRA: Multi-Resolution Analysis
- STFT: Short Time Fourier Transform
- CWT: Continuous Wavelet Transform
- DWT: Discrete Wavelet Transform

Chapter 1

Introduction

1.1 Background

Induction motors are most commonly used electrical machines in industry because of their low cost, reasonably small size, ruggedness, low maintenance, and operation with an easily available power supply. Although these are very reliable, they are subjected to different modes of failures / faults. These faults may be inherent to the machine itself or due to operating conditions. The inherent faults may be are due to the mechanical or electrical forces acting on the machine enclosure. If a fault is not detected or if it is allowed to develop further it may lead to a failure. A variety of machine faults have been studied in the literature [1, 2] such as winding faults, unbalanced stator and rotor parameters, broken rotor bars, eccentricity and bearing faults. Several fault identification method have been developed and been effectively applied to detect machine faults at different stages by using different machine variables, such as current, voltage, speed, efficiency, temperature and vibrations. Thus, for safety and economic considerations, it is essential to monitor the behavior of motors of different sizes such as large and small.

Traditionally maintenance procedures in industry follow two approaches as follows. The first one is to perform fixed time interval maintenance, where the engineers take advantage of slower production cycles to fully inspect all aspects of the machinery. The second is to simply respond to the plant failure as and when it happens. However, making use of today's technology, new scientific approach was becoming possible for maintenance management. One of the key elements to this new approach is predictive maintenance through condition monitoring, which depends upon the condition of the plant. Condition monitoring is used for achieves performance of machinery, reducing consequential damage, increasing machine life, reducing spare parts inventories and reducing breakdown maintenance. An efficient condition-monitoring scheme is one that provides warning and predicts the faults at early stages. Monitoring system obtains information about the machine in the form of primary data and through the use of modern signal

processing techniques; it is possible to give vital diagnostic information to equipment operator before it catastrophically fails. The problem with this approach is that the results require constant human interpretation. The logical progression of the condition-monitoring technologies is the automation of the diagnostic process. To automate the diagnostic process, recently a number of soft computing diagnostic techniques have been proposed [3, 4, 5].

Recently soft computing techniques such as expert system, neural network, fuzzy logic, adaptive neural fuzzy inference system, genetic algorithm etc. have been employed to assist the diagnostic task to correctly interpret the fault data. These techniques have gained popularity over other conventional techniques. These are easy to extend and modify besides their improved performance. The neural network can represent any non-linear model without knowledge of its actual structure and can give result in a short time. From the early stages of developing electrical machines, researchers have been engaged in developing a method for machine analysis, protection and maintenance. The use of above technique increases the precision and accuracy of the monitoring systems. The area of condition monitoring and faults diagnostic of electrical drives is essentially related to a number of subjects, such as electrical machines, methods of monitoring, reliability and maintenance, instrumentation, signal processing and intelligent systems.

1.2 Different Types of Faults in an Induction Motor

This section presents a comprehensive description of the most common faults to be found in induction machines. The faults are classified according to their location: stator and rotor which are as shown in Fig. 1.1.

1.2.1 Stator Faults

Stator faults may be divided into two types these are as follows

1. Stator winding related faults
2. Stator core related faults

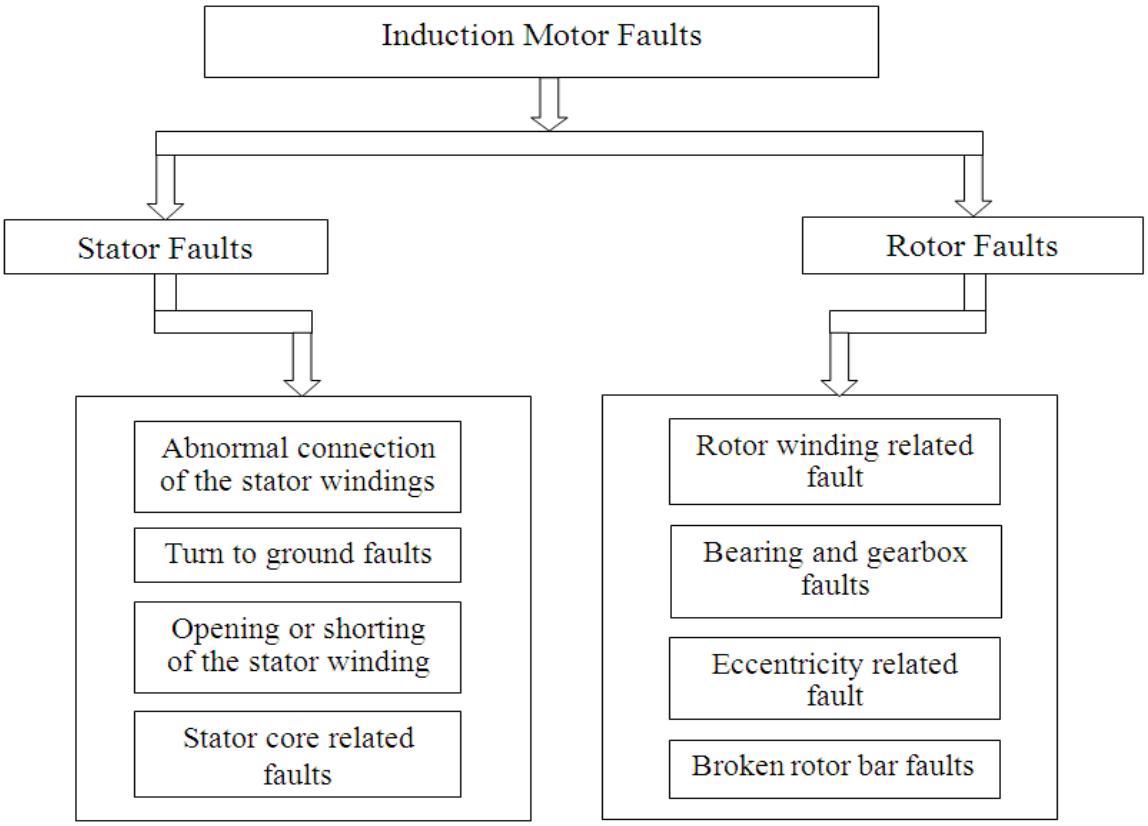

Fig.1.1 Sources of Induction Motor Faults

1.2.1.1 Stator Winding related Faults

According to an IEEE and Electric Power Research Institute motor reliability study [6], stator faults are mostly responsible for 37% of the failures in an induction motor. Many works have indicated that the majority of induction motor stator winding failures result from the destruction of the turn insulation. In most cases, this failure starts as a turn-to-turn (inter-turn) fault which finally grows and reaches in major ones such as coil-to-coil, phase-to-phase or phase-to-ground failures, and ultimately causing motor breakdown.

Very often Stator winding of an induction machine is subjected to stresses induced by a variety of factors, such as thermal overloads, mechanical vibrations and voltage spikes caused by adjustable frequency drives. Some of the most frequent causes of stator winding failures are as follows.

- Due to high stator core or winding temperatures
- Due to Loose bracing for end windings

- Due to Contaminations caused by oil, moisture etc
- Due to short circuits
- Due to starting stresses
- Due to electrical discharges
- Due to leakage of cooling systems

1.2.1.2 Stator Core related Faults

Stator core problems are rare compared to stator winding problems are not usually a major concern for small machines [7]. However, the repair/rebuild process is more costly in the case of the stator core failure, since it usually requires the entire core to be replaced. Therefore, there has been interest in identifying the causes of core problems and finding ways of monitoring the core in order to detect and prevent stator core failure.

The stator cores of induction machine are built from thin insulated steel laminations with a view to minimize the eddy current losses at higher operational efficiency. In the case of medium or large machines, the core is compressed after the core laminations are stacked in order to prevent the individual lamination sheets from vibrating and to maximize the thermal conductance in the core.

The main causes of stator core failures are as follows:

- Core end-region heating resulting from axial flux in the end winding region
- Core melting caused by ground fault currents
- Lamination vibration resulting from core clamping relaxation
- Loosening of core tightening at the core end resulting from vibration during operation
- Manufacturing defects in laminations
- Inter laminar insulation failure
- Stator-rotor rubs during assembly and operation
- Arcing from winding failure

1.2.2 Rotor related Faults

The most common rotor faults in an induction machine may be classified as:

1. Rotor winding related faults
2. Broken rotor bar fault
3. Bearing and gearbox faults
4. Eccentricity related faults

1.2.2.1 Rotor Winding related Faults

Short circuit turns in induction machine rotor windings cause operational problems such as high vibration levels; therefore early detection is essential. Normally the resistance of the windings on opposite poles is identical. The heat produced by Joule's effect is distributed symmetrically about the rotor forging. If the inter-turn insulation is damaged, then the rotor winding become short circuited. The resistance of the damaged coil diminishes and if the poles are connected in series, less heat is generated than in the symmetrical coil on the opposite pole. The rotor body thus experiences asymmetric heating, which produces a thermal bow in the rotor body, causing vibration. The unbalanced magnetic forces on the rotor produced by the change in the magneto motive force (MMF) from the winding contribute to increased vibration [8].

1.2.2.2 Broken Rotor Bar Fault

Under normal operating conditions, large mechanical and thermal stresses are presents, especially if the machine is being continually stopped and restarted or if the machine is heavily loaded. It is well known that the rotor current during starting can be as much as ten times the normal full load current and that the effects of these large currents are represented by very large thermal stresses in the rotor circuit. The starting period is also characterized by minimal cooling and maximum mechanical forces, which over stresses the rotor bars.

The cracked bar will increase in resistance and will over heat at the crack. The bar will break completely and arcing will occur across the break. This arcing will then damage the rotor laminations around the faulted bar. The neighboring bars will carry an increased current and will

be subjected to increased stresses, eventually causing these bars to fail. Finally the broken bars may lift outwards because of centrifugal forces and could damage the stator winding [9].

1.2.2.3 Bearing and Gearbox Faults

As reported in [10] EPRI(1982), bearing faults may account for 42%-50% of all motor failures, motor bearings may cost between 3%-10% of the actual cost of the motor, but the hidden costs involved in downtime and lost production combine to make bearing failure a rather expensive abnormality [11]. Ball-bearing related defects can be categorized as outer bearing race defects, inner bearing race defects and ball defects.

Different stresses acting upon a bearing may lead to excessive audible noise, uneven running, reduced working accuracy, and the development of mechanical vibrations and as a result, increased wear. More than twenty years ago, few bearing failures were electrically induced but at the beginning of the 90's a study by [12] showed that bearing failures are about 12 times as common in converter-fed motors as in direct on-line motors. However mechanical issues remain the major cause of bearing failure as discussed in [11].

1.2.2.3 Eccentricity related Faults

Machine eccentricity is defined as a condition of the asymmetric air-gap that exists between the stator and rotor [13]. The presence of a certain level of eccentricity is common in rotating electrical machines; some manufacturers and users specify a maximum permissible level of 5%, where as in other cases, a maximum level of 10% of the air gap length is allowed by the users [14]. However, manufacturers normally try to keep the total eccentricity level even lower in order to reduce vibration, noise and minimize unbalanced magnetic pull [15]. Since the air gap of an induction machine is considerable smaller than in other types of machines with a similar size and performance, this type of machine is more sensible to changes in the length of the air gap.

There are two types of air gap eccentricity: static air gap eccentricity and dynamic air gap eccentricity. In the case of static air gap eccentricity the position of the minimal radial air gap length is fixed in space, while in the case of dynamic eccentricity the center of the rotor is not at the center of the rotation and the position of the minimum air gap rotates with the rotor. Unless

detected early, the eccentricity becomes large enough to develop high unbalanced radial forces that may cause stator-to-rotor rub, leading to a major breakdown of the machine [16].

1.3 Literature Review on Different Fault Diagnosis Techniques

Various fault monitoring techniques for induction motors reported in literature can be broadly categorized as shown in Fig. 1.2.

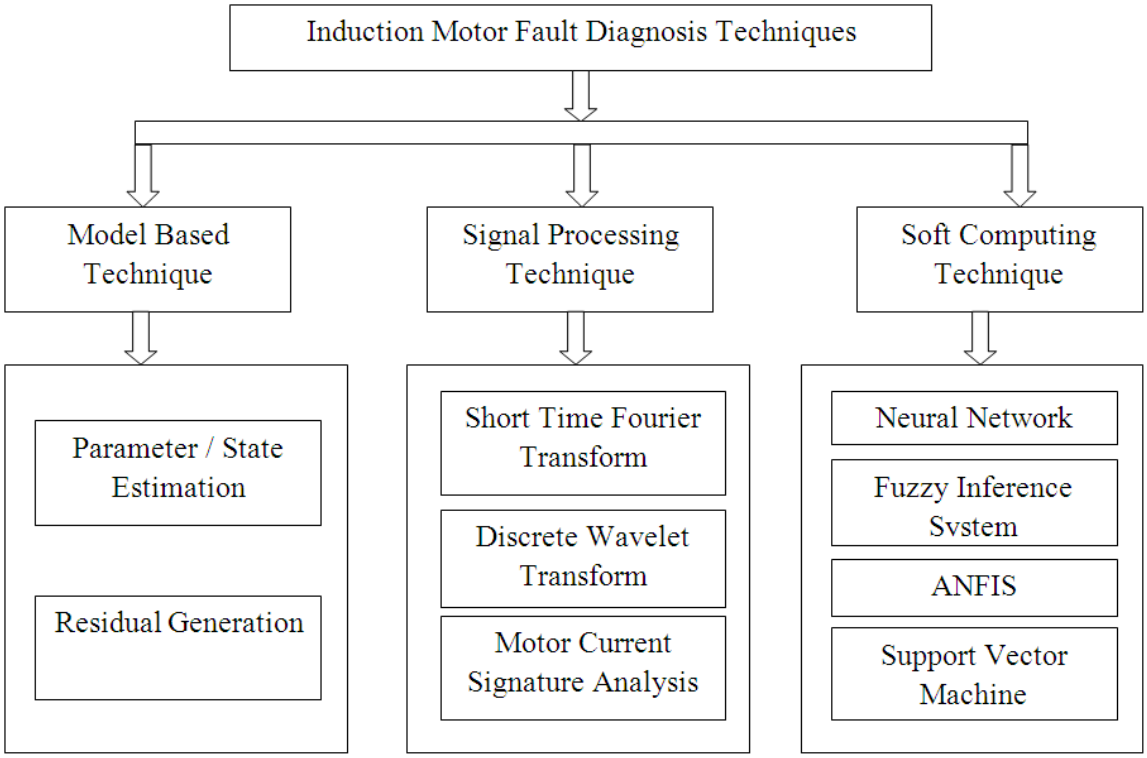

Fig.1.2 Types of Fault Diagnosis Techniques of Induction Motor

1.3.1 Model Based Technique

Isermann [17] has presented a novel, unified model-based fault detection and prediction (FDP) technique is developed for non linear multiple-input-multiple-output (MIMO) discrete time systems. The proposed scheme addresses both state and output faults by considering separate time profiles. The faults, which could be incipient or abrupt, are modeled using input and output signals of the system. The fault detection (FD) scheme comprises online approximator in discrete time (OLAD) with a robust adaptive term. An output residual is generated by comparing the fault detection (FD) estimator output with that of the measured system output. A fault is detected

when this output residuals exceeds a predefined threshold. The asymptotic stability of the fault detection and prediction (FDP) scheme enhances the detection and time to failure accuracy. The effectiveness of the proposed approach is demonstrated by using a fourth-order MIMO satellite system.

Arkan, Kostic-Perovic and Unsworth [18] have presented two orthogonal axis models of a three phase induction motor. From these two models first one having asymmetrical windings and the other one having inter-turn short circuits on the stator winding. The machine is modeled by using classical two axis theory, and the equations are modified to take into account the stator inter-turn faults. A state space form of the system is presented for dynamic simulations. The simulation results from the models are compared with experiment carried out on a specially wound motor with taps to allow different number of turns to be shorted. The above models have been successfully used to study the transient and steady state behavior of the induction motor with short circuited turns.

Sahraoui, Ghoggal, Zouzou, Aboubou and Razik [19] have proposed a new mathematical model of the induction motor operating under stator inter-turns short circuits. The model is based on the multiplied coupled circuit approach. The inductances calculation is performed an extension in 2-D of the modified winding function approach (EMWFA), which was able to take into account the space harmonics in addition to the effects of rotor bar skewing and to the linear rise of MMF across the slots. From the results it is shown that the inter-turn short circuit gives rise to some spectral components which appear in the current line spectrum.

Bachir, Tnani, Trigeassou and Champenois [20] have suggested a new model of squirrel cage induction motors under stator and rotor faults. First, they study an original model that takes into account the effects of inter-turn faults resulting in the shorting of one or more circuits of stator-phase winding. Then, they propose a new faulty model dedicated to broken rotor bars detection. The corresponding diagnosis procedure based on parameter estimation of the stator and rotor faulty model is proposed. The estimation technique is performed by taking into account prior information available on the safe system operating in nominal conditions. In this paper the output error (OE) identification technique is used to estimate the parameters.

1.3.2 Signal Processing Technique

Stainislaw, A.H.M sadrul Ula and Andrzej [21] have proposed a new methodology for the signature analysis of induction motors, namely the instantaneous power. In this paper in place of stator current the instantaneous power is used for the motor signature analysis for the detection of mechanical abnormalities in a drive system. The information carried by the instantaneous power is the product of the supply voltage and current is higher than that deducible from the current alone. In the power spectrum of stator current the highest magnitude will appear is -52 dB, but in case of spectrum of instantaneous power the highest magnitude appears is -47dB. From the above the instantaneous power is higher by 5dB than that of the strongest non fundamental spectral component.

Yen and Lin [22] have employed a wavelet packet for extracting useful information from vibration signals of an induction motor. Though the measured vibration signals contain non-stationary part, Fourier transform cannot provide sufficient information to detect some machine faults. The results of employing wavelet packet are used with the aid of statistical based feature selection criteria to discard the feature components containing little discriminate information. The extracted reduced dimensional feature vector is then used as the input to the neural network classifier. The results show improvement in neural network generalization capability and significant reduction in training time.

Thomson and Fenger [23] have used the current signature analysis approach to detect the induction motor faults. This approach uses the motor current signature to detect the author detects different faults such as broken rotor bars in squirrel cage induction motor, detection of shorted turns in an industrial motor. In this paper the author has taken four case studies which is used to detect the different faults in an induction motors. From the results the author have clearly demonstrate that the motor current signature analysis is a powerful technique for monitoring the health of three phase induction motors.

Kim, Parlos and Bharadwaj [24] have developed a speed sensorless fault diagnosis system for induction motors. In this paper they have used to find out both the electrical (turn to turn stator winding short circuit) and mechanical (broken rotor bars, Eccentric air gap, bearing) faults respectively. Here, they have used the combination of recurrent neural networks and signal

processing algorithms such as standard Fourier based and wavelet based techniques for detecting faults in induction motors. The motor terminal voltages and current have been used as the input to the diagnosis system. The Fourier based signal processing technique is applicable if the motor is operating under steady state and the wavelet based signal processing technique is applicable if the motor operating in transient mode.

Douglas, Pillay and Ziarani [25] have introduced a new algorithm, where they followed the least squares error minimization using the method of gradient descent in a time varying set of equations. The algorithm is used for transient motor current signature analysis using wavelets. Here the residual currents are analyzed using wavelets for the detection of broken rotor bars. The advantage of this method is that it does not required parameters such as speed or number of rotor bars. Here a high order notch filter is used to separate the fundamental frequency from the rotor bar frequencies. Once the fundamental frequency has been removed, the residual current can be examined by using discrete wavelet transform analysis. Hence Daubechies 8 wavelet is used as the mother wavelet function. From the results it is clear that the broken rotor bar can be detected using measured transient in rush current.

In [26] an online diagnosis approach has been proposed for an induction motor that uses the motor current signature analysis (MCSA) with advanced signal processing algorithms. The above proposed system was able to diagnosis of induction motors having four types of faults such as breakage of rotor bars and end rings, short circuit of stator windings, bearing cracks and air-gap eccentricity faults. The motor diagnosis using MCSA depends on the slip, so if the detected slip has an error then the result of the motor diagnosis is incorrect. Hence, to detect the correct slip, an optimal slip algorithm based on the Bayesian method of estimation. In this paper the advanced signal processing techniques such as the “Proper Sample Selection Algorithm” and “Frequency Auto Search Algorithm” are used. The Proper Sample selection Algorithm is used to determine the standard of suitable samples for the MCSA process. The Frequency Auto Search Algorithm is used to detect the abnormal harmonic frequency of 1 kHz.

Aderiano, Richard and Nabed [27] have presented an induction motor fault diagnosis method using the three phase stator current envelopes for broken rotor bars and inter-turn short circuits in stator windings. The above methods not only identifies an induction motor as healthy or faulty but also identify the severity of the fault through the identification of the number of broken bars

or the number of short circuit turns in the stator windings. The training and testing sets are generated from the three phase stator current of an induction motor at both healthy and faulty operating conditions using the Gaussian Mixture models (GMMs) of the reconstructed phase space (RPSs) transforms. The author has claimed that the proposed method can constitute a powerful tool for induction motor fault diagnosis due to its high accuracy.

Riera-Guasp [28] has presented a discrete wavelet transform based technique for detection an asymmetries in the rotor of an induction motor by using the startup current and plugging stopping current, as well as the mixed eccentricities by using the startup current. He has used the Daubechies-44 and dmeyer as the mother wavelets for the discrete wavelet transform analysis. To avoid overlapping between two adjacent frequency bands such as a high order mother wavelet has been used. The author has also found out the parameters for the quantification of the severity of the fault in case of the startup rotor asymmetry and the plugging rotor asymmetry.

1.3.3 Soft Computing Technique

Nejjari and Benbouzid [29] have used the Park's vector patterns for detecting different types of supply faults, such as voltage imbalance and single phasing. In addition a neural network based back propagation algorithm is used to obtain the machine condition by testing the shape of the Park's vector patterns. Two neural network based approach have been used, these are classical and decentralized. The generality of the proposed methodology has been experimentally tested and the authors claim that the results provide a satisfactory level of accuracy.

Fillippetti [30] has introduced a comprehensive study about the application of artificial intelligence in machine monitoring and fault diagnosis. Here, expert system has been used as a tool for the fault diagnosis. The authors show the validity of using neural network along with fuzzy logic for fault identification and fault severity evaluation. The paper also covers a diagnosis of the inverter system, which is used to drive the motor.

Awadallah [31] has introduced a comprehensive adaptive neuro-fuzzy inference system for identification of stator short circuits in brushless DC motors, where the diagnosis of the fault was done through two independent ANFISES, first one is used to find out the shorted turns and the second one is used to identify out the faulty phase. The inputs to the first ANFIS are the diagnostic indices to determine the number of shorted turns, while the output was taken zero

during the normal operation and integers under fault conditions. Input to the second ANFIS were the three phase identification indices and its output was an integer indicating the faulty phase.

Tan and Huo [32] have suggested a generic neuro-fuzzy model based approach to the detection of rotor broken bar faults in an induction motor. In this paper the data for training the neuro-fuzzy system to model the generic static torque-speed relationship of the class of induction motors used in the practical evaluation of the fault detector. Modeling error was found by comparing the output speed of the neuro-fuzzy model and the speed which is obtained from the experimental torque-speed equation. This approach overcomes the practical limitations of model based strategies as it reduces the amount of experimental data that are needed to design the fault detector. This method is also able to identify the absence/presence of cracked rotor bars under varying load conditions.

Makarand, Zaffer, Hirallal and Ram [33] have been applied an adaptive neural fuzzy inference system for the detection of inter-turn insulation and bearing wear faults in induction motor. Here, the authors have given five inputs to the ANFIS; these are motor intakes current, speed, winding temperature, bearing temperature and the noise. The neural fuzzy architecture takes into account both ANN and fuzzy logic technology. They have used multilayer feed forward network as the ANN and sugeno type fuzzy rules as fuzzy inference systems. First they have developed both the detectors with two input parameters. Then the remaining three parameters are included. In case of the two inputs for insulation detector the training error was 0.068 and the accuracy was 94.03%, for bearing condition the training error was 0.0905 and the accuracy was 90.5%.In case of the five inputs, for insulation detector the training error was 0.001209 and the accuracy was 96.67%, for bearing condition the training error was 0.000945 and the accuracy was 98.77%. It was observed from the performance results that the five inputs ANFIS technique provides more accurate results in comparison with two input system.

Rodriguez and Arkkio [34] have used a methodology using for detection of stator winding fault in induction motor. In this paper, the stator three phase rms values of currents and the variance have been used as the input to the fuzzy logic system. The input data are generated with the motor working in different load conditions by using the FEM analysis. The fuzzy logic method was able to detect the motor condition with high accuracy for both with noise and without noise.

The drawback of the method is that a current unbalance originating from the supply source may be identified as a fault condition of the motor.

Abiyev [35] has integrated both fuzzy logic system with a wavelet neural network for identification and control of an uncertain system. In this paper he has used the gradient decent algorithm for the parameter updation. Two examples have been presented for identification and control performance studies. It has been demonstrated that the fuzzy wavelet neural networks can converge faster and is more adaptive to new data.

Bouzid [36] has suggested a neural network approach for the detection and location automatically of an inter-turn short circuit fault in the stator windings of an induction motor. In this paper they have used a feed forward multi layer perceptron neural network which is trained by the back propagation technique. The phase shift between the phase voltage and line current of an induction motor is used as the input to the neural network. The desired output is set to either 'one' or 'zero'. If a short circuit is detected and located on one of the three phases, the corresponding neural network output is set to 'one'; otherwise, it is 'zero'.

1.4 Objectives of the Thesis

The objectives of the thesis are as follows

- To develop an experimental setup for the generation of induction motor parameters under both healthy and inter-turn fault condition.
- To emulate the phase currents for both healthy and inter-turn fault condition and find out their behavior.
- To find out the phase shifts under different load conditions which are used as the input for the soft computing techniques.
- To apply different soft computing techniques such as MLPNN, RNN, RBFNN, and ANFIS for the detection of stator inter-turn short circuit fault in an induction motor.

- To propose discrete wavelets transform approach to detect and locate stator inter-turn short circuit fault together with identification of the severity of this fault in the stator winding of an induction motor.

1.5 Motivation

Maintenance of induction motors is one of the serious problems faced by many industries and utilities. According to Electric Power Research Institute motor reliable study [6], stator faults are responsible for 37% of the induction motor failures. According to Neale [37], the purchasing and installation costs of the equipments usually cost less than half of the total expenditure over the life of the machine for maintenance. According to Wowk [38], maintenance expenditure typically presents 15 to 40% of the total cost and it can be up to 80% of the total cost.

Having reviewed most of the techniques for fault diagnosis of an induction machine it is seen that accurate models of the faulty machine and model based techniques are essentially required for achieving a good fault diagnosis. Sometimes it becomes difficult to obtain accurate models of the faulty machine and also in applying model based techniques. On the other hand, soft computing approaches such as neural networks, fuzzy logic technique, wavelet techniques provide good analysis of a system even of accurate models are unavailable. Further Multilayer perceptron (MLP) architecture using Back Propagation (BP) algorithm has been extensively applied earlier for fault detection of machines [39]. This thesis extends the other Neuro-Computing paradigms such as Recurrent Neural Network (RNN), Radial Basis Function Neural Network (RBFNN) to the detection and location of an inter-turn short circuit fault in the stator winding of an induction motor. Adaptive neural fuzzy inference system (ANFIS) has been employed for a single phase induction motor to the detection and location of an inter-turn short circuit fault [33]. The results of the fault diagnosis using this technique are good. Thus, it gave a motivation in extending the ANFIS approach to fault detection of a three phase induction motor. By using neural networks, one can identify the particular phase of the induction motor where the fault occurs from the neural network output. Subsequently, a discrete wavelet technique is exploited not only to the detection and location of an inter-turn short circuit fault but also we can know the severity of such faults in the stator winding of an induction motor.

1.6 Thesis Organization

The contents are divided in 6 chapters. Besides this introductory chapter, the following chapters are presented.

Chapter–2 illustrates an experimental set up for the calculation of induction motor parameters both under healthy and stator inter-turn short circuit faulty condition. These induction motor parameters are used to generate the induction motor phase currents and the phase angle between the line currents and phase voltages under both healthy and faulty condition.

Chapter–3 deals with different neural network techniques such as MLPNN, RNN and RBFNN for the detection of stator inter-turn short circuit fault of an induction motor. Here we have used the three phase shifts between the line currents and phase voltages of an induction motor as inputs to above all the techniques. Then we have compared both training and testing errors of the above techniques.

Chapter–4 describes the adaptive neural fuzzy inference system (ANFIS) technique for detection of the stator inter-turn short circuit fault of an induction motor. Here also we have used the three phase shifts between the line currents and phase voltages of an induction motor as inputs to the above techniques. Lastly we have compared the performance of ANFIS with the RBFNN technique.

Chapter–5 presents the wavelet technique for the detection of stator inter-turn short circuit fault of an induction motor. In this technique the motor phase currents are used as the sampling signal for diagnosis. This chapter also describes the quantification of the degree of severity of such fault.

Chapter–6 concludes the thesis and gives some suggestions for future work.

Chapter 2

Experimental Setup and Data Generation for Induction Motor Fault Diagnosis

2.1 Introduction

Stator winding faults are one of the most important causes of faults in induction motors. Such faults are caused by several types of stress such as thermal, mechanical, electrical and environmental acting on the insulation system. All these stresses interact with each other in such a way that to degrade in the insulation system. Different types of stator faults [40] can develop under such stresses. From which inter-turn short circuit fault is one of the most common types of stator fault [41-43]. In most cases, the inter-turn short circuit fault progresses to a coil to coil, phase to phase, or phase to ground fault, causing the final breakdown of the motor.

This chapter presents an experimental set up for the calculation of induction motor parameters such as stator resistance, rotor resistance, stator inductance, rotor inductance, and magnetizing inductance both under healthy and stator inter-turn short circuit fault conditions. For this experimental set up, we have used a 2-hp squirrel cage induction motor. These parameters which are calculated from the experimental set up are used in a model [36] to generate the current in the different phases and the phase shift between the line currents and phase voltages of an induction motor under both healthy and stator inter-turn fault conditions.

2.2 Experimental Setup

The experimental set up is developed by reconfiguring of an existing induction motor rated at 2-hp. The advantage of using a 2-hp induction motor is that we can limit the short circuit loop current simply by using a variable external resistor. In case of large machines these short circuit loop currents are very large as compared to the rated current. So for this reason we have taken a 2-hp induction motor.

The stator core consists of 36 slots. There are 9 slots per pole (for a 4-pole motor) and 3 slots per pole per phase. A cross-sectional view of the motor is depicted in Fig. 2.1. To minimize the inherent cogging torque effects due to the space harmonics arising from the magnetic circuit geometric configurations and the effects of winding layouts the stator core was skewed by one slot pitch by 30^0 electrical. The skewed stator including its winding coils is shown in Fig. 2.2. The stator phase windings are double-layered, lap-connected with short pitched coils, each of a span of 150^0 electrical.

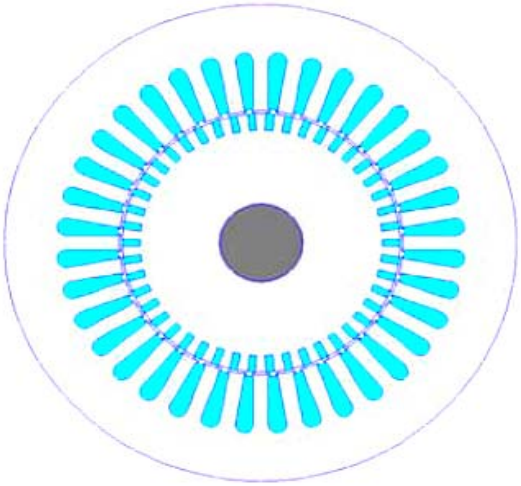

Fig. 2.1 Cross-sectional view of 2-hp IM

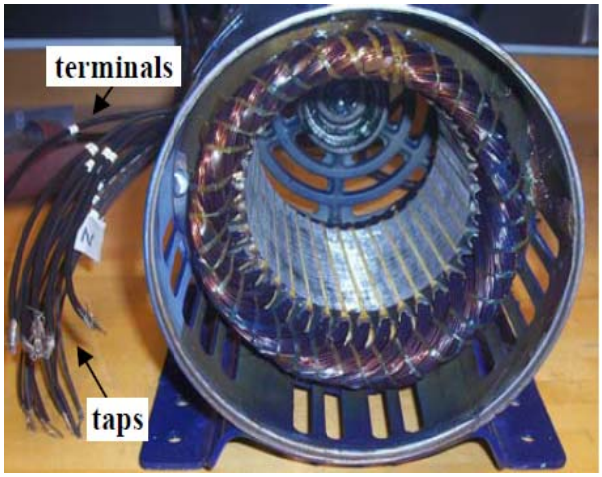

Fig. 2.2 Skewed stator with winding coils and taps

In order to emulate stator inter-turn short-circuit faults, the motor has a phase winding that was prepared with taps for the purpose of "experimental mimicking" of incipient inter-turn faults. The taps were soldered sequentially every two turns, beginning with the "start" point of turn #1 and ending with the "end" point of turn #45 of the machine as shown in Fig. 2.3.

The number of taps to be soldered in the windings is restricted by the amount of space available inside the motor housing. These taps are specially added at the motor terminal of one of the phases since the stator faults are likely to occur closest to the terminal end of the windings. To limit the short-circuit loop current; a variable external resistor is connected between the taps of the shorted portion of the winding turns (Fig. 2.3). The design characteristics of this reconfigurable induction motor are given in Table I.

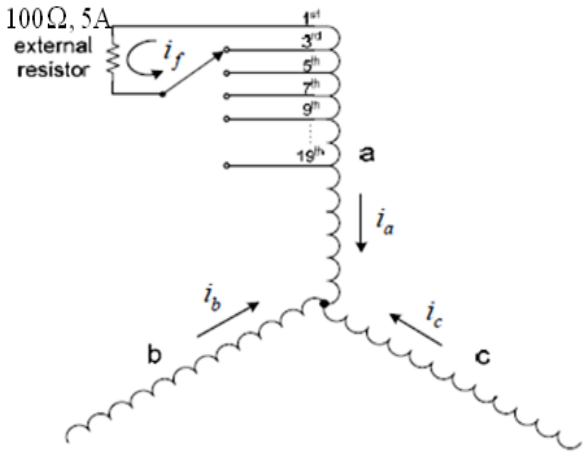

Fig. 2.3 Schematic diagram of stator windings with taps

TABLE I
2-HP INDUCTION MOTOR CHARACTERISTICS

Power (hp)	2
Voltage (V)	220/400
Current (I)	13.63/ 3.75
Speed (r/min)	1410
Number of poles	4
Number of coils per phase	12
Number of turns per coil	46
Number of turns per phase	552
Type of stator windings	Double Layer, Lap
Number of stator slots	36

2.3 Induction Motor Parameters

The equivalent circuit of an Induction Machine is very useful for determining its response to change in load. However, if a model is to be used for a real machine, it is necessary to determine the machine parameters. This information may be found by performing a series of tests such as No-load test, DC test and short-circuit tests on induction motor.

2.3.1 No- Load Test

The no-load test on an induction motor is conducted to measure the rotational losses of the motor to obtain information about the magnetizing current. The test circuit for this test is shown in Fig. 2.4. A voltmeter and three ammeters are connected to an induction motor. Wattmeters W_1 and W_2 are connected to an induction motor. As the motor is not connected to any load, all the power supplies to the motor are converted to the friction and windage losses. The equivalent circuit of the motor is shown in Fig. 2.5. With a small slip, the resistance corresponding to its power converted, $\frac{R_S(1-s)}{s}$ is much larger than the resistance corresponding to the rotor copper losses R_r and much larger than the rotor reactance X_r.

At no-load conditions, the input power measured by the meters W_1 and W_2 gives the losses occurs in the motor. The rotor copper losses are negligible because the current I_2 is extremely small so may be neglected. The stator copper losses are given by

$$P_{SCL} = 3I_1^2 R_S$$

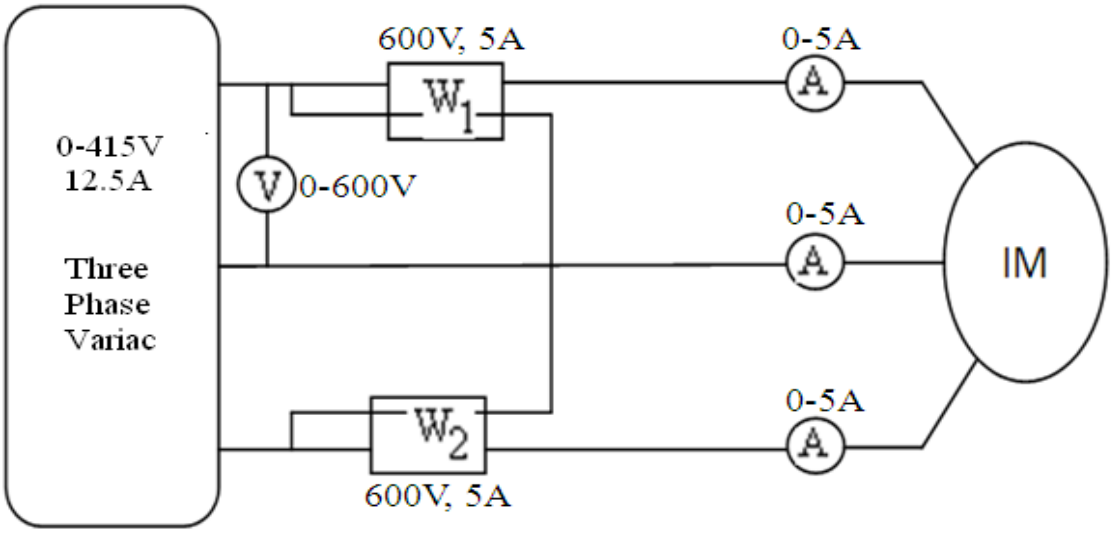

Fig.2.4 Circuit for No-Load test of an Induction Motor

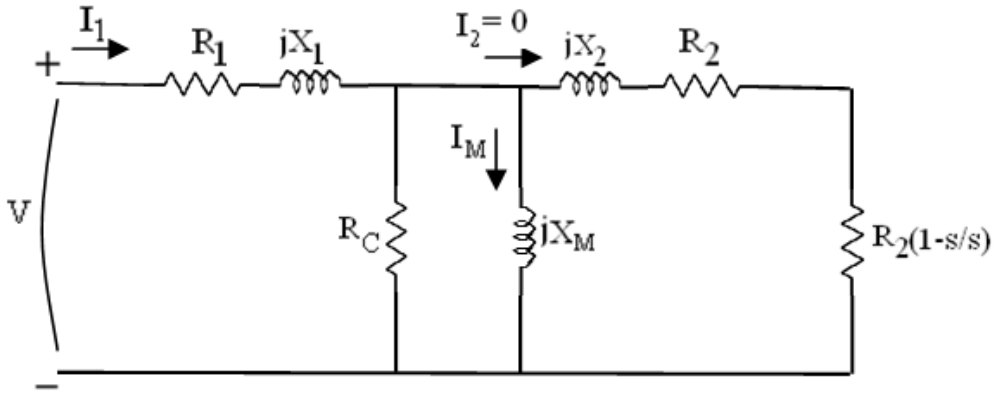

Fig.2.5 Induction Motor equivalent circuit

Hence the input power must equal

$$P_{in} = P_{SCL} + P_{Core} + P_{F\&W}$$
$$= 3I_1^2 R_S + P_{rot}$$

where P_{rot} is the rotational losses of the motor, given by

$$P_{rot} = P_{Core} + P_{F\&W}$$

Thus, given the input power to the motor, the rotational losses of the machine may be determined.

2.3.2 DC Test for Stator Resistance

The rotor resistance R_r plays an extremely critical role in the operation of an induction motor. A standard motor test called the block rotor test can be used to determine the total motor circuit resistance. However, this test gives only the total resistance. To find the rotor resistance R_r accurately, it is necessary to know R_s so that it can be subtracted from the total value of resistance.

There is a test for R_s independent of R_r. This test is called the dc test. Basically, a dc voltage is applied to the stator windings of an induction motor. Because the current is dc, there is no induced voltage in the rotor circuit and no resulting current flow. Therefore, the only quantity limiting current flow in the motor is the stator resistance, and that resistance can be determined.

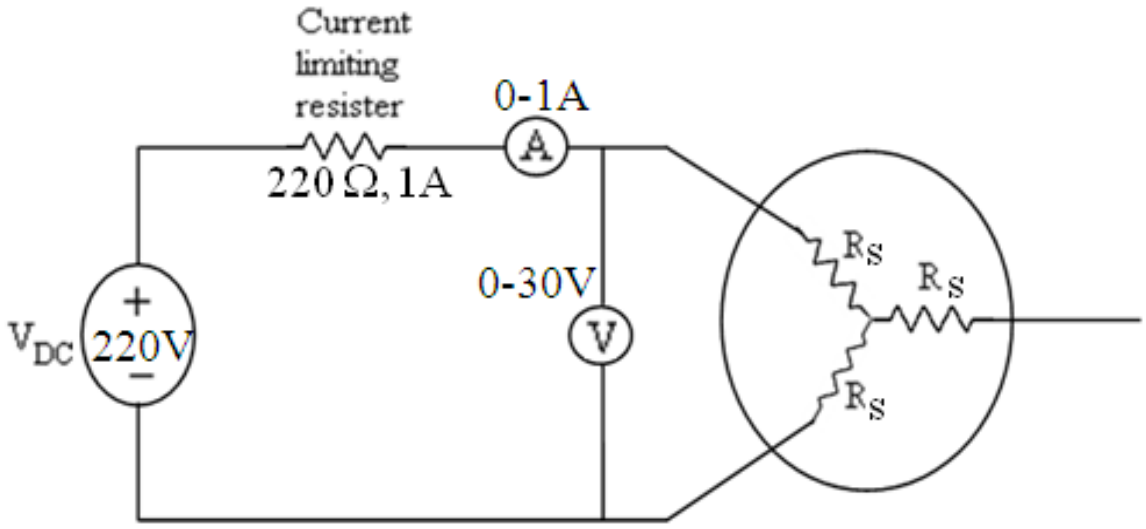

Fig.2.6 Test circuit for a dc resistance test

The basic circuit for conducting the dc test is shown in Fig.2.6, which shows a dc power supply connected to two of the three terminals of a Y-connected induction motor. To perform the test, current in the stator windings is adjusted to its rated value, and the voltage between the terminals is measured. The current in the stator windings is adjusted to the rated value in an attempt to heat the windings to the same temperature they would have during normal operation.

Fig. 2.6 shows the flow of current through two of the windings of the induction motor. The total resistance in the current path is $2R_s$. Therefore,

$$2R_S = \frac{V_{DC}}{I_{DC}}$$

$$R_S = \frac{V_{DC}}{2I_{DC}}$$

With this value of R_S the stator copper losses at no load may be determined.

2.3.3 Block Rotor Test

The third test that can be performed on an induction motor to determine its circuit parameters is the block-rotor or short-circuit test. In this test, the rotor is blocked so that it cannot move. A voltage is applied to the motor terminals, and the resulting voltage, current, and power is measured.

Fig. 2.7 shows the connections for the block rotor test. To perform the block rotor test, an ac voltage (approximately 100V) is applied to the stator, and the current flow is adjusted to a value approximately full-load value. When the current reaches the full-load value, the voltage, current, and power flowing into the motor are measured. The equivalent circuit for this test is shown in Fig. 2.8. Since the rotor is static, the slip s = 1, and so the rotor resistance R_r/s is just equal to R_r which is quite a small value. Since R_r and X_r are small values, almost all the input current will flow through them, instead of through the much larger magnetizing reactance X_M. Therefore, the circuit under these conditions looks like a series combination of X_S, R_S, X_r, and R_r.

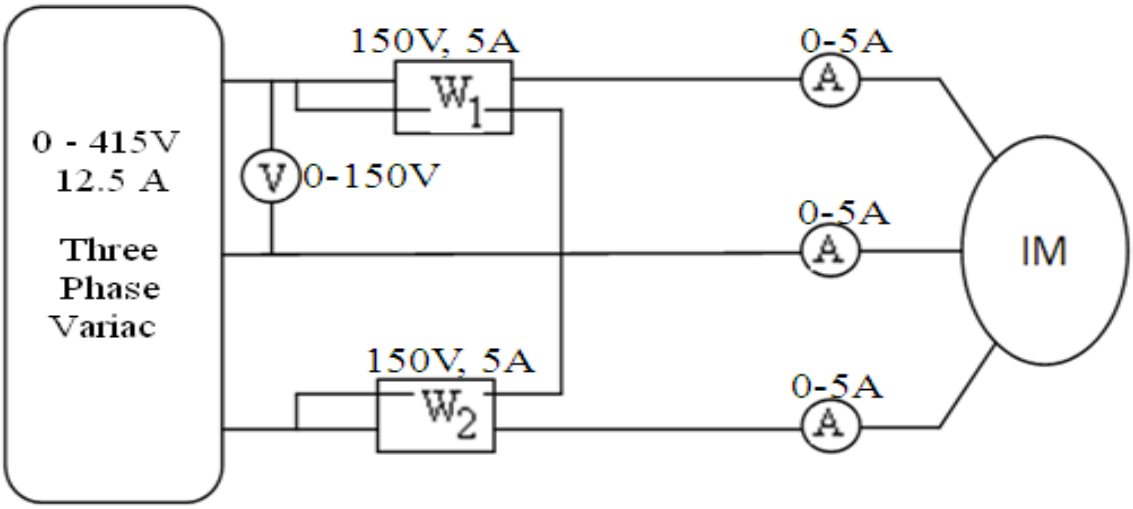

Fig. 2.7 Test circuit for block rotor test for an Induction Motor

There is one problem with this test. i.e. in normal operation, the stator frequency is the line frequency of the power system. At starting condition the rotor is also at line frequency. However, at normal operating conditions, the slip of the motor is only 2 to 4 percent, and the resulting rotor frequency is in the range of 1 to 3 Hz. This creates a problem in that the line frequency does not represent the normal operating conditions of the rotor. Since effective resistance is a function of frequency.

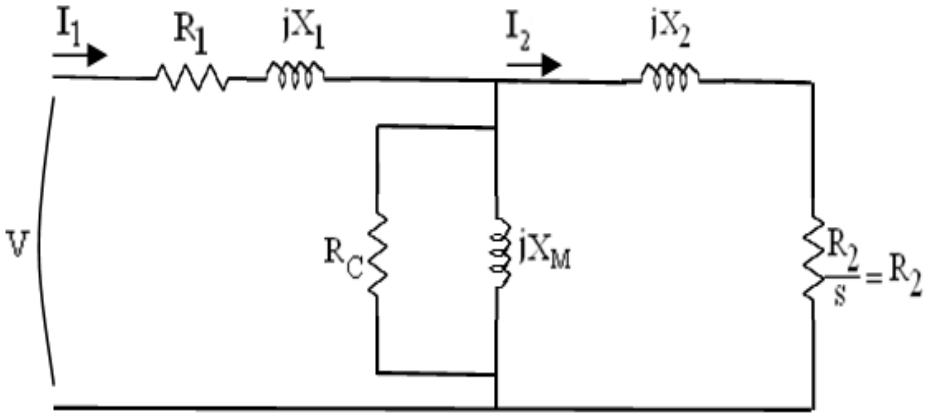

Fig.2.8 Induction Motor equivalent circuit

After a test voltage and frequency have been set up, the current flow in the motor is quickly adjusted to about the rated value, and the input power, voltage, and current measured before the rotor can heat up too much. The input power to the to the motor is given by

$$P = \sqrt{3} V_L I_L \cos\theta$$

where V_L, I_L and $\cos\theta$ are Line voltage, Line current and power factor respectively.

Hence, for blocked-rotor test power factor can be found by

$$PF = \cos\theta = \frac{p_{in}}{\sqrt{3} V_T I_L}$$

The magnitude of the total impedance in the motor circuit at this time is

$$Z_{LR} = \frac{V_T}{\sqrt{3} I_L}$$

and the angle of the total impedance is θ. Therefore,

$$Z_{LR} = R_{LR} + jX'_{LR}$$

$$= Z_{LR}\cos\theta + jZ_{LR}\sin\theta$$

The rotor resistance R_{LR} is equal to

$$R_{LR} = R_1 + R_2$$

While the rotor reactance is equal to

$$X'_{LR} = X'_1 + X'_2$$

Where X'_1 and X'_2 are the stator and rotor reactances at the test frequency, respectively.

The rotor resistance R_2 can now be found as

$$R_2 = R_{LR} - R_1$$

where R_1 was determined in the dc test. The total rotor reactance referred to the stator can also be found. Since the reactance is directly proportional to the frequency, the total equivalent reactance at the normal operating frequency can be found as

$$X_{LR} = X_1 + X_2$$

2.4 Induction Motor Parameters under Healthy Condition

From the above three tests (No load test, DC test and Block rotor test) one has to find out the Induction Motor Parameters under healthy condition. These are given in table II.

Table II
Induction Motor Parameters under Healthy Condition

Sl. No	R_s (ohm)	R_r (ohm)	L_s (Henry)	L_r (Henry)	L_m (Henry)
1	6.2	7.91	0.418	0.418	0.3942

2.5 Induction Motor Parameters under Stator Inter-Turn Fault Condition

From the above three tests (No load test, DC test and Block rotor test) we have found out the Induction Motor Parameters have been calculated when a stator inter-turn fault occurs in the phase-A of an induction motor. These are given in table III.

Table III
Induction Motor Parameters under Inter-Turn Faulty Condition

Sl. No	No. of shorted turns	Stator Resistance (ohm)			Rotor Resistance (ohm)	Fault Inductance (Henry)			Rotor Inductance (Henry)	Magnetizing Inductance		
		R_{sa}	R_{sb}	R_{sc}	R_r	L_{fa}	L_{fb}	L_{fc}	L_r	L_{ma}	L_{mb}	L_{mc}
1	1-3	2.3	7.66	3.68	6.1	0.01497	0.05	0.024	0.418	0.390	0.48	0.4
2	3-5	2.08	7.905	3.32	6.1	0.0139	0.052	0.02118	0.418	0.386	0.488	0.389
3	5-7	1.92	8.508	3.20	6.1	0.01266	0.05632	0.01999	0.418	0.381	0.504	0.378
4	7-9	1.85	8.95	3.04	6.1	0.01126	0.05941	0.01851	0.418	0.373	0.521	0.364
5	9-11	1.75	9.40	2.92	6.1	0.01038	0.06251	0.01741	0.418	0.369	0.532	0.357
6	11-13	1.63	9.96	2.86	6.1	0.009475	0.06637	0.0167	0.418	0.362	0.545	0.346
7	13-15	1.52	10.54	2.78	6.1	0.008522	0.0704	0.01545	0.418	0.355	0.564	0.337
8	15-17	1.40	11.1	2.66	6.1	0.007655	0.07425	0.01467	0.418	0.349	0.578	0.329
9	17-19	1.33	11.8	2.59	6.1	0.00679	0.07912	0.014	0.418	0.343	0.590	0.318
10	19-21	1.24	12.5	2.51	6.1	0.006277	0.08404	0.01328	0.418	0.337	0.605	0.309
11	21-23	1.11	13.25	2.40	6.1	0.005659	0.08936	0.01251	0.418	0.331	0.618	0.297
12	23-25	1.02	13.9	2.26	6.1	0.004888	0.09402	0.0116	0.418	0.319	0.631	0.284
13	25-27	0.91	14.30	2.12	6.1	0.004418	0.09698	0.01065	0.418	0.308	0.648	0.271
14	27-29	0.82	14.96	2.01	6.1	0.003825	0.10165	0.00984	0.418	0.294	0.663	0.257
15	29-31	0.71	15.5	1.86	6.1	0.00334	0.10557	0.00886	0.418	0.281	0.678	0.243

As we know that under normal operation and balanced conditions, the three phase parameters of an induction motor are same as shown in the table II. When a stator inter-turn fault will occur in an induction motor the three phase parameters are different for different phases.

2.6 State Space Representation of a Faulty Induction Motor

The model in [36] is used here to generate both healthy and faulty currents of a three phase induction motor. In faulty condition, this model can be characterized by two modes such as common mode and differential mode. The common mode refers to the dynamic modes in healthy operation of the machine whereas the differential mode refers to the faulty operation. The model of the differential mode introduces two parameters defining the faults in the stator. These are as follows

(i) $\theta_{cck,}$ (location parameter): is the angle between the inter turn short circuit stator winding and the first stator phase axis. This parameter can take only three values 0, $2\pi/3$, $4\pi/3$, corresponding to the short circuit on the phase a_s, b_s, c_s respectively.

(ii) λ_{cck}, (detection parameter): is the ratio between the numbers of inter-turn short circuit windings and the total number of turns in the healthy phase. These parameters are to quantify the unbalance.

$$\lambda_{cck} = \frac{\text{Number of inter - turns short circuit windings}}{\text{Total number of inter - turns in healthy phase}}$$

The state space representation of a faulty induction motor is given by

$$\dot{X} = AX + BU$$

$$Y = CX + DU$$

where

$$X = [i_{ds}\ i_{qs}\ \varphi_{dr}\ \varphi_{qr}]^T$$

$$U = [V_{ds}\ V_{qs}]^T$$

$$A = \begin{bmatrix} -\frac{R_s + R_r}{L_f} & \omega & \frac{R_r}{L_m L_f} & \frac{\omega}{L_f} \\ -\omega & -\frac{R_s + R_r}{L_f} & -\frac{\omega}{L_f} & \frac{R_r}{L_m L_f} \\ R_r & 0 & -\frac{R_r}{L_m} & 0 \\ 0 & R_r & 0 & -\frac{R_r}{L_m} \end{bmatrix}$$

$$B = \begin{bmatrix} \frac{1}{L_f} & 0 & 0 & 0 \\ 0 & \frac{1}{L_f} & 0 & 0 \end{bmatrix}^T$$

$$C = \begin{bmatrix} 1 & 0 & 0 & 0 \\ 0 & 1 & 0 & 0 \end{bmatrix}$$

$$D = \left[\frac{2}{3R_s} \sum_{k=1}^{3} \lambda_{cck} P(-\theta) Q(\theta_{cck}) p(\theta) \right]$$

$$Q_{cck} = \begin{bmatrix} \cos(\theta_{cck})^2 & \cos(\theta_{cck})\sin(\theta_{cck}) \\ \cos(\theta_{cck})\sin(\theta_{cck}) & \sin(\theta_{cck})^2 \end{bmatrix}$$

$$P(\theta) = \begin{bmatrix} \cos(\theta) & -\sin(\theta) \\ \sin(\theta) & \cos(\theta) \end{bmatrix}$$

i_{ds}, i_{qs} : dq stator current components;

ϕ_{dr}, ϕ_{qr} : dq rotor flux linkage;

V_{ds}, V_{qs} : dq stator voltage;

θ : Electrical angle;

$\omega = d\theta / dt$

R_s, L_f, R_r, and L_m are the stator resistance, global leakage inductance referred to the stator, rotor resistance, and magnetizing inductance, respectively.

2.7 Data Generation for Induction Motor Fault Diagnosis

Under normal operation and balanced conditions, phase voltages and line currents equal in magnitude and shifted by 120^0 electrical due to the induction motor parameters. However, under faulty operation, the phase currents are unequal and also their phase shifts. The different phase currents of the induction motor under both before and after the inter-turn short circuit fault have been investigated through simulation study using MATLAB software.

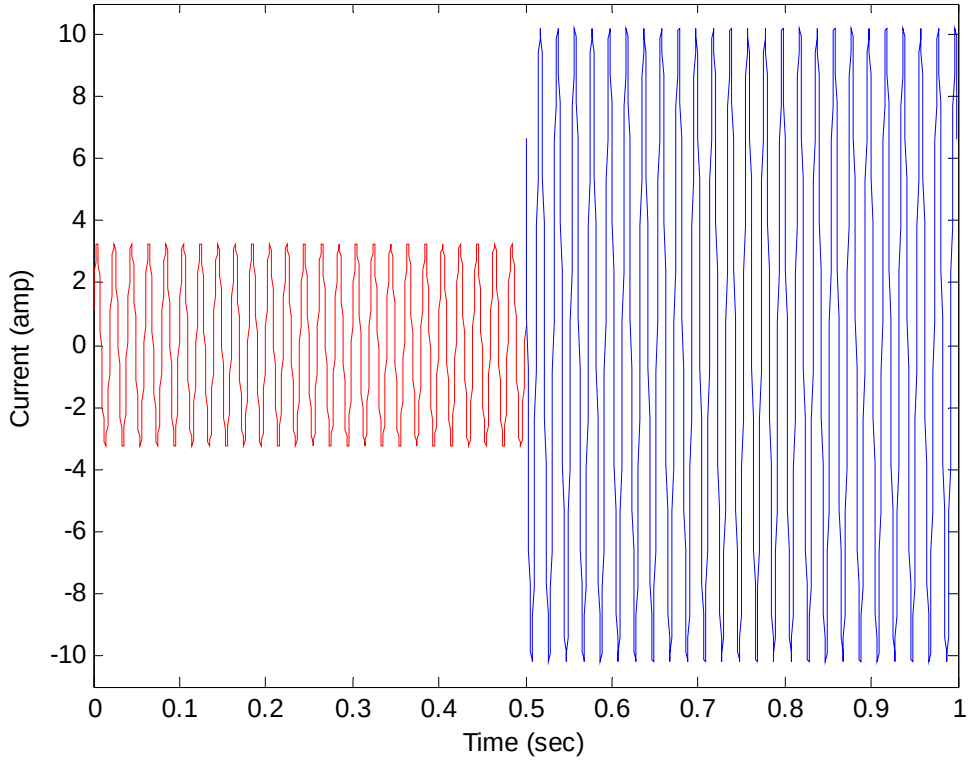

Fig. 2.9 Current on phase A before and after fault

Fig. 2.9 shows the profiles of the simulated current on phase A before and after fault condition with no load torque. When a stator inter-turn fault will occur on phase A of an induction motor introduced at 0.5 Sec, the current in that phase rises to its peak value.

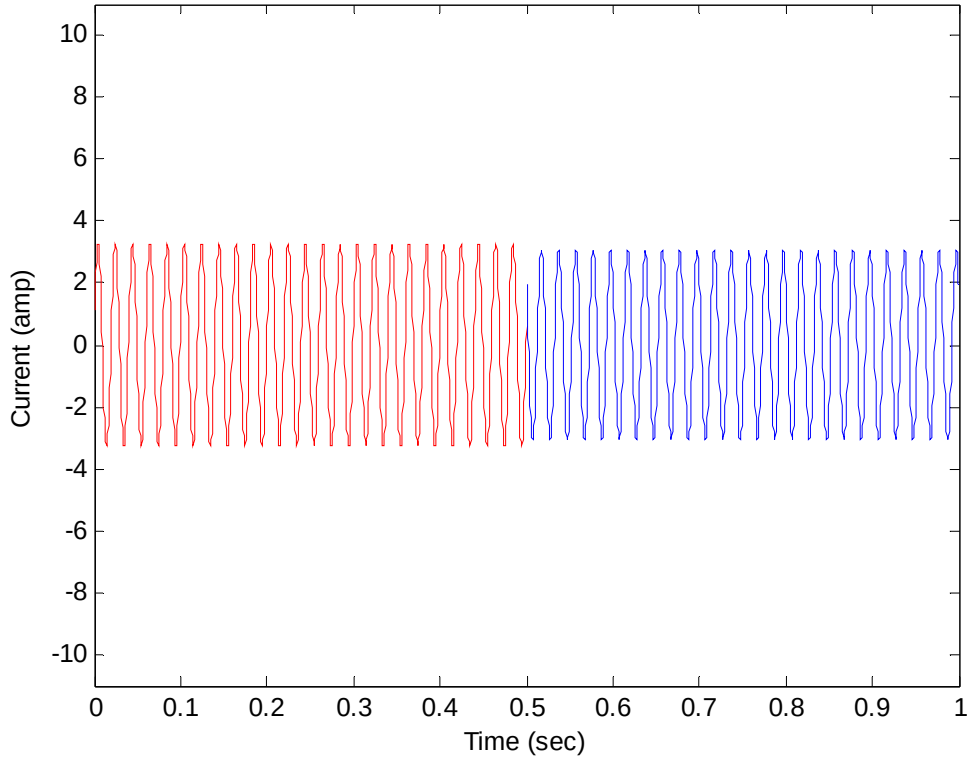

Fig. 2.10 Current on phase B before and after fault

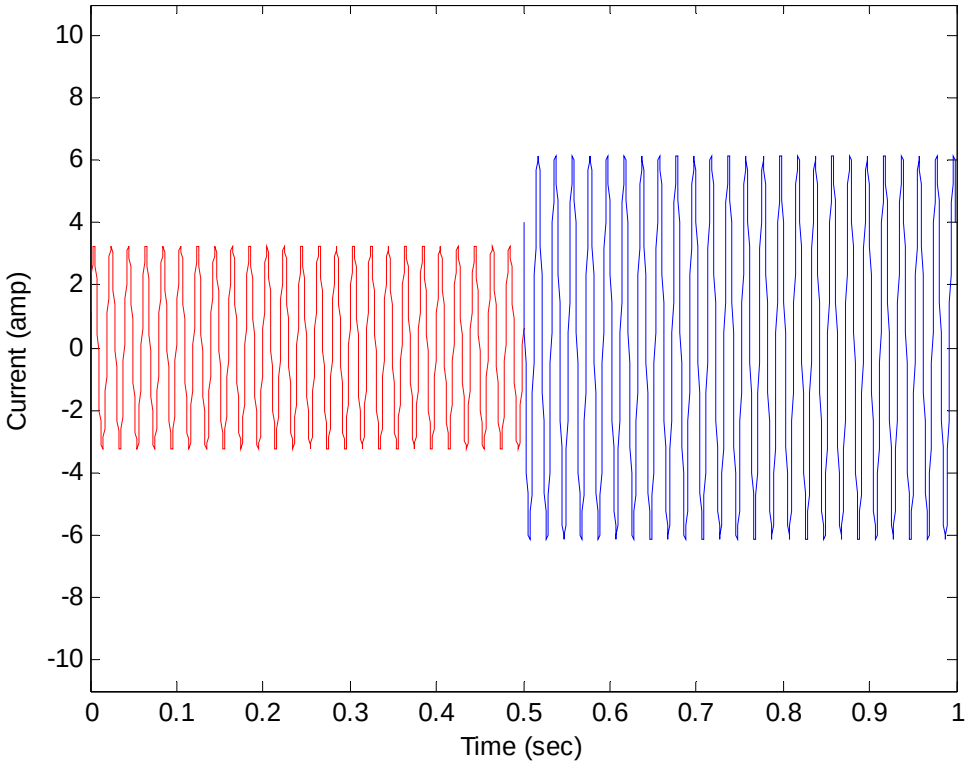

Fig. 2.11 Current on phase C before and after fault

Fig. 2.10 indicates the profiles of the simulated current on phase B before and after fault condition with no load torque. When a stator inter-turn fault will occur on phase A of an induction motor introduced at 0.5 sec, the current in phase B is less influenced.

Fig. 2.11 illustrates the profiles of the simulated current on phase C before and after fault condition with no load torque. When a stator inter-turn fault will occur on phase A of an induction motor introduced at 0.5 sec, the current in phase C has smaller influence compared to phase A. From Figs. 2.9, 2.10 and 2.11 we can observe that, when a fault occurred in one of the three phases, the current appears particularly in the corresponding phase increases to its peak value compared with other phases. Thus, it is clear that an inter-turn short circuit fault affects the stator current of the faulty phase in peak value where the other stator phase currents have smaller influences.

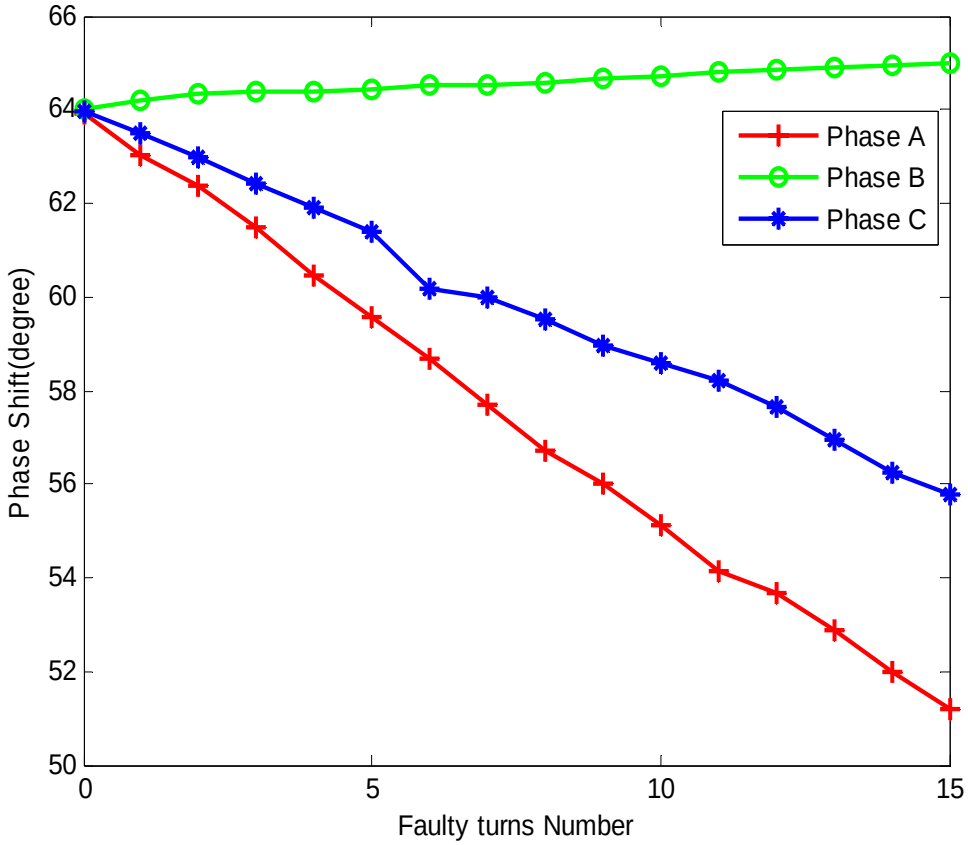

Fig. 2.12 Phase shift characteristics for fault on phase A

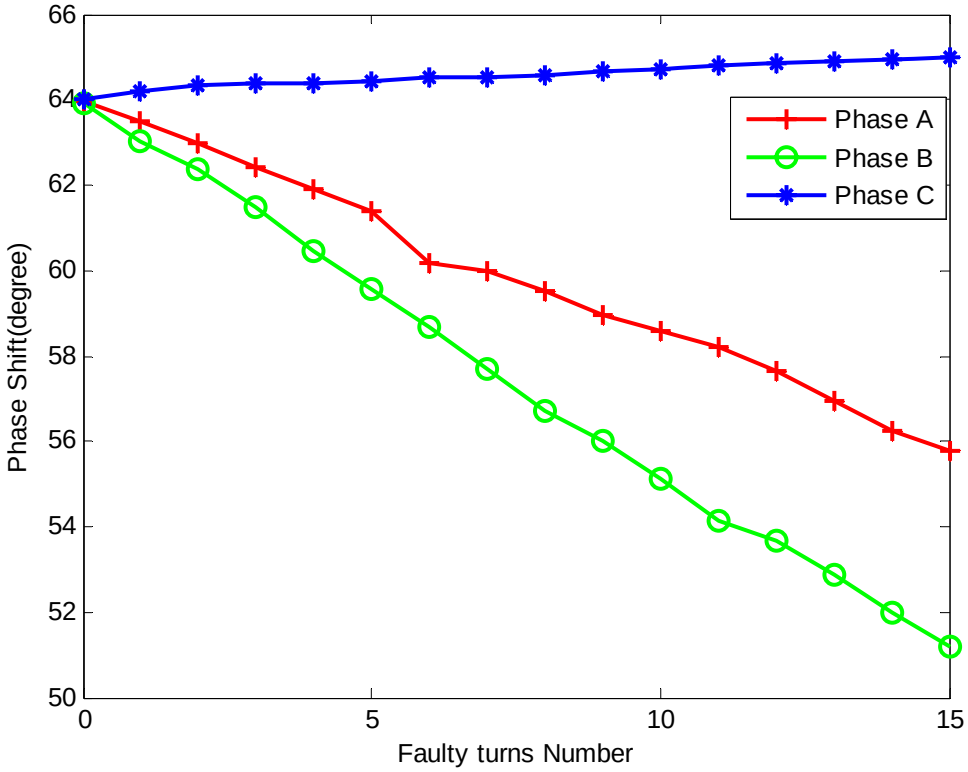

Fig. 2.13 Phase shift characteristics for fault on phase B

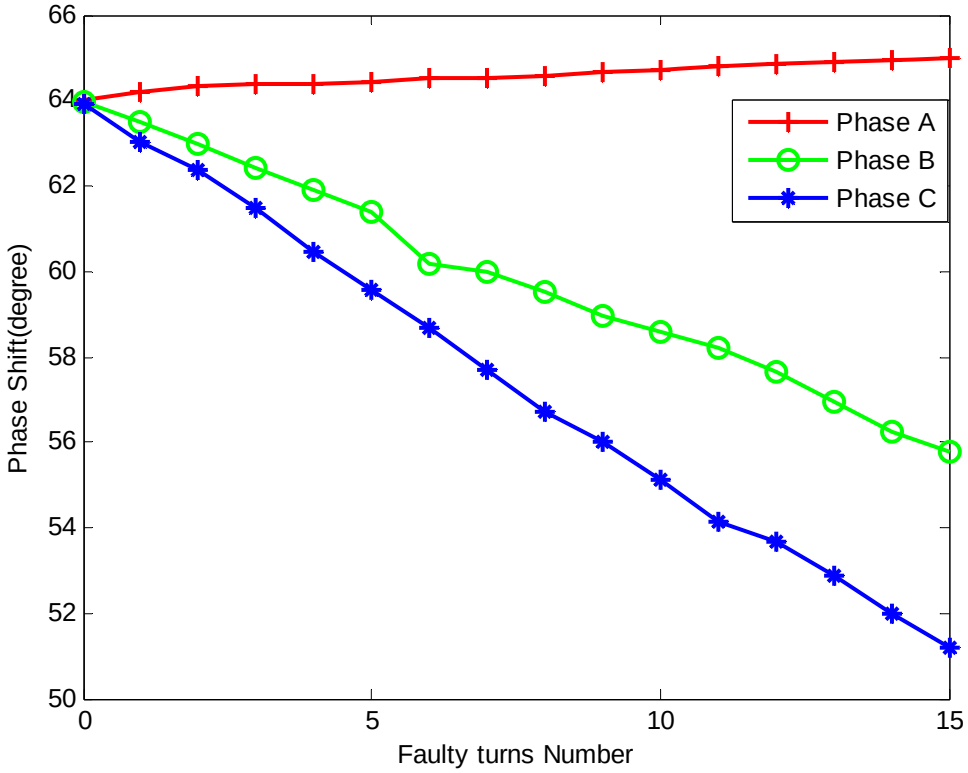

Fig. 2.14 Phase shift characteristics for fault on phase C

Effect of occurrence on stator inter-turn short circuit fault on the phase shift, can be analyzed from Figs. 2.12, 2.13, and 2.14. The characteristics of the phase shifts under a load torque of 3 N-m, as function of the faulty turn number in the case of stator inter-turn short circuit fault on the phases A, phase B, and phase C as shown in Figs. 2.12, 2.13, and 2.14 respectively. As the number of short circuit turn changes, the induction motor parameters such as stator resistance (R_s), leakage inductance (L_f), and magnetizing inductance (L_m) also changes. It can be also noted that, in the case of a stator fault on one of the three phases, the smallest value of the three-phase shifts is the phase where the fault has occurred.

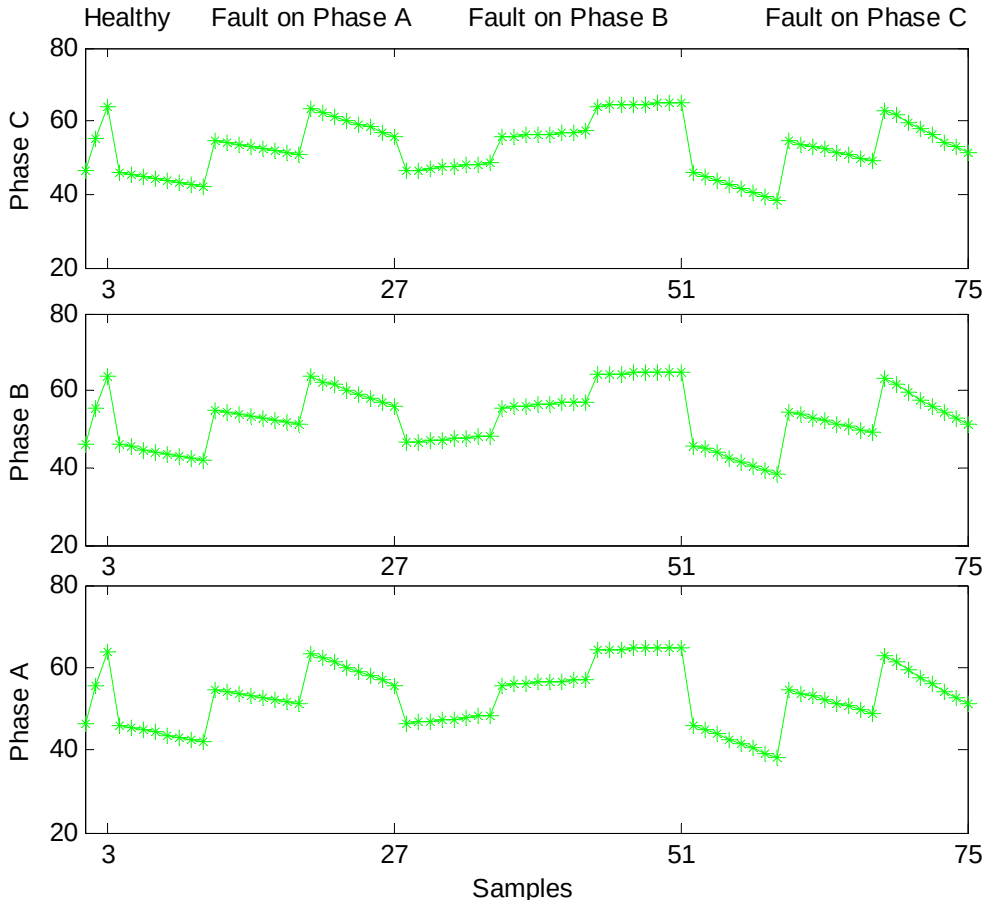

Fig. 2.15 Simulated training input data set

The input data are collected through simulations by Matlab. The data collected above will be useful in subsequent chapters for studying stator inter-turn fault conditions. To achieve the location of the induction motor faulty phase, the training data should represent the complete range of the operating conditions, which contain all possible fault occurrences and even the healthy cases.

For this purpose, the input data set, which is shown in Fig. 2.15 are composed by a successive range of several examples in different operating conditions of the induction motor. All these examples are used in the subsequent chapters under three load torques (τ_1 = 3 N-m, τ_2 = 5 N-m, τ_3 = 7 N-m) and represent the following different operating cases of the induction motor: healthy (three points) and fault of an odd number of shorted turns (1, 3, 5, 7, 9, 11, 13, and 15) on each stator phase [24 (8 × 3) points]. Thus, a total of 75(24 × 3 + 3) training samples has been collected and will be useful in subsequent chapters for studying stator inter-turn fault conditions.

2.8 Chapter Summary

This chapter presents an experimental setup for the generation of induction motor parameters such as stator resistance, rotor resistance, stator inductance, rotor inductance, and magnetizing inductance both under healthy and stator inter-turn short circuit fault conditions. For the generation of those parameters, we have conducted several tests (no-load test, DC test, and block rotor test) under both healthy and shorting the stator winding for every two turns sequentially, beginning with the start point of turn '1' and ending with the end point of turn '45' of the induction motor. A variable resistor is connected between the taps of the shorted portion of the winding turns to limit the circular loop current. Those induction motor parameters are used in the model equation [36] to generate the currents in the different phases under both conditions. By using the model equation, the data (phase shifts between the line currents and phase voltages) have been generated under both conditions at different load torques i.e τ_1 = 3 N-m, τ_2 = 5 N-m, τ_3 = 7 N-m. These generated data have been incorporated for studying stator inter-turn fault conditions which is presented in the subsequent chapters.

Chapter 3

Fault Detection Schemes using Different Neural Network Paradigms

3.1 Introduction

In this chapter, neural networks have been exploited to diagnose the stator inter-turn short circuit fault. Neural networks have gained popularity over other techniques due to their generalization capability [44], which means that they are able to perform satisfactorily even for unseen fault. Neural networks [45-47] can perform fault detections based on measurements and training without the need of complex and rigorous mathematical models. In addition, heuristic interpretation of motor conditions which sometimes only humans are capable of doing can be easily implemented in the neural networks through supervised learning. For many fault detection schemes redundant information is available and can be used to achieve more accurate results. This concept can be easily implemented in neural network exploiting its multiple input parallel processing features to enhance the robustness of the network performance.

In this chapter, application of different paradigms of neural networks (NNs) are chosen such as multilayer perceptron neural network (MLPNN), recurrent neural network (RNN), and radial basis function neural network (RBFNN) for inter-turn short circuit fault detection and location in the stator winding of an induction motor has been proposed. Different kinds of inputs are used to the neural networks such as current and speed [47, 48], negative and positive sequence stator currents, slip, and rated slip [30] for the induction motor stator fault diagnosis. It is reported in [49], that the phase shift is more preferable than the others. Hence we have used the three phase shift between the line currents and the phase voltages of the induction motor as inputs to the neural networks.

3.2 Propose NNs Approach to Induction Motor Fault Diagnosis

The proposed fault diagnosis system consists of detection and the location of an inter-turn short fault on the stator windings of a three phase induction motor by using the Neural Networks. The Fig 3.1 shows the block diagram of the fault location procedure in the stator winding of an induction motor.

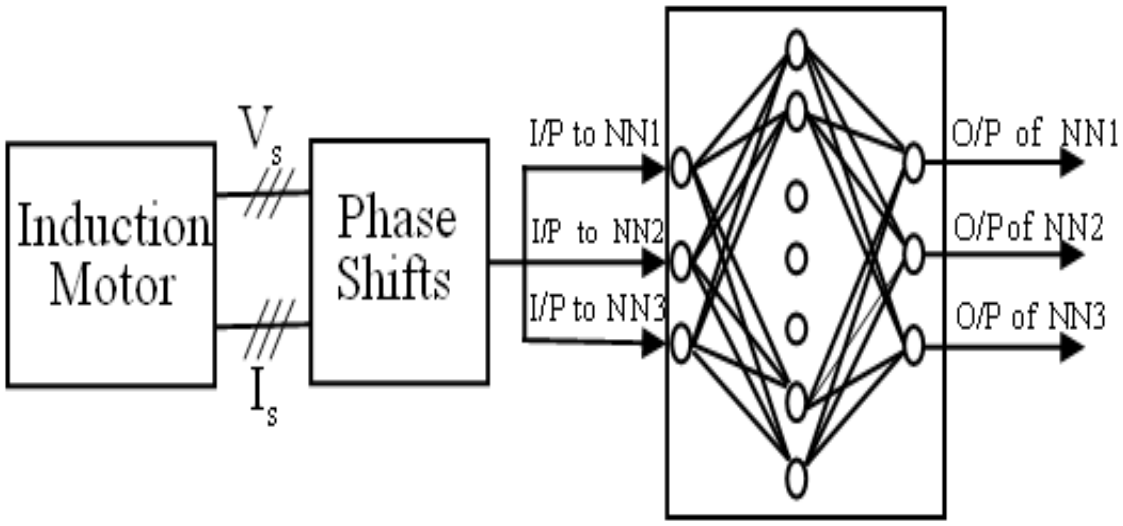

Fig.3.1 Block diagram of the fault location procedure

The first step of this procedure is the acquisition of the three line currents and phase voltages from the induction motor in order to extract the three phase shift between the line currents and the phase voltages.

The three phase shifts are considered as the inputs to input layer neural networks, which are be to trained offline using the gradient descent algorithm. Neural Network had to learn the relationships between the NNs inputs (three phase shift between the line currents and phase voltage) and the NNs outputs (either 0 for healthy condition or 1 for inter-turn short circuit condition) due to its input-output mapping characteristics to locate the faulty phase in the stator winding of an induction motor.

The neural networks employed for fault diagnosis consists of three inputs, which are the three phase shifts and three outputs corresponding to the three phase of the induction motor as shown

in Fig. 3.1. If a short circuit is detected and located on one of the three phases, the corresponding output is set to 'one', otherwise it is 'zero'.

The design of the neural networks based fault diagnosis comprises of the following four steps.

i. Preparation of a suitable training data set for the NNs.
ii. Selection of a suitable NNs Structure.
iii. Training of the NNs.
iv. Evaluation of the test pattern.

3.2.1 Preparation of a Suitable Training Data Set for the NNs

A training data set constituted by input and output data sets has been applied to the neural network. The input data set, which is shown in chapter 2 (section 2.7) are composed by a successive range of several examples in different operating conditions of the induction motor. All these examples are presented to the NNs under three load torques (τ_1 = 3 N-m, τ_2 = 5 N-m, τ_3 = 7 N-m) which represent the following different operating cases of the induction motor: healthy (three points) and fault of an odd number of shorted turns (1, 3, 5, 7, 9, 11, 13, and 15) on each stator phase [24 (8 × 3) points]. Thus, a total of 75(24 × 3 + 3) samples have been collected and applied as the inputs to the neural networks for stator inter-turn fault diagnosis.

The desired outputs (T_i) of the neural networks are decided as below.

T_1 = 1 for a short circuit at phase A; otherwise, T_1 = 0;
T_2 = 1 for a short circuit at phase B; otherwise, T_2 = 0;
T_3 = 1 for a short circuit at phase C; otherwise, T_3 = 0;

Therefore, the output states of the neural networks are set as the following.

[0; 0; 0] no fault (healthy condition);
[1; 0; 0] fault occurred at phase A;
[0; 1; 0] fault occurred at phase B;
[0; 0; 1] fault occurred at phase C;

3.2.2 Selection of a Suitable NNs Structure

3.2.2.1 Selection of a Suitable MLPNN Structure

Fig. 3.2 shows the structure of the multi layer perceptron neural network used for the location of the faulty phase of induction motor. The first neural network paradigm studied for the proposed fault diagnosis is a feed-forward multi layer perceptron neural network. It is trained by using back propagation algorithm [50]. The numbers of input and output neurons are fixed i.e three for three phases of an induction motor, but the number of neurons in the hidden layer is not known.

If the number of neurons in the hidden layer is too few, the neural network cannot learn well, and if this number is too large, the neural network may simply memorize the training set.

First we start with only two neurons in the hidden layer we then add on until a small mean square error (MSE) is obtained. With the above procedure it was found the training performance in terms of MSE of the neural network is obtained with five neurons in the hidden layer.

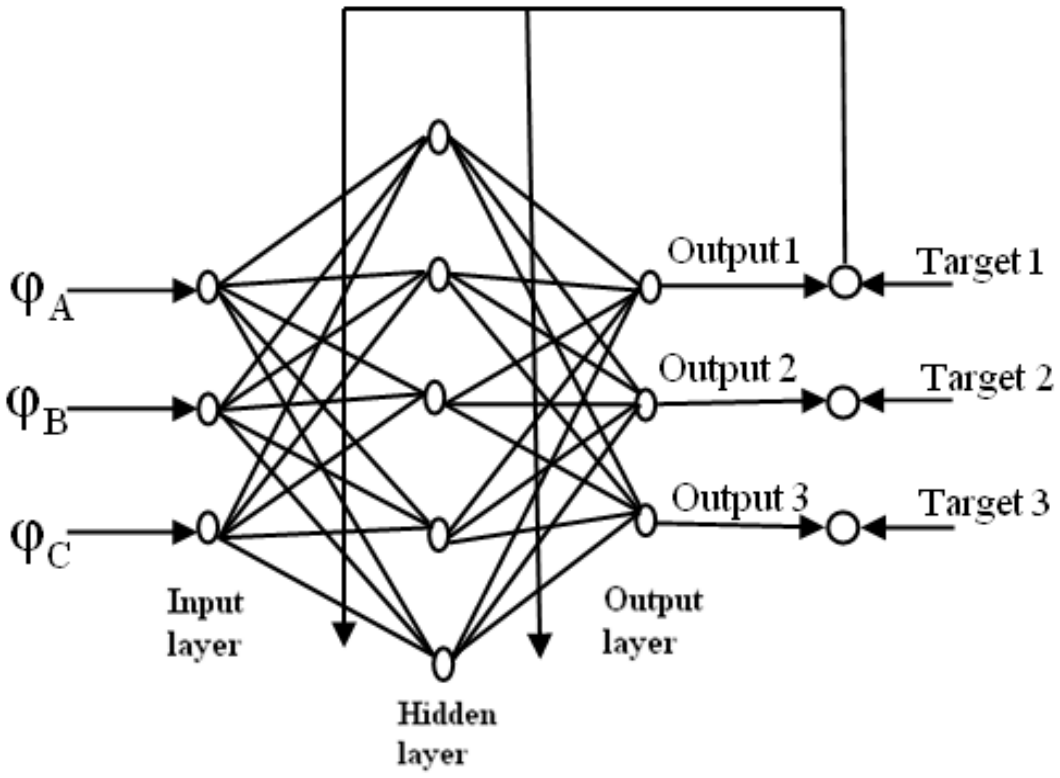

Fig.3.2.MLPNN Architecture

3.2.2.2 Selection of a Suitable RNN Structure

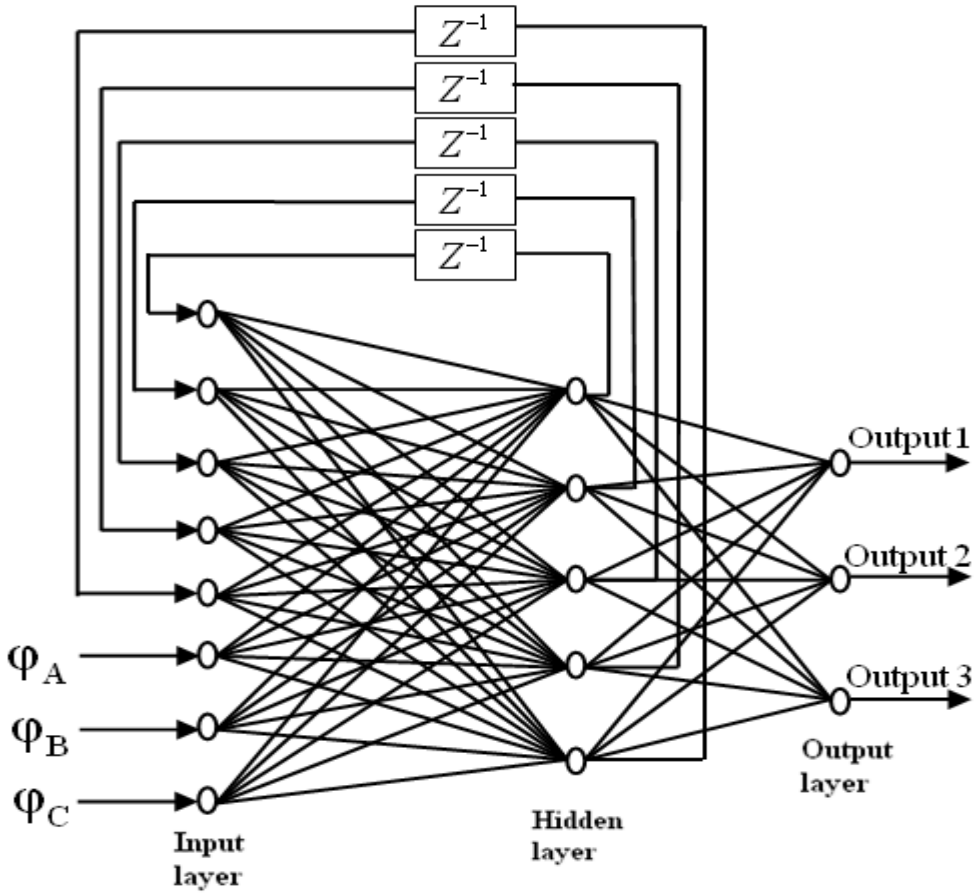

Fig.3.3 RNN Architecture

Fig 3.3 shows recurrent neural network architecture used for the location of the faulty phase of an induction motor. Though the MLPNN is already used but it could not give the better identification performance. The proposed network architecture is used to make the identification faster and accurate for achieving better convergence of neural network optimization. It is trained by using real time recurrent learning algorithm.

The numbers of input and output neurons are fixed i.e three for three phases of an induction motor, but the number of neurons in the hidden layer is not known. The same trial and error procedure is used for choosing the number of neurons in the hidden layer. First we start with only two neurons in the hidden layer we then add on until a small mean square error (MSE) is obtained. With the above procedure it was found the training performance in terms of MSE of the neural network is obtained with five neurons in the hidden layer.

3.2.2.3 Selection of a Suitable RBFNN Structure

RBF neural network is a feed forward network whose structure is shown in Fig. 3.4. Though the MLPNN and RNN are used but it could not give the better identification performance so we further go for another one neural network structure i.e radial basis function neural network (RBFNN). The structure of a RBF neural network consists of three different layers, namely the input layer, the hidden layer, and output layer. The input layer is made up of source nodes whose number is equal to the dimension of the input vector; the second layer is hidden layer (Gaussian transfer functions typically used) which is composed of non-linear units that are connected directly to all of the nodes in the input layer. Here fixed centers selected at random learning strategy has used.

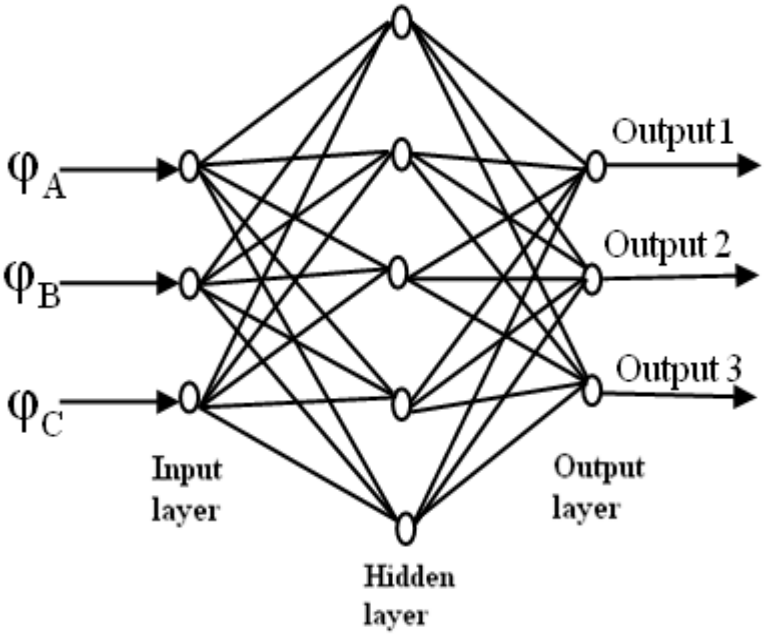

Fig.3.4 RBFNN Architecture

The numbers of input and output neurons are fixed i.e three for three phases of an induction motor, but the number of neurons in the hidden layer is not known. The same trial and error procedure is used for choosing the number of neurons in the hidden layer. First we start with only two neurons in the hidden layer we then add on until a small mean square error (MSE) is obtained. With the above procedure it was found the training performance in terms of MSE of the neural network is obtained with five neurons in the hidden layer.

3.2.3 Training methodology of the NNs

If the weights are updated after presentation of the entire set of training patterns to the network, then it is called batch training. In second approach, the weights are updated after presentation of each training pattern; this is called pattern training or online updating. When the NNs are trained, the weights of the links are changed / adjusted so as to achieve minimum error. During this process a part of the entire data set is used as training set, and the error is minimized on this set. Calculations of error may be done using various functions. One of the most commonly used errors is the mean square error. Different training algorithms such as back propagation, real time recurrent learning and fixed centers selected at random learning strategy are used for updating the weights of the MLPNN, RNN, and RBFNN respectively.

3.2.3.1 Training methodology of MLPNN

The multilayer perceptron neural network is trained with a supervised learning algorithm called back propagation. The feed-forward neural networks consist of an input layer representing the input data to the network, some hidden layers and output layer representing the response of the network. Each layer consists of a certain number of neurons. Each neuron is connected to other neurons of the previous layer through adaptable synaptic weight W and biases b, as shown in Fig. 3.5.

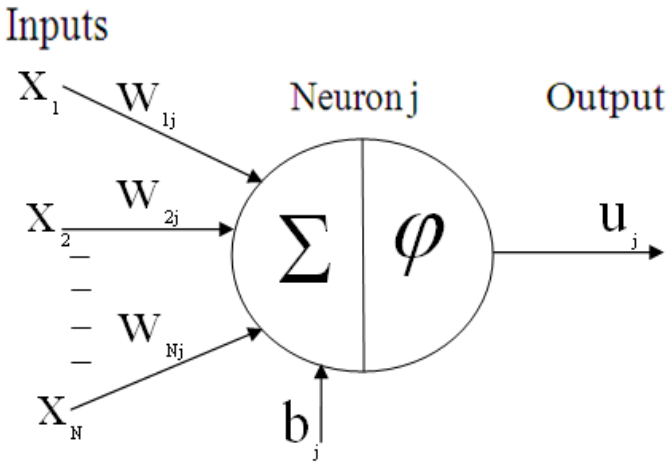

Fig.3.5 Information processing in a neuron

If the inputs to the neuron j are the variables x_1, x_2, x_3 ……..x_N, the output u_j of the neuron j is obtained as follows.

$$u_j = \varphi(\sum_{i=1}^{N} w_{ij} x_i + b_j) \quad (3.1)$$

where

w_{ij} : weight of the connection between neuron j and the i^{th} input.

b_j : bias of the neuron j.

φ : transfer function (activation function) of neuron j.

N: number of inputs.

A feed-forward neural network shown in Fig. 3.5 consists of three layers (one hidden layer) with N, M and Q neurons for the input, hidden and output layers respectively. The input patterns of the ANN represented by a vector of variables $x = (x_1, x_2, x_3 \ldots\ldots x_N)$ submitted to the ANN by the input layer are transferred to the hidden layer. Using the weight of the connection between the input, the hidden layer and the bias of the hidden layer, the output vector $u = (u_1, u_2, u_3 \ldots\ldots u_M)$ of the hidden layer is then determined. The output u_j of neuron j is obtained as follows.

$$u_j = \varphi_{hid}(\sum_{i=1}^{N} w_{ij}^{hid} x_i + b_j^{hid}) \quad (3.2)$$

where

w_{ij}^{hid} : weight of connection between neuron j in the hidden layer and the i^{th} neuron of the input layer.

b_j^{hid} : bias of neuron j.

φ_{hid} : activation functions of the hidden layer.

The values of the vector u of the hidden layer are transferred to the output layer. Using the weight of the connection between the hidden layer and output layers and the bias of the output layer, the output vector $y = (y_1, y_2, y_3 \ldots\ldots y_Q)$ of the output layer is determined.

The output y_k of the neuron k (of the output layer) may obtained as follows.

$$y_k = \varphi_{out}(\sum_{j=1}^{M} w_{jk}^{out} u_j + b_k^{out}) \quad (3.3)$$

where

w_{jk}^{out} : weight of the connection between neuron k in the output layer and the j^{th} neuron of the hidden layer.

b_k^{out} : bias of the neuron k.

φ_{out} : activation function of the output layer.

The output y_k (corresponding to the given input vector x) is compared with the desired output (target value) y_k^d that is (y_k^d - y_k) is minimized using the mean square error at the output layer (which is composed of Q output neurons), defined by

$$E = \frac{1}{2}\sum_{k=1}^{Q}(y_k^d - y_k)^2 \qquad (3.4)$$

Training of the neural network is the process of adjusting connection weights w and biases b. In the first step, the network outputs and the difference between the actual output and the desired (target) output (i.e. the error) is calculated for the initialized weights in all links and biases in all neurons are adjusted to minimize the error by propagating the error backwards (the back propagation algorithm). The network outputs and the error are calculated again with the adopted weights and biases, and the process (the training of the ANN) is repeated at each epoch until a satisfied output y_k (corresponding to the values of the input variables x) is obtained and the error is acceptably small.

The adjustment in weights and biases can be accomplished by the back propagation algorithm. Following the principle, minimizing the total mean square error computed as follows.

$$\Delta w = w^{new} - w^{old} = -\eta\frac{\partial E}{\partial w} \qquad (3.5)$$

$$\Delta b = b^{new} - b^{old} = -\eta\frac{\partial E}{\partial b} \qquad (3.6)$$

where

η = learning rate.

The computation in (3.5) and (3.6) reflects the generic rule used by the back propagation algorithm. Equations (3.7) to (3.10) illustrated this generic rule of adjusting the weights and biases. For the output layer, we have

$$w_{jk}^{new} = \alpha \Delta w_{jk}^{old} + \eta \delta_k y_k \tag{3.7}$$

$$b_k^{new} = \alpha \Delta b_k^{old} + \eta \delta_k \tag{3.8}$$

where

$\alpha =$ momentum factor (a constant between 0 and 1)

$$\delta_k = y_k^d - y_k$$

For the hidden layer, we get

$$\Delta w_{ij}^{new} = \alpha \Delta w_{ij}^{old} + \eta \delta_j y_j \tag{3.9}$$

$$\Delta b_j^{new} = \alpha \Delta b_j^{old} + \eta \delta_j \tag{3.10}$$

where

$$\delta_j = \sum_{k=1}^{Q} \delta_k w_{jk}$$

$$\delta_k = y_k^d - y_k$$

Once the network is trained with the back propagation algorithm and appropriate weights and biases are obtained, neural networks can be used as a predictor to identify the output pattern when an input pattern is presented.

3.2.3.2 Training methodology of RNN

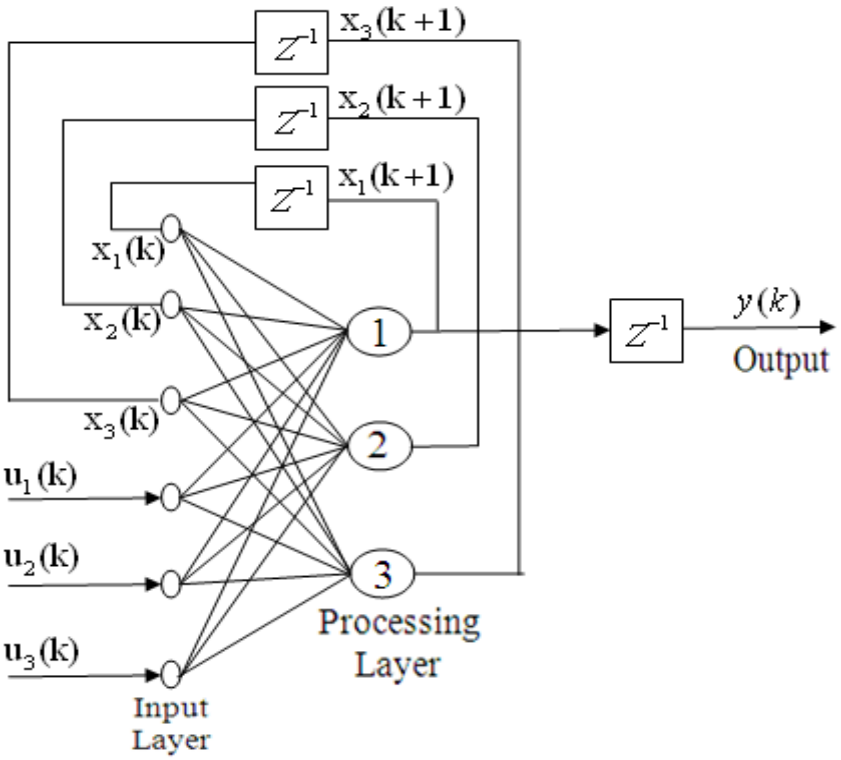

Fig.3.6. A Fully Recurrent Neural Network

The training of the RNN is carried out by using the real time recurrent learning algorithm. Fig 3.6 shows the layout of a fully recurrent neural network. It consists of q neurons with m external inputs. The state space description of the network is defined by equations

$$x(k+1) = \varphi(W_a x(k) + W_b u(k)) \tag{3.11}$$

$$y(k) = Cx(k) \tag{3.12}$$

The equation (3.11) can be expanded in the form

$$x(K+1) = \begin{bmatrix} \varphi(w_1^T \xi(k)) \\ \bullet \\ \varphi(w_j^T \xi(k)) \\ \bullet \\ \varphi(w_q^T \xi(k)) \end{bmatrix} \tag{3.13}$$

where it is assumed that all the neurons have a common activation function $\varphi(\cdot)$. The (q + m + 1) vector w_j is the synaptic weight vector of neuron j in the recurrent network, that is given by

$$w_j = \begin{bmatrix} w_{a,j} \\ w_{b,j} \end{bmatrix} \quad j = 1, 2, ..., q \tag{3.14}$$

where $w_{a,j}$ and $w_{b,j}$ are the jth columns of the transposed weight matrices w_a^T and w_b^T, respectively. The (q + m + 1) vector $\xi(k)$ is defined by

$$\xi(k) = \begin{bmatrix} x(k) \\ u(k) \end{bmatrix} \tag{3.15}$$

where x(k) is the state vector and u(k) is the input vector.

To simplify the representation, three new matrices have been introduced. These are $\Lambda_j(k)$, $U_j(k)$, and $\phi(k)$.

1. $\Lambda_j(k)$ is defined as the partial derivative of the state vector x(k) with respect to the weight vector w_j.

$$\Lambda_j(k) = \frac{\partial x(k)}{\partial w_j}, \quad j = 1, 2, ..., q \tag{3.16}$$

2. $U_j(k)$ is a matrix whose rows are all zero, except for the jth row that is equal to the transpose of vector $\xi(k)$:

$$U_j(k) = \begin{bmatrix} 0 \\ \xi^T(k) \\ 0 \end{bmatrix}, \quad j = 1, 2, ..., q \tag{3.17}$$

3. $\phi(k)$ is a diagonal matrix whose kth diagonal element is the partial derivative of the activation function with respect to its argument, evaluated at $w_j^T \xi(k)$:

$$\phi(k) = diag(\varphi'(w_1^T \xi(k)), ...\varphi'(w_j^T \xi(k)), ...\varphi'(w_j^T \xi(k))) \tag{3.18}$$

Differentiating equation (3.13) with respect to w_j and then, using the chain rule of calculus, we obtain the following recursive equation:

$$\Lambda_j(k+1) = \varphi(k)\left[w_a(k)\Lambda_j(k) + U_j(k)\right], \quad j = 1, 2, ..., q \tag{3.19}$$

This recursive equation describes the nonlinear state dynamics of the real-time recurrent learning process. The error vector can be described as

$$\begin{aligned} e(k) &= d(k) - y(k) \\ &= d(k) - Cx(k) \end{aligned} \tag{3.20}$$

The mean square errors at time k is defined in terms of e(k) by

$$\xi(k) = \frac{1}{2} E\left[e(k)^2\right] \tag{3.21}$$

The objective of the learning process is to minimize a cost function obtained summing $\xi(k)$ over all time k: that is,

$$\xi_{Total} = \sum_k \xi(k) \tag{3.22}$$

To accomplish this objective we may use the method of steepest descent, which requires knowledge of the gradient matrix, written as

$$\nabla_W \xi_{Total} = \frac{\partial \xi_{Total}}{\partial w} = \sum_k \frac{\partial \xi(k)}{\partial w} = \sum_k \nabla_W \xi(k) \tag{3.23}$$

where $\nabla_W \xi(k)$ is the gradient of $\xi(k)$ with respect to the weight matrix W. In order to develop a learning algorithm can be used to train the recurrent network in real time, we use an instantaneous estimate of the gradient, namely $\nabla_W \xi(k)$, which results in an approximator to the method of steepest descent.

To minimize the cost function, we differentiate it with respect to the weight vector w_j,

$$\frac{\partial \xi(k)}{\partial w_j} = \left(\frac{\partial e(k)}{\partial w_j} \right) e(n)$$
$$= -C \left(\frac{\partial x(k)}{\partial w_j} \right) e(k)$$
$$= -C\Lambda_j(k)e(k), \qquad j = 1, 2, ..., q \tag{3.24}$$

The adjustment applied to synaptic weight vector $w_j(k)$ of neuron j is therefore determined by

$$\Delta w_j(k) = -\eta \frac{\partial \xi(k)}{\partial w_j}$$
$$= \eta C\Lambda_j(k)e(k), \qquad j = 1, 2, ..., q \tag{3.25}$$

3.2.3.3 Training Methodology of RBFNN

The radial basis function based neural network (RBFNN) consists of an input layer made up of source nodes and a hidden layer of large dimension. The number of input and output nodes is maintained same and while training the same pattern is simultaneously applied at the input and the output. The linear weights associated with the output layer of the network tend to evolve on a different time scale compared to the nonlinear activation functions of the hidden layer. Thus, as the hidden layer's activation functions evolve slowly in accordance with some nonlinear optimization strategy, the output layer's weights adjust themselves rapidly through a linear optimization strategy.

The fixed radial basis functions approach is used for defining the activation functions of the hidden layer. The locations of the centers are chosen randomly from the training data set. A radial basis function centered at t_i is given by

$$G\left(\left\| x - t_i \right\|^2 \right) = \exp\left(-\frac{m_1}{d_{\max}^2} \left\| x - t_i \right\|^2 \right), \qquad i = 1, 2, ..., m_1 \tag{3.26}$$

where m_1 is the number of centers and d_{max} is the maximum distance between the chosen centers. The standard deviation (width) of all the Gaussian radial basis functions is fixed at

$$\sigma = \frac{d_{\max}}{\sqrt{2m_1}} \tag{3.27}$$

Equation (3.27) ensures that the individual radial basis functions are not too peaked or too flat; both of these two extreme conditions should be avoided. The only parameters that would need to be learned in this approach are the linear weights in the output layer of the network. For this pseudoinverse method have been used and given by

$$w = G^{+}d \tag{3.28}$$

where d is the desired response vector in the training set. The matrix G^{+} is the pseudoinverse of the matrix G, which is defined as

$$G = \{g_{ji}\} \tag{3.29}$$

where

$$g_{ji} = \exp\left(-\frac{m_1}{d^2}\left\|x_j - t_i\right\|^2\right), \quad \mathrm{j} = 1, 2, ..., \mathrm{N}; \quad \mathrm{i} = 1, 2, ..., \mathrm{m}_1 \tag{3.30}$$

where x_j is the jth input vector of the training sample.

For the computation of a pseudoinverse of a matrix, the singular value decomposition method is used:

If G is a real matrix, there exist orthogonal matrices

$$U = \{u_1, \mathrm{u}_2, ..., \mathrm{u}_\mathrm{N}\}$$

and

$$V = \{v_1, \mathrm{v}_2, ..., \mathrm{v}_\mathrm{M}\}$$

such that

$$U^T GV = diag(\sigma_1, \sigma_2, ..., \sigma_\mathrm{K}), \qquad \mathrm{K} = \min(\mathrm{M}, \mathrm{N}) \tag{3.31}$$

where

$$\sigma_1 \geq \sigma_2 \geq ..... \geq \sigma_K \succ 0$$

The column vectors of the matrix U are called the left singular vectors of G, and the column vectors of the matrix V are called its right singular vectors. The $\sigma_1, \sigma_2, ..., \sigma_K$ are called the singular values of the matrix G. According to the singular value decomposition theorem, the pseudoinverse of matrix G is defined by

$$G^+ = V \sum^+ U^T \tag{3.32}$$

where $\sum^+$ is defined in terms of singular values of G by

$$\sum^+ = diag\left(\frac{1}{\sigma_1}, \frac{1}{\sigma_2}, ..., \frac{1}{\sigma_K}, 0, ..., 0\right) \tag{3.33}$$

The random selection of centers method is relatively insensitive in the field of pattern classification.

3.2.4. Evaluation of the Test Pattern

The performance of NNs on the testing data set represents its generalization ability. The data set is divided into two. One set is used for training and the other for testing. In fact a generalized neural network will perform well for both training and testing data. The test procedure is conducted by a test data set that is different from the training data set to assess the generalization capacity of the adopted network.

The test data set are presented to the neural networks under three load torques (τ_1 = 3 N-m, τ_2 = 5 N-m, τ_3 = 7 N-m) and represent the following different operating cases of the induction motor: healthy (three points) and fault of an even number of shorted turns (2, 4, 6, 8, 10, and 12) on each stator phase [18 (6 × 3) points]. Thus, a total of 21(18 + 3) testing samples have been collected for testing the each phase stator inter-turn fault.

3.3 Results and Discussions

3.3.1 Fault Detection Performance of MLPNN

3.3.1.1 Training Results for MLPNN

Training data of all the three input parameters (three phase shifts θ_a, θ_b, θ_c) are applied for obtaining the optimized architecture for the detection of inter-turn short circuit fault in the stator winding of an induction motor.

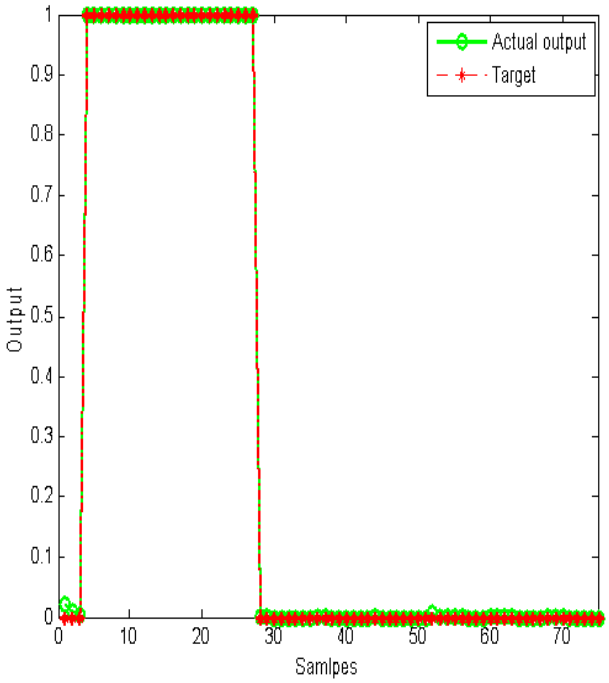

Fig.3.7 MLPNN Output for fault on phase A

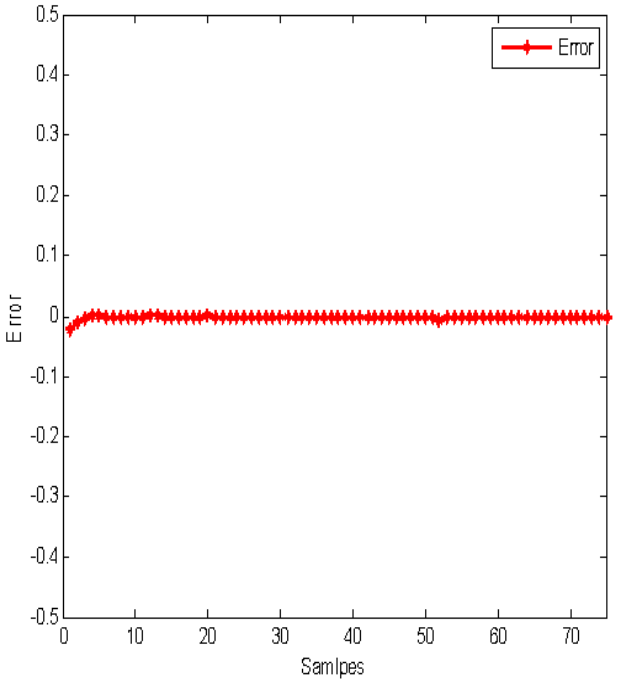

Fig.3.8 MLPNN Error for fault on phase A

Figs.3.7 and 3.8 show the MLPNN output and error when a stator inter-turn short circuit fault occurs on phase A of an induction motor respectively. Fig.3.7 describes that the output of the MLPNN from which the star one is the target value (either 0 or 1 for healthy and inter-turn faulty condition respectively) and the circle one is the output of the MLPNN. When a stator inter-turn fault occurs on phase A, then the output of that phase is one and others are zero. From Fig. 3.7 it is clear that the MLPNN has well learned the input data and correctly reproduced the desired output. Hence, the error which is the difference between the target value and the actual output is 9.1701×10^{-6} which is shown in Fig.3.8.

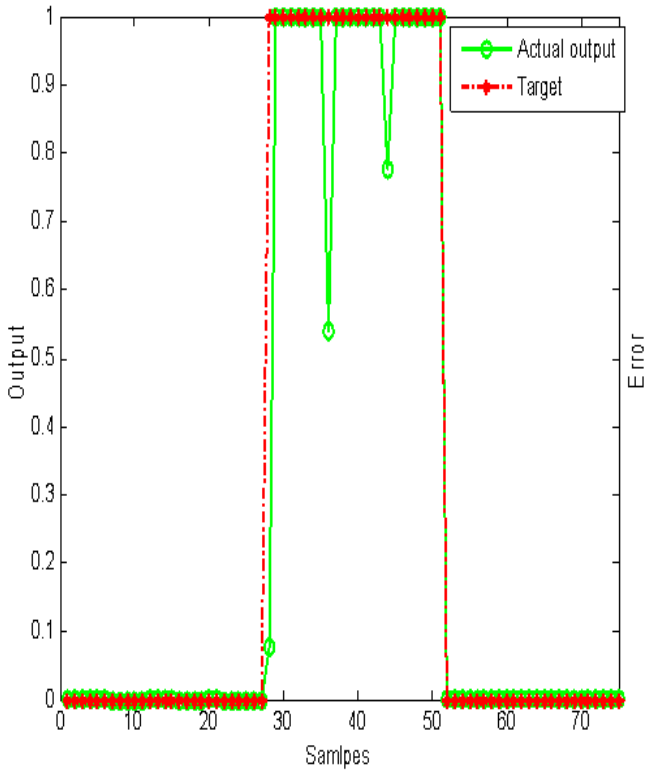

Fig.3.9 MLPNN Output for fault on phase B

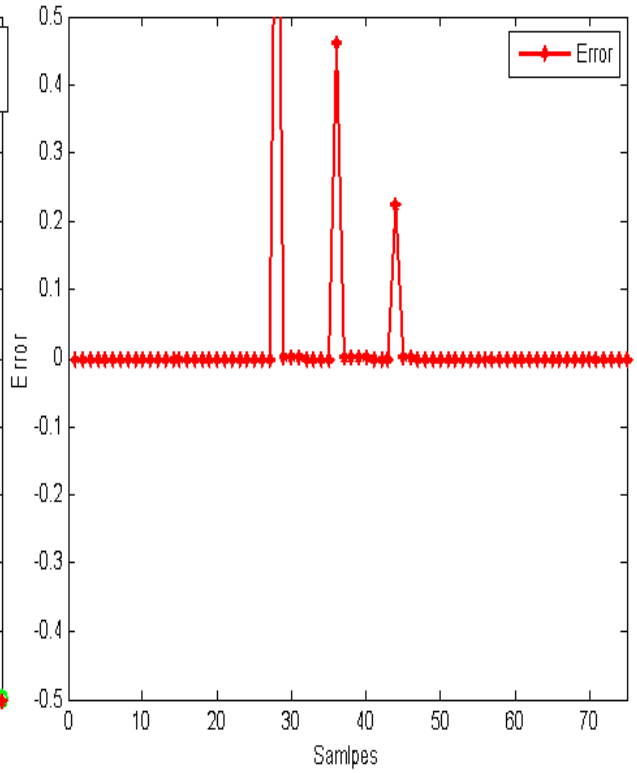

Fig.3.10 MLPNN Error for fault on phase B

The MLPNN output and error when a stator inter-turn short circuit fault occurs on phase B of an induction motor respectively as shown in Figs.3.9 and 3.10. Fig.3.9 shows that the output of the MLPNN from which the star one is the target value (either 0 or 1 for healthy and inter-turn faulty condition respectively) and the circle one is the output of the MLPNN. From Fig. 3.9 it is clear that the MLPNN has not properly learned the input data Hence, the error which is the difference between the target value and the actual output is 1.4800×10^{-2} as shown in Fig.3.10.

Figs.3.11 and 3.12 illustrate that the MLPNN output and error when a stator inter-turn short circuit fault occurs on phase C of an induction motor respectively. The target output (either 0 or 1 for healthy and inter-turn faulty condition respectively) of the MLPNN i.e the star one and the circle one is the actual output of the MLPNN as shown in Fig. 3.11. When a stator inter-turn fault occurs on phase C then the output of that phase is one and others are zero. From Fig. 3.11 it is clear that the MLPNN has well learned the input data and correctly reproduced the desired output. The error which is the difference between the target value and the actual output is 9.0743×10^{-7} as shown in Fig.3.12.

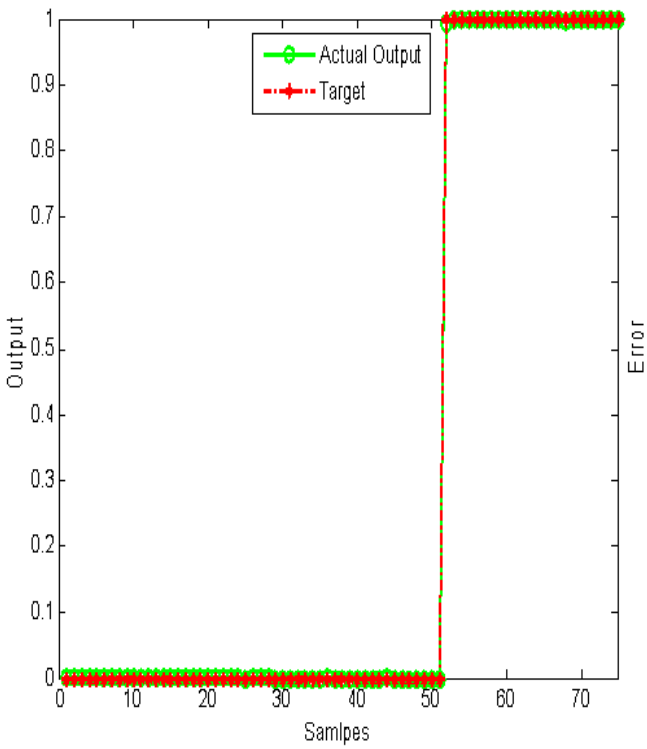

Fig.3.11 MLPNN Output for fault on phase C

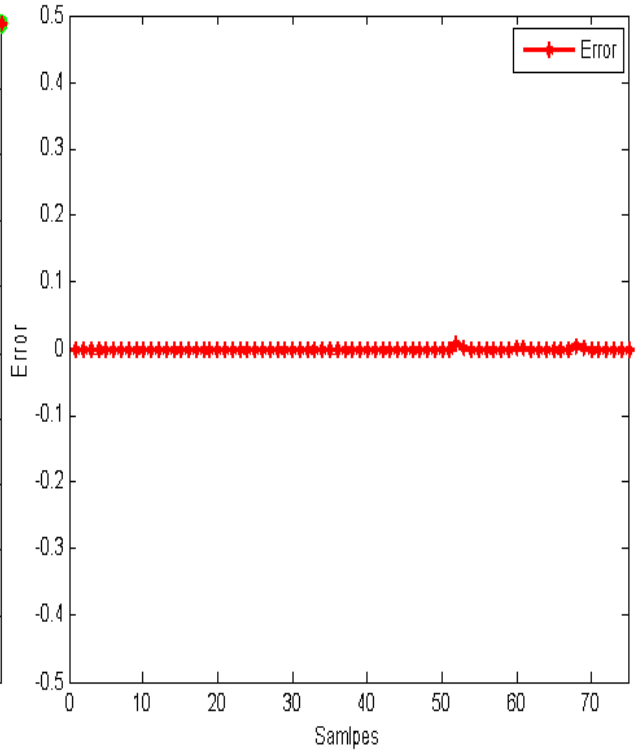

Fig.3.12 MLPNN Error for fault on phase C

3.3.1.2. Testing Results for MLPNN

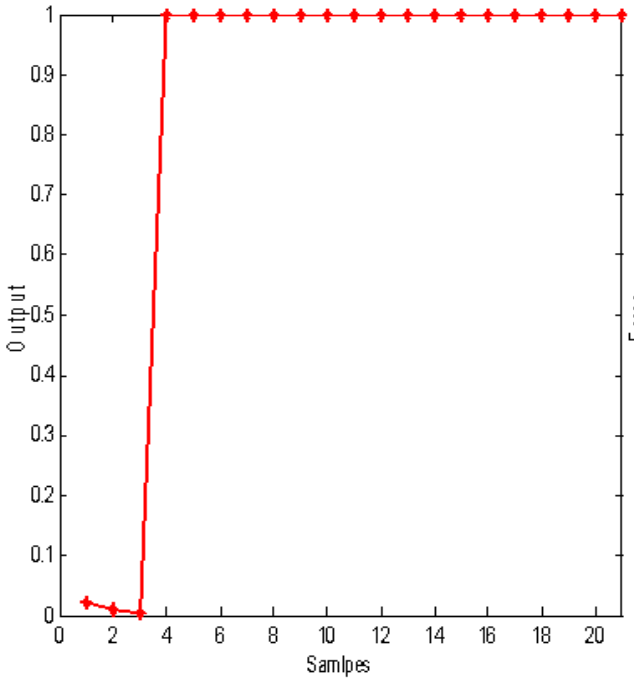

Fig.3.13 Test Output of phase A for fault on phase A

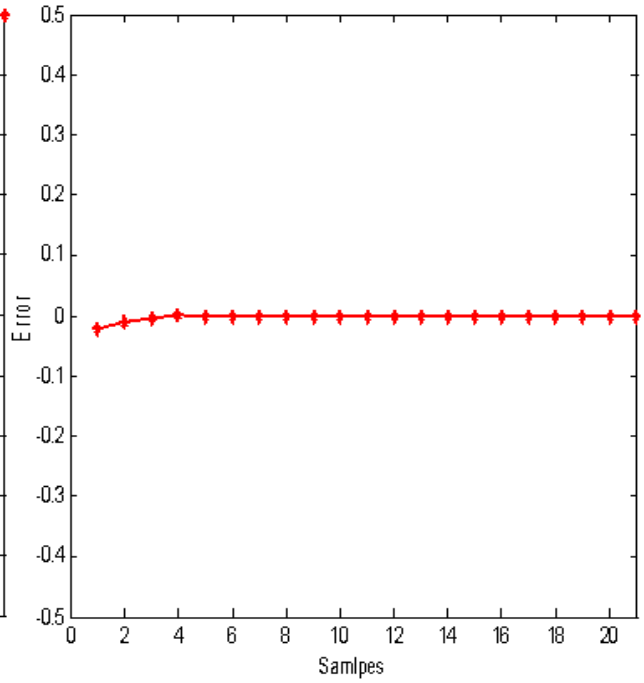

Fig.3.14 Test Error of phase A for fault on phase A

Figs. 3.13 and 3.14 show the MLPNN test output and error of phase A when an inter-turn fault occurs on phase A inside the stator of an induction motor. From Fig. 3.13 the MLPNN test output is nearly equal to zero for first three samples and is equal to one for the faulty condition from 4 to 21 samples with good accuracy. This means that the MLPNN is able to locate correctly the fault occurring on phase A. The testing error is 2.84×10^{-5} as shown in Fig.3.14.

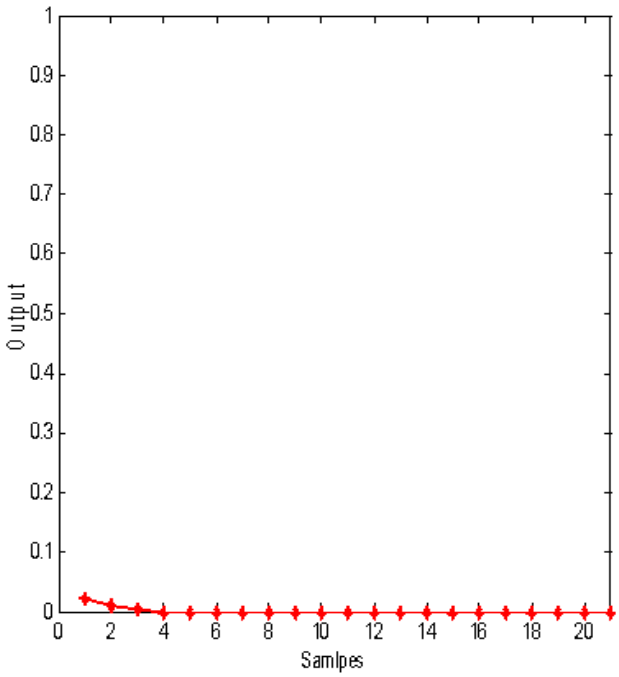

Fig.3.15. Test Output of phase B for fault on phase A

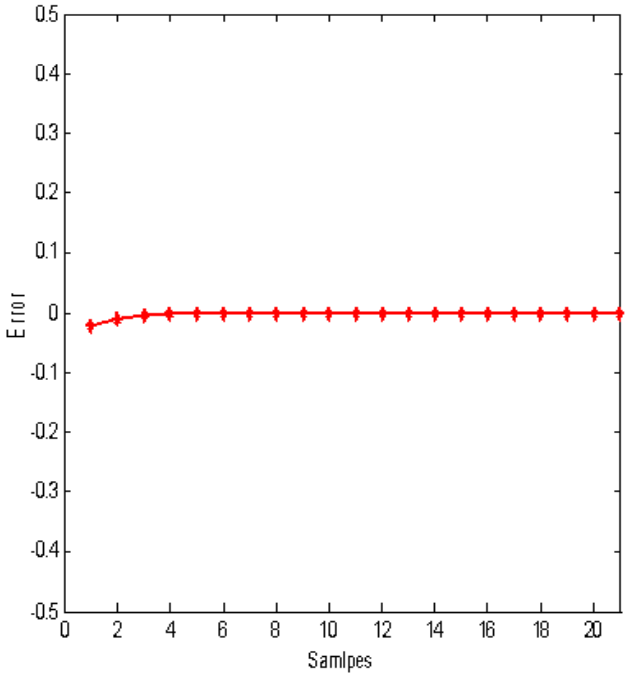

Fig.3.16. Test Error of phase B for fault on phase A

The MLPNN test output and error of phase B when an inter-turn short circuit fault occurs on phase A inside the stator of an induction motor as shown in Figs. 3.15 and 3.16. From Fig. 3.15 it is clear that the MLPNN well learn the test data with good accuracy. Hence the MLPNN is able to locate correctly the stator inter-turn short circuit fault occurring on phase A. The testing error is very low i.e 2.8297×10^{-5} as shown in Fig.3.16.

Figs. 3.17 and 3.18 show the MLPNN test output and test error of phase C when an inter-turn short circuit fault occurs on phase A inside the stator of an induction motor. Fig. 3.17 shows that the MLPNN well learn the test data and gives the test output with good accuracy. The testing error is 3.1063×10^{-5} as shown in Fig.3.18. Hence we conclude that the MLPNN is able to locate correctly the fault occurring on phase A.

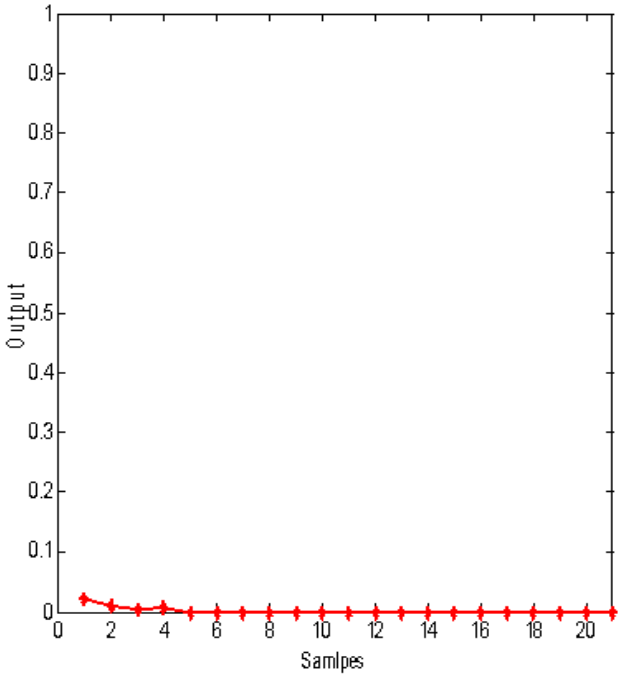

Fig.3.17. Test Output of phase C for fault on phase A

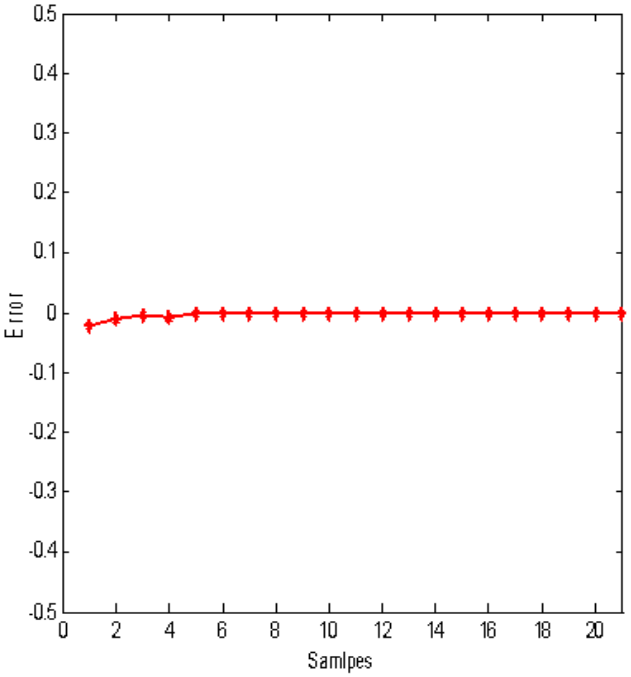

Fig.3.18. Test Error of phase C for fault on phase A

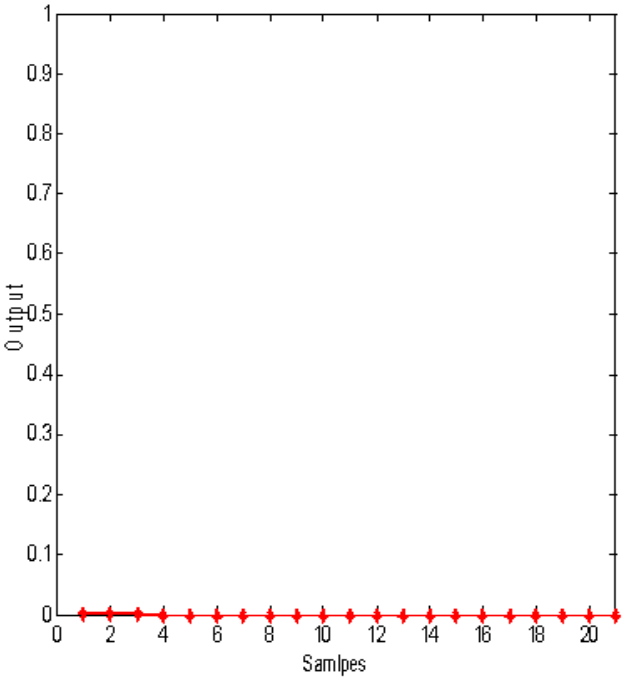

Fig.3.19. Test Output of phase A for fault on phase B

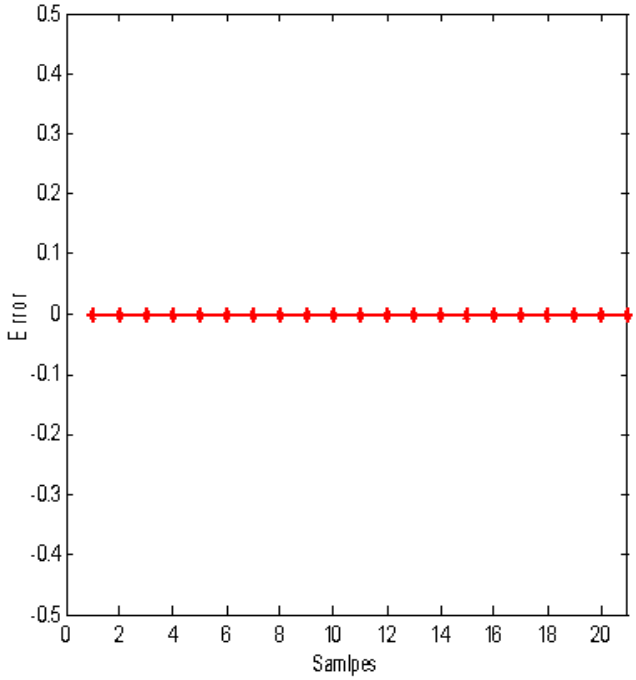

Fig.3.20. Test Error of phase A for fault on phase B

The MLPNN test output and test error of phase A when an inter-turn short circuit fault occurs on phase B inside the stator winding of an induction motor as shown in Figs. 3.19 and 3.20. From Fig. 3.19 it is clear that the MLPNN test output is equal to zero for all the samples with good

accuracy. The testing error for this case is very low i.e 4.9091×10^{-8} as shown in Fig.3.20. Hence the MLPNN is able to locate correctly the inter-turn short circuit fault on phase B.

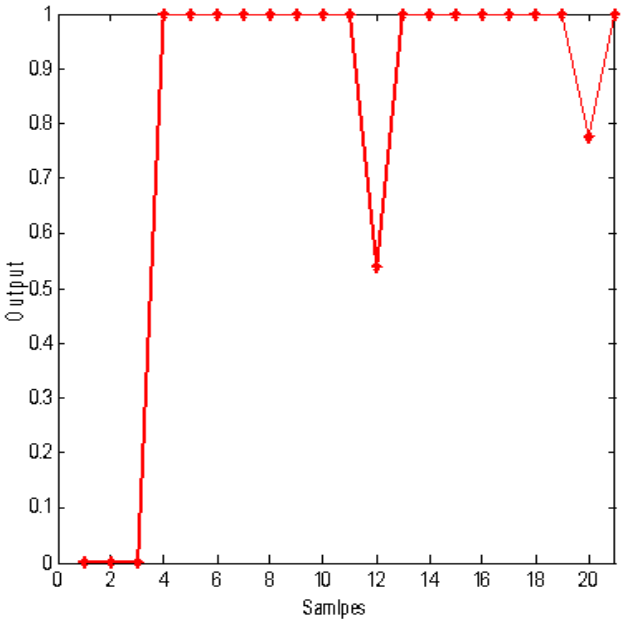

Fig.3.21. Test Output of phase B for fault on phase B

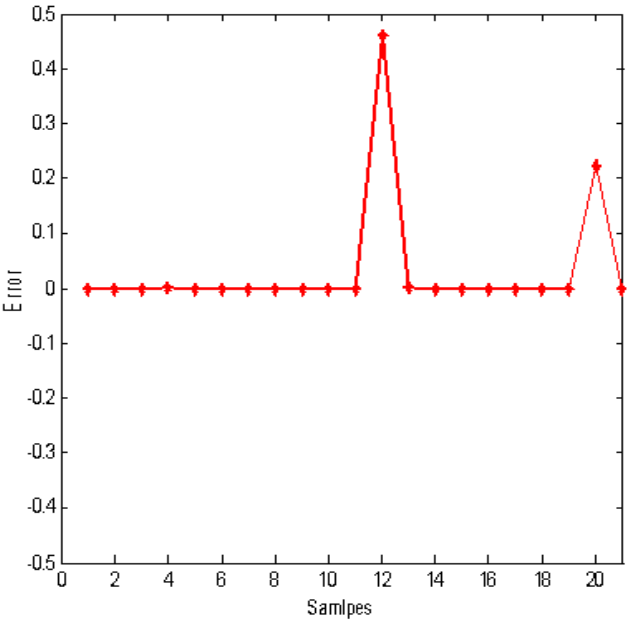

Fig.3.22. Test Error of phase B for fault on phase B

The MLPNN test output and error of phase B when an inter-turn short circuit fault occurs on phase B inside the stator of an induction motor as shown in Figs. 3.21 and 3.22. From Fig. 3.21 it is clear that the MLPNN not well learn the test data. The testing error is i.e 1.1900×10^{-2} as shown in Fig.3.22.

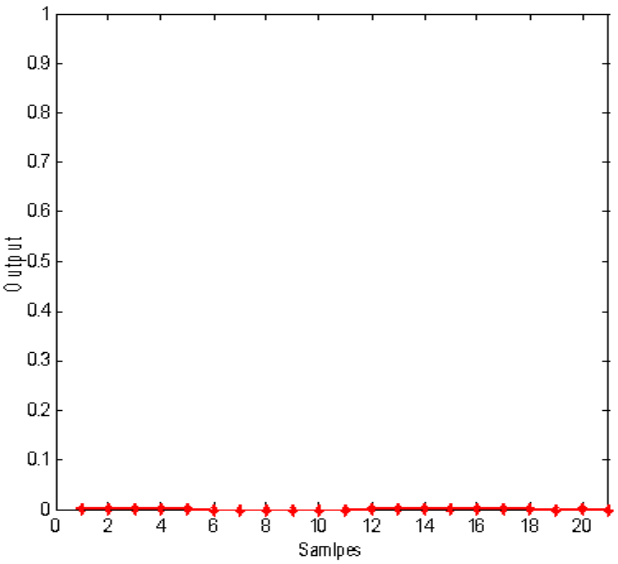

Fig.3.23. Test Output of phase C for fault on phase B

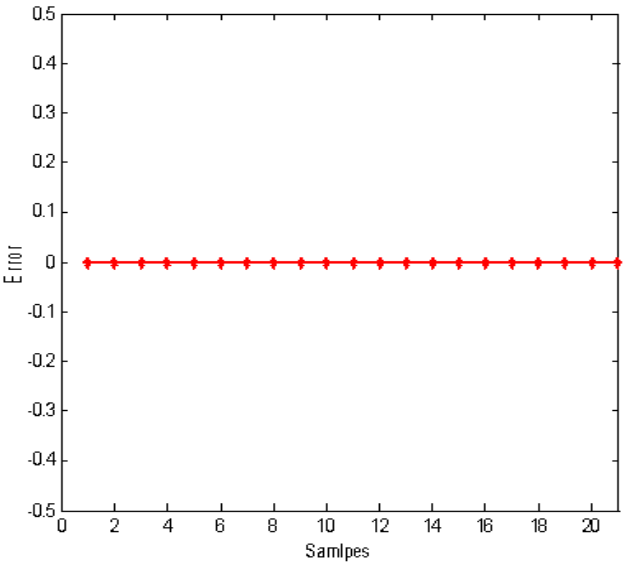

Fig.3.24. Test Error of phase C for fault on phase B

Figs. 3.23 and 3.24 show the MLPNN test output and error of phase C when an inter-turn fault occurs on phase B inside the stator of an induction motor. Fig. 3.23 shows the MLPNN well learn the test data and gives the test output is equal to zero for all samples with good accuracy. Hence the MLPNN is able to locate correctly the stator inter-turn fault occurring on phase B. From Fig 3.24 the testing error is 7.0909×10^{-8}.

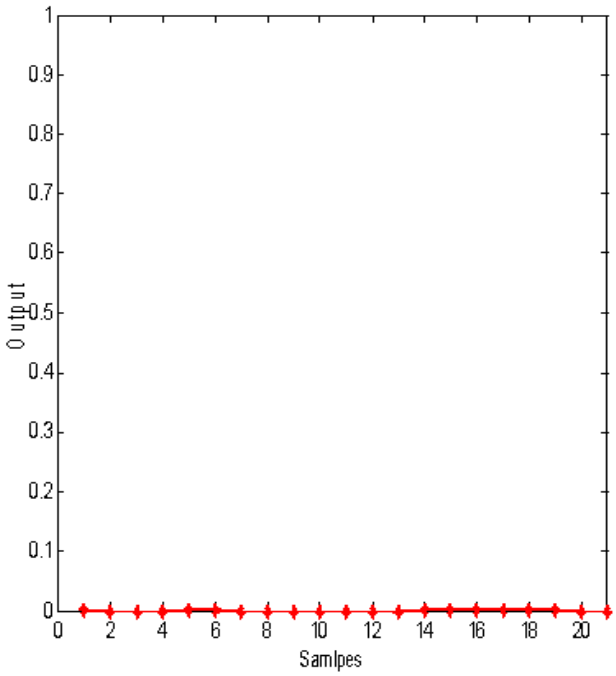

Fig.3.25. Test Output of phase A for fault on phase C

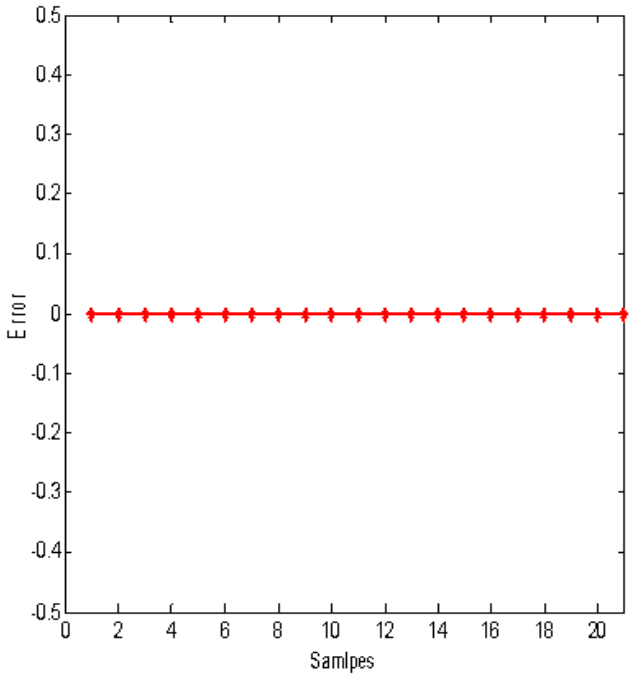

Fig.3.26. Test Error of phase A for fault on phase C

Figs. 3.25 and 3.26 show the MLPNN test output and test error of phase A when an inter-turn short circuit fault occurs on phase C inside the stator of an induction motor. Fig. 3.25 shows that the MLPNN well learn the test data and gives the test output with good accuracy. The testing error is 1.9227×10^{-7} as shown in Fig.3.26. Hence we conclude that the MLPNN is able to locate correctly the fault occurring on phase C.

Figs. 3.27 and 3.28 show the MLPNN test output and test error of phase B when an inter-turn short circuit fault occurs on phase C inside the stator of an induction motor. The MLPNN well learn the test data and gives the test output with good accuracy as shown in Fig. 3.27. The testing error is very low i.e 4.5455×10^{-8} as shown in Fig.3.28. Hence we conclude that the MLPNN is able to locate correctly the stator inter-turn short circuit fault occurring on phase C.

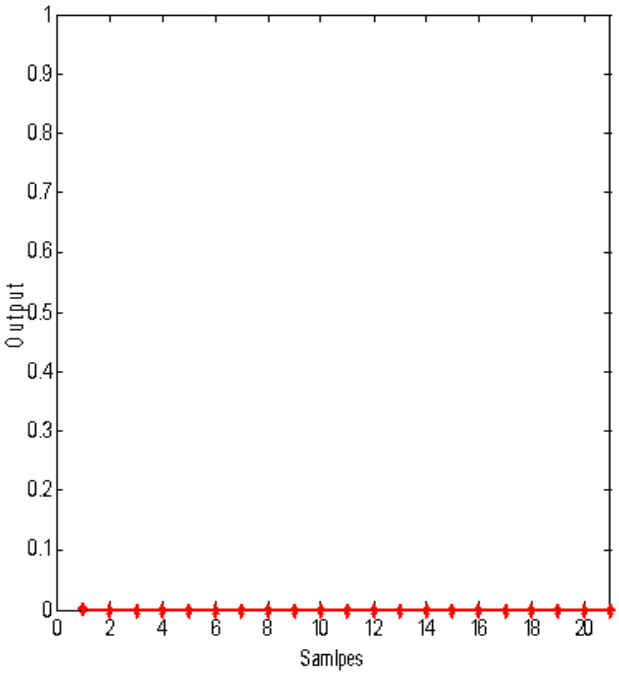

Fig.3.27. Test Output of phase B for fault on phase C

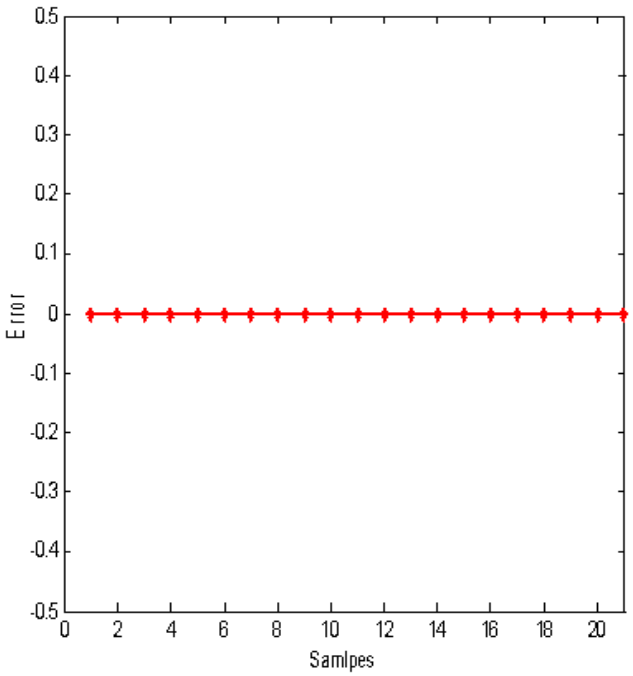

Fig.3.28. Test Error of phase B for fault on phase C

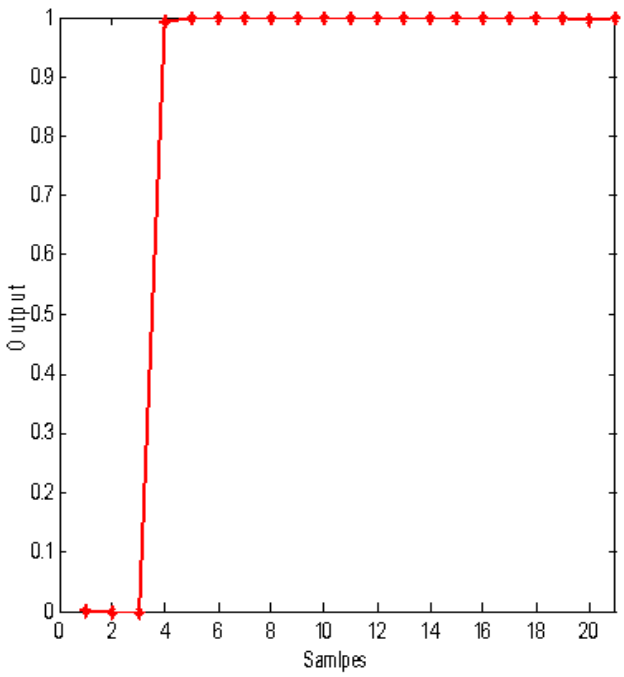

Fig.3.29. Test Output of phase C for fault on phase C

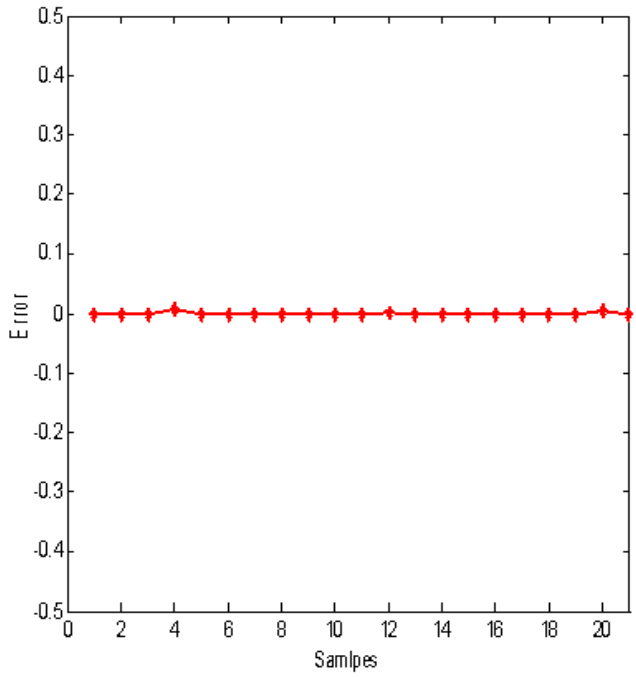

Fig.3.30. Test Error of phase C for fault on phase C

Figs. 3.29 and 3.30 show the MLPNN test output and test error of phase C when an inter-turn short circuit fault occurs on phase C inside the stator winding of an induction motor. From Fig. 3.29 MLPNN test output is equal to zero for first three samples and is equal to one for the faulty

condition from 4 to 21 samples with good accuracy. Fig.3.29 shows that the MLPNN is able to locate correctly the fault occurring on phase C. The testing error is 2.9314×10^{-6} as shown in Fig.3.30.

3.3.2 Fault Detection Performance of RNN

3.3.2.1 Training Results for RNN

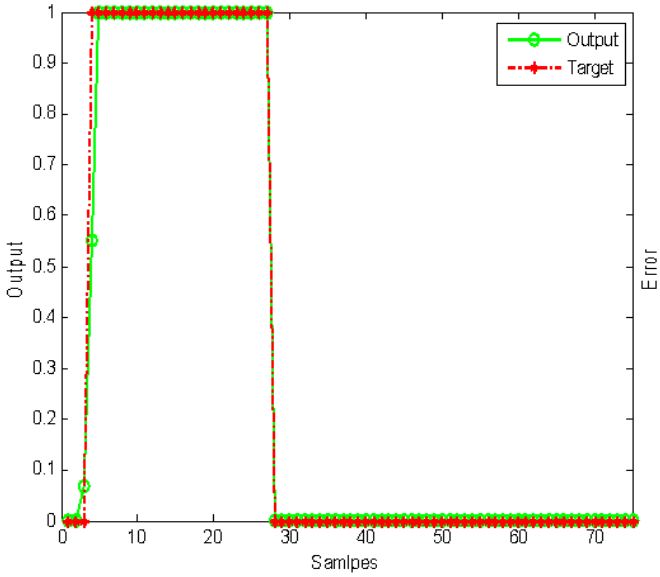

Fig.3.31 RNN Output for fault on phase A

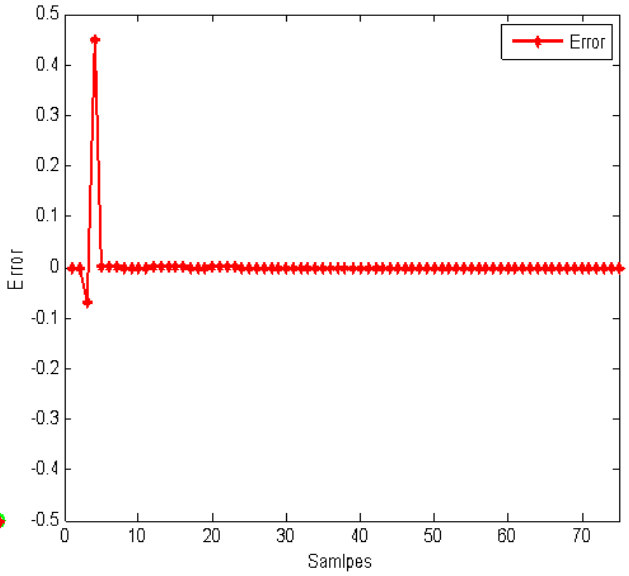

Fig.3.32 RNN Error for fault on phase A

Figs.3.31 and 3.32 show the RNN output and error when a stator inter-turn short circuit fault occurs on phase A of an induction motor respectively. Fig.3.31 shows that the output of the RNN from which the star one is the target value (either 0 or 1 for healthy and inter-turn faulty condition respectively) and the circle one is the output of the RNN. When a stator inter-turn fault occurs on phase A, then the output of that phase is one and others are zero. Fig. 3.31 shows that the RNN has well learned the input data and correctly reproduced the desired output. Hence, the error which is the difference between the target value and the actual output is 2.7000×10^{-3} as shown in Fig.3.32.

The RNN output and error when a stator inter-turn short circuit fault occurs on phase B of an induction motor respectively as shown in Figs.3.33 and 3.34. Fig.3.33 shows that the output of the RNN from which the star one is the target value (either 0 or 1 for healthy and inter-turn faulty condition respectively) and the circle one is the output of the RNN. From Fig. 3.33 it is

clear that the MLPNN has properly learned the input data Hence, the error which is the difference between the target value and the actual output is 5.6651×10^{-4} as shown in Fig.3.34.

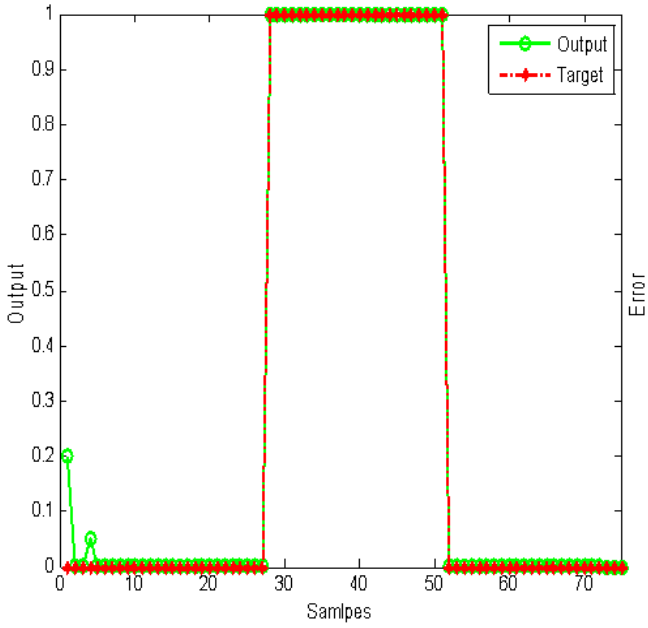

Fig.3.33 RNN Output for fault on phase B

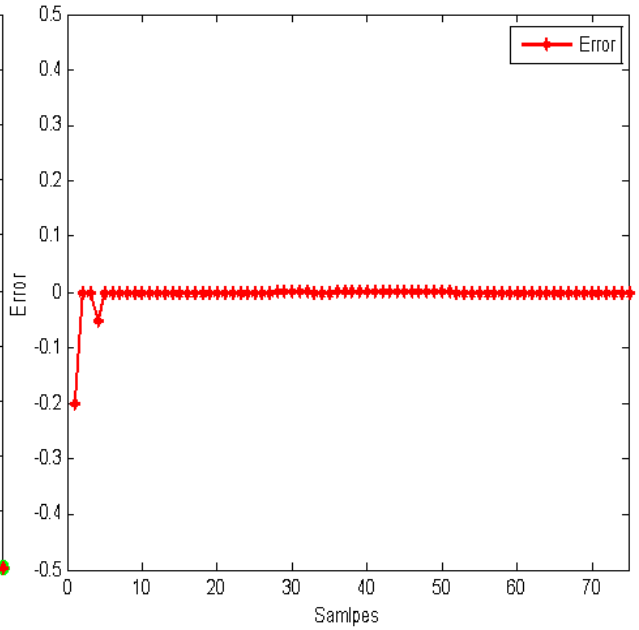

Fig.3.34 RNN Error for fault on phase B

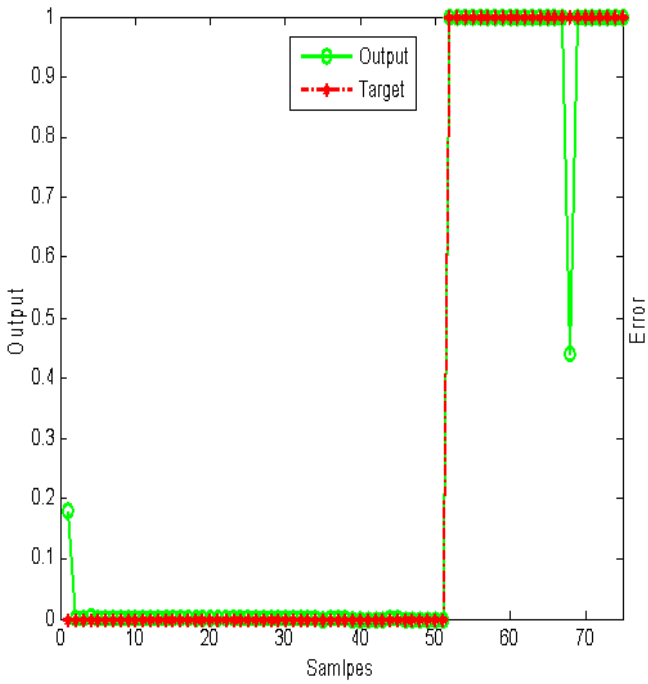

Fig.3.35 RNN Output for fault on phase C

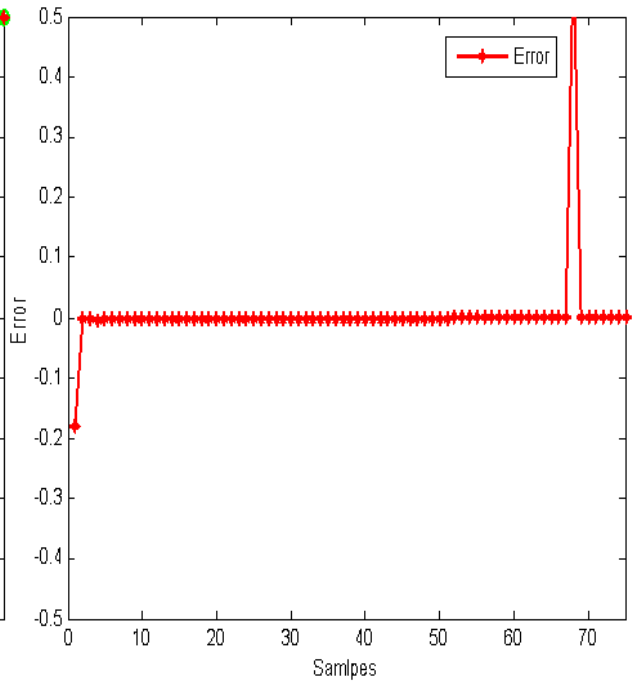

Fig.3.36 RNN Error for fault on phase C

Figs.3.35 and 3.36 show that the RNN output and error when a stator inter-turn short circuit fault occurs on phase C of an induction motor respectively. The target output (either 0 or 1 for healthy

and inter-turn faulty condition respectively) of the RNN i.e the star one and the circle one is the actual output of the RNN as shown in Fig. 3.35. When a stator inter-turn fault occurs on phase C then the output of that phase is one and others are zero. From Fig. 3.35 it is clear that the RNN has not well learned the input data. The error which is the difference between the target value and the actual output is 4.6000×10^{-3} as shown in Fig.3.36.

3.3.2.2 Testing Results for RNN

Figs. 3.37 and 3.38 show the RNN test output and error of phase A when an inter-turn fault occurs on phase A inside the stator of an induction motor. From Fig. 3.37 the RNN test output is nearly equal to zero for first three samples and is equal to one for the faulty condition from 4 to 21 samples with good accuracy. This shows that the RNN is able to locate correctly the fault occurring on phase A. The testing error is 2.1089×10^{-4} as shown in Fig.3.38.

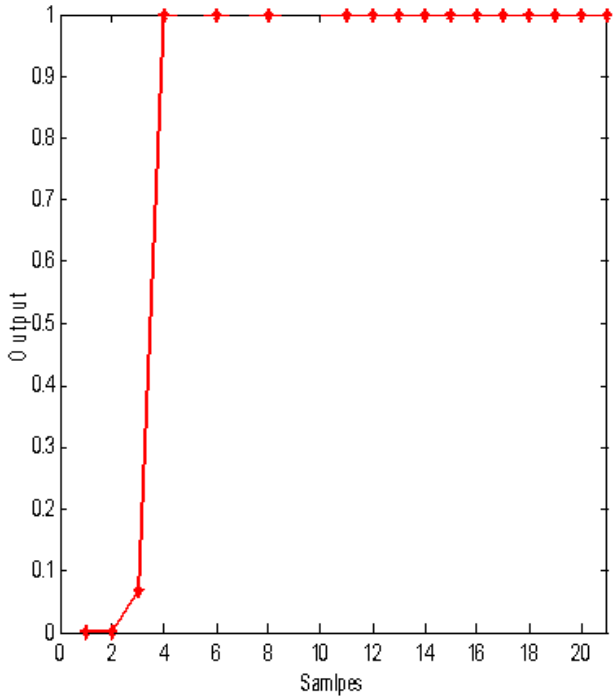

Fig.3.37 Test Output of phase A for fault on phase A

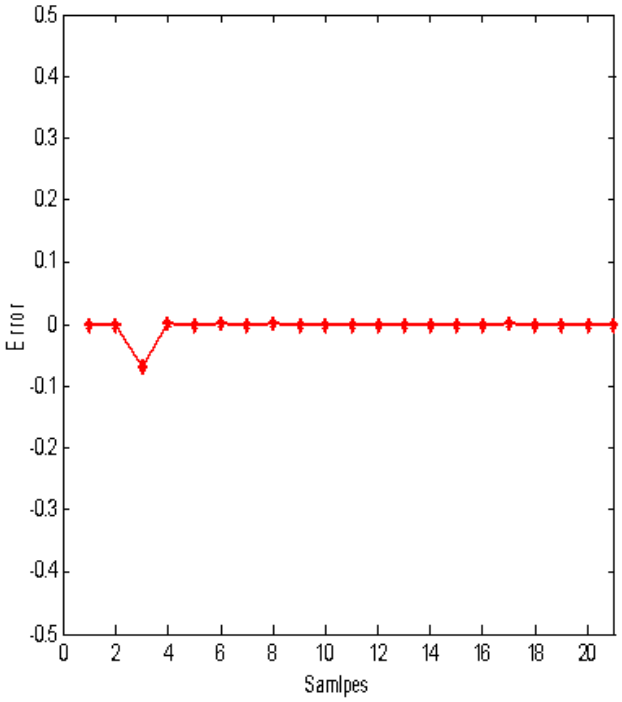

Fig.3.38 Test Error of phase A for fault on phase A

The RNN test output and error of phase B when an inter-turn short circuit fault occurs on phase A inside the stator of an induction motor as shown in Figs. 3.39 and 3.40. From Fig. 3.39 it is clear that the RNN well learn the test data with good accuracy. Hence the RNN is able to locate

correctly the stator inter-turn short circuit fault occurring on phase A. The testing error is very low i.e 2.1083×10^{-4} as shown in Fig.3.40.

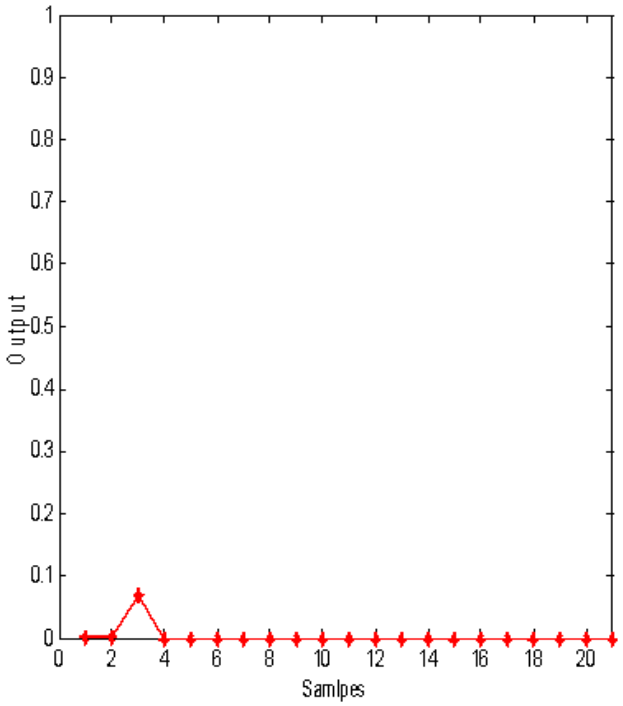

Fig.3.39 Test Output of phase B for fault on phase A

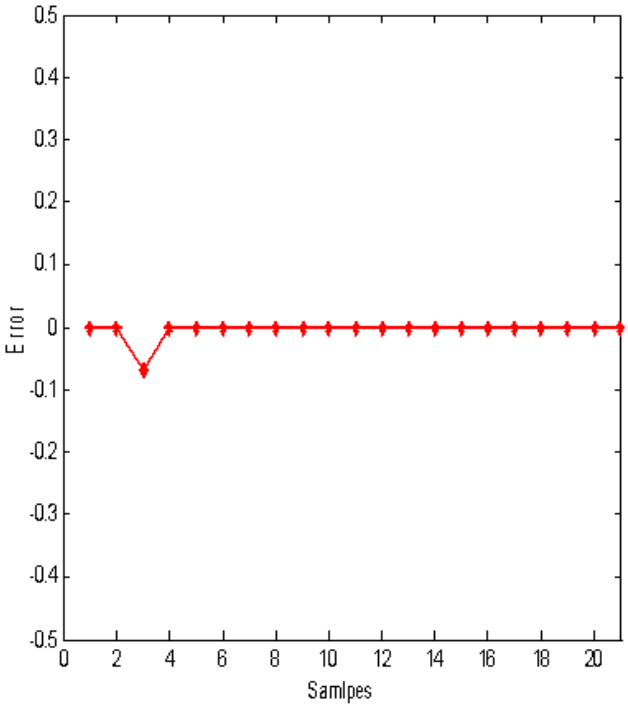

Fig.3.40 Test Error of phase B for fault on phase A

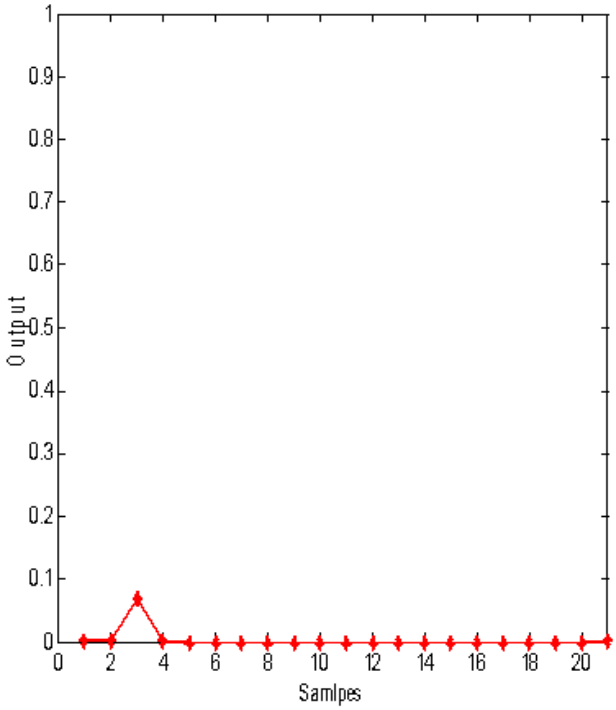

Fig.3.41 Test Output of phase C for fault on phase A

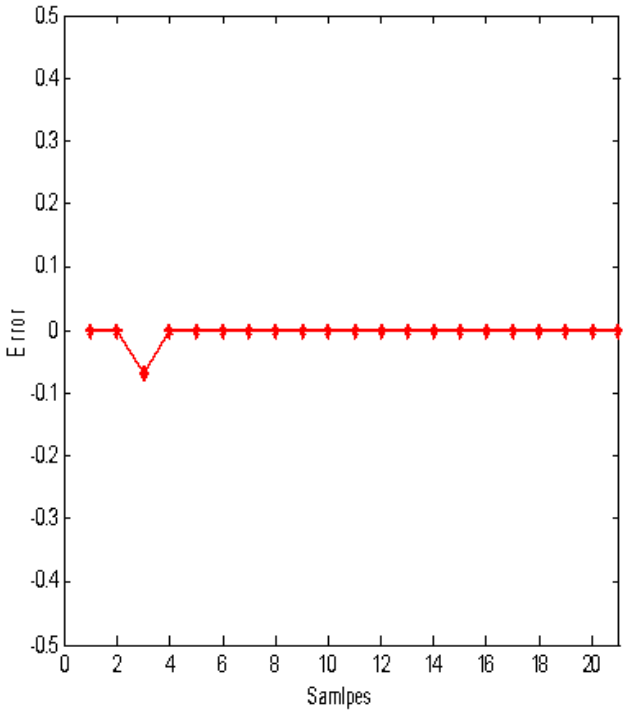

Fig.3.42 Test Error of phase C for fault on phase A

Figs. 3.41 and 3.42 show the RNN test output and test error of phase C when an inter-turn short circuit fault occurs on phase A inside the stator of an induction motor. Fig. 3.41 shows that the RNN well learn the test data and gives the test output with good accuracy. The testing error is 2.1083×10^{-4} as shown in Fig.3.42. Hence we conclude that the RNN is able to locate correctly the fault occurring on phase A.

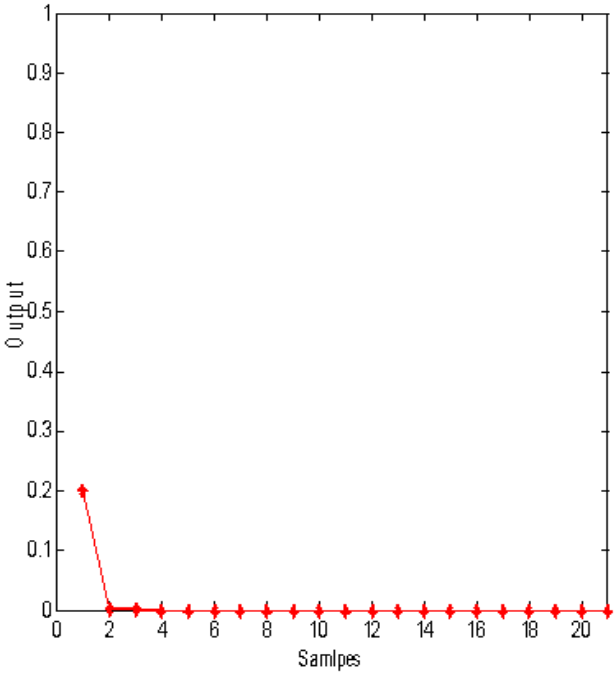

Fig.3.43 Test Output of phase A for fault on phase B

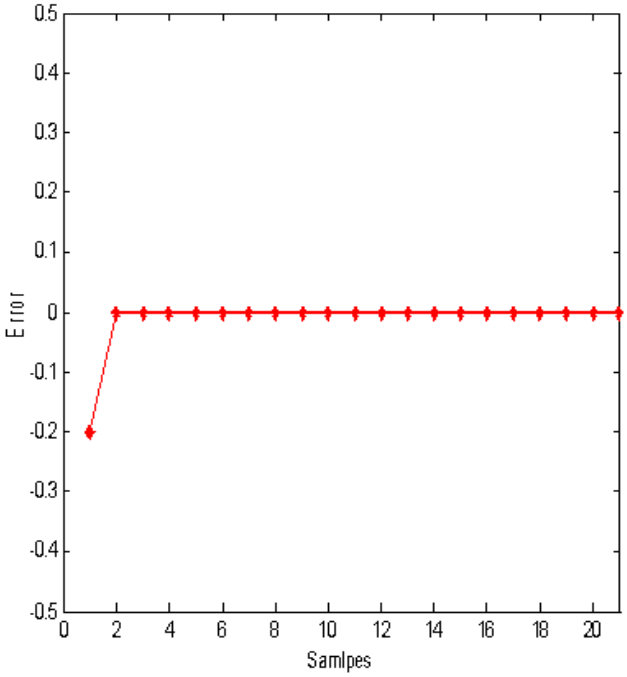

Fig.3.44 Test Error of phase A for fault on phase B

The RNN test output and test error of phase A when an inter-turn short circuit fault occurs on phase B inside the stator winding of an induction motor as shown in Figs. 3.43 and 3.44. From Fig. 3.43 it is clear that the RNN well learn the test data. The testing error for this case is very low i.e 1.8000×10^{-3} as shown in Fig.3.44. Hence the RNN is able to locate correctly the inter-turn short circuit fault on phase B.

The RNN test output and error of phase B when an inter-turn short circuit fault occurs on phase B inside the stator winding of an induction motor as shown in Figs. 3.45 and 3.46. From Fig. 3.45 it is clear that the RNN is able to learn the test data. The testing error is 1.8000×10^{-3} as shown in Fig.3.46.

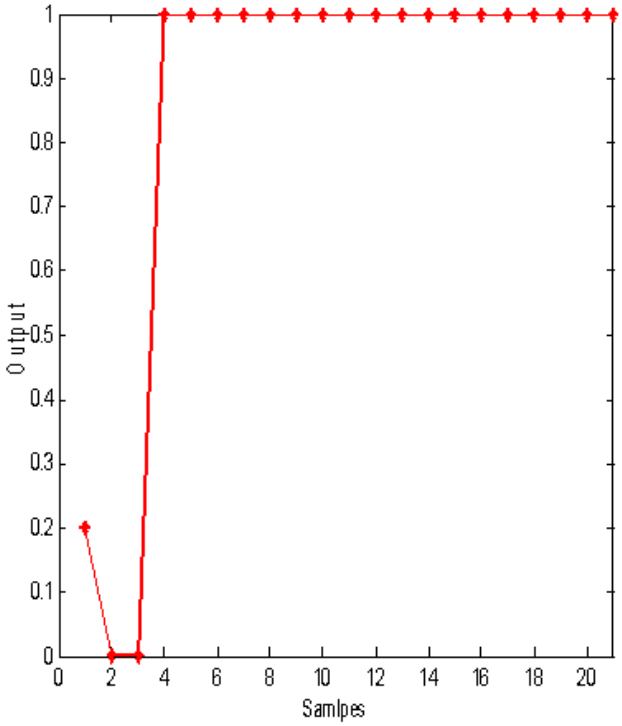

Fig.3.45 Test Output of phase B for fault on phase B

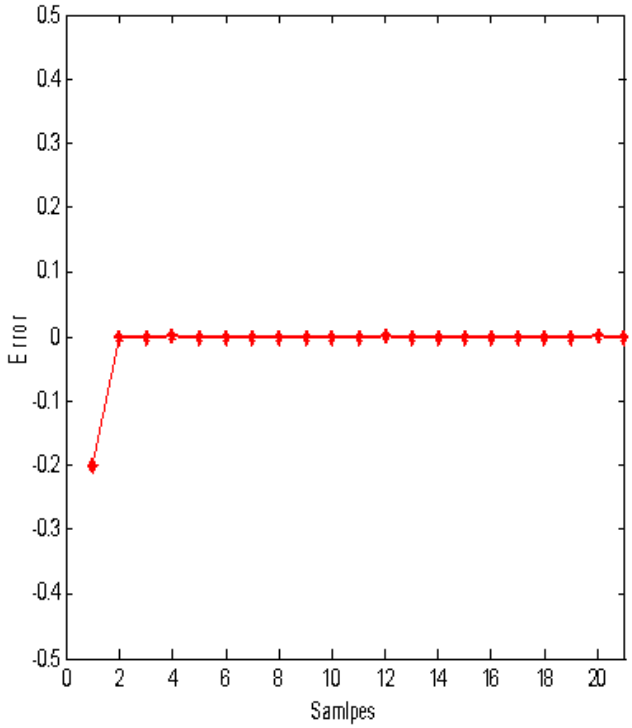

Fig.3.46 Test Error of phase B for fault on phase B

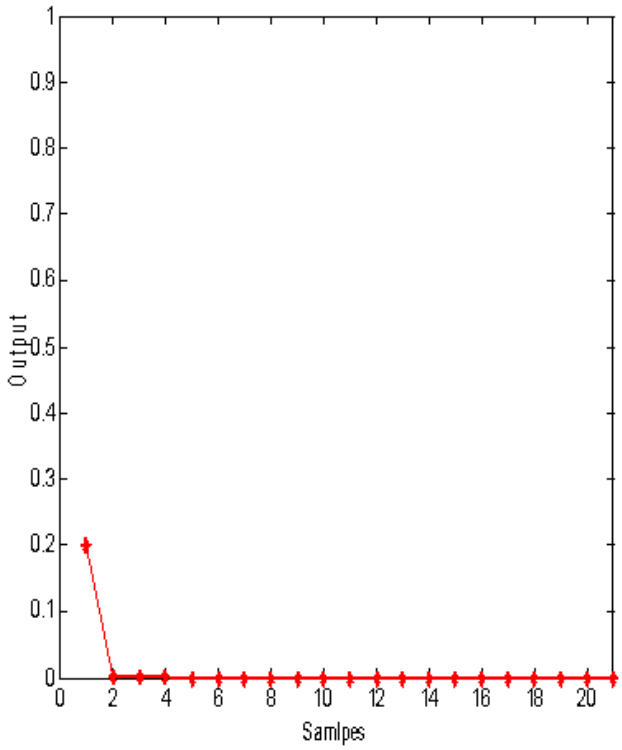

Fig.3.47 Test Output of phase C for fault on phase B

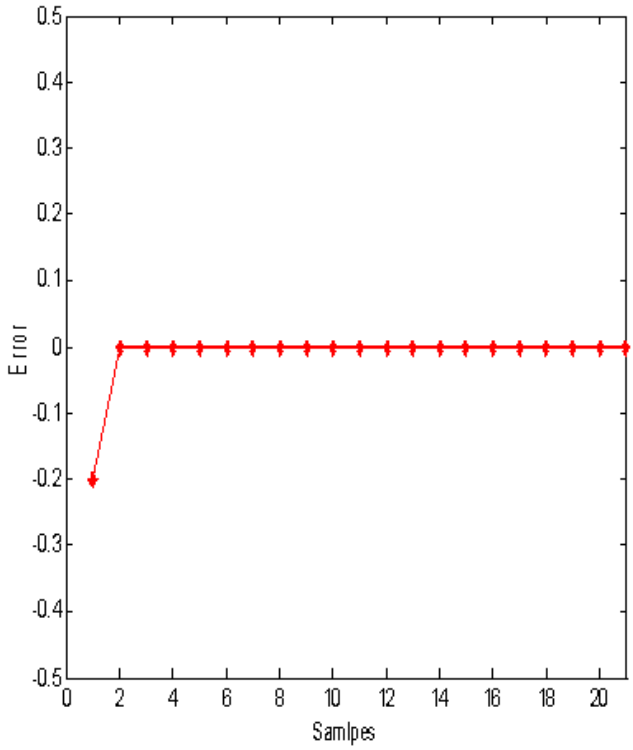

Fig.3.48 Test Error of phase C for fault on phase B

Figs. 3.47 and 3.48 show the RNN test output and error of phase C when an inter-turn fault occurs on phase B inside the stator of an induction motor. Fig. 3.47 shows the RNN well learn the test data and gives the test output is equal to zero for all samples expect one sample. Hence the RNN is able to locate correctly the stator inter-turn fault occurring on phase B. From Fig 3.48 the testing error is 1.8000×10^{-3}.

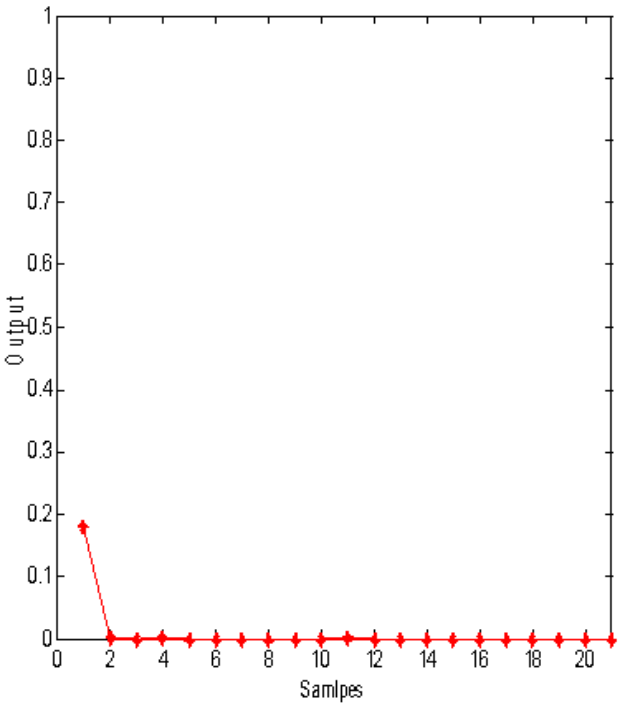

Fig.3.49 Test Output of phase A for fault on phase C

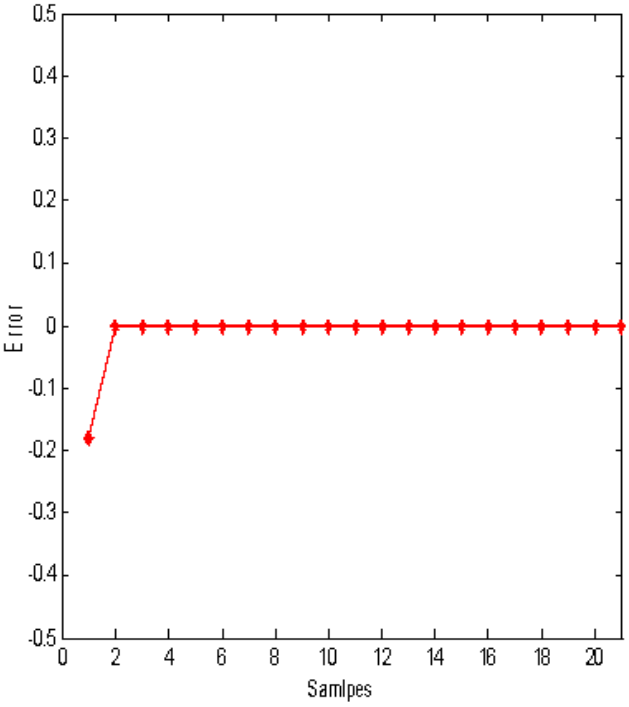

Fig.3.50 Test Error of phase A for fault on phase C

Figs. 3.49 and 3.50 show the RNN test output and test error of phase A when an inter-turn short circuit fault occurs on phase C inside the stator of an induction motor. Fig. 3.49 shows that the RNN well learn the test data and gives the test output with good accuracy. The testing error is 1.5000×10^{-3} as shown in Fig.3.50. Hence we conclude that the RNN is able to locate correctly the fault occurring on phase C.

Figs. 3.51 and 3.52 show the RNN test output and test error of phase B when an inter-turn short circuit fault occurs on phase C inside the stator of an induction motor. The RNN well learn the test data and gives the test output with good accuracy as shown in Fig. 3.51. The testing error is 1.5000×10^{-3} as shown in Fig.3.52. Hence we conclude that the RNN is able to locate correctly the stator inter-turn short circuit fault occurring on the stator C phase.

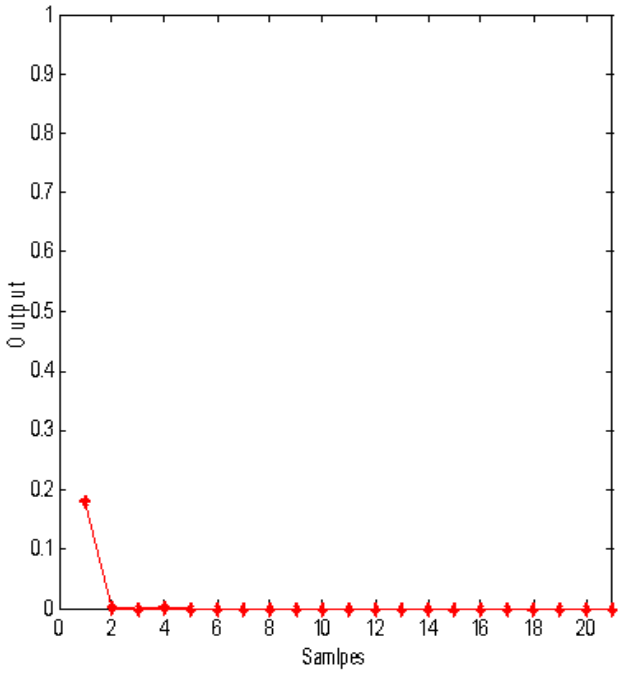

Fig.3.51 Test Output of phase B for fault on phase C

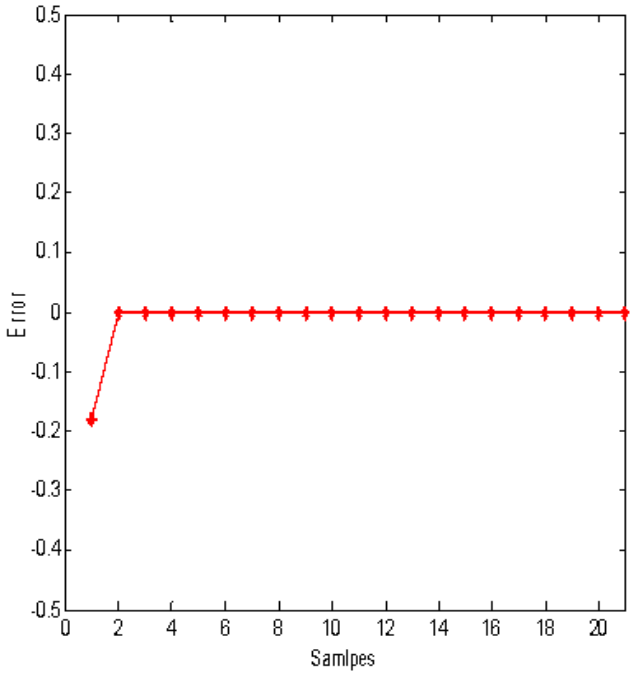

Fig.3.52 Test Error of phase B for fault on phase C

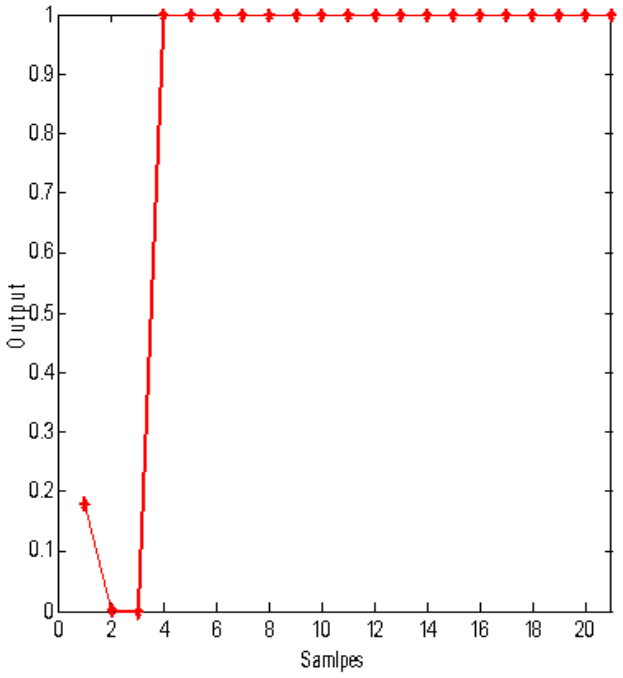

Fig.3.53 Test Output of phase C for fault on phase C

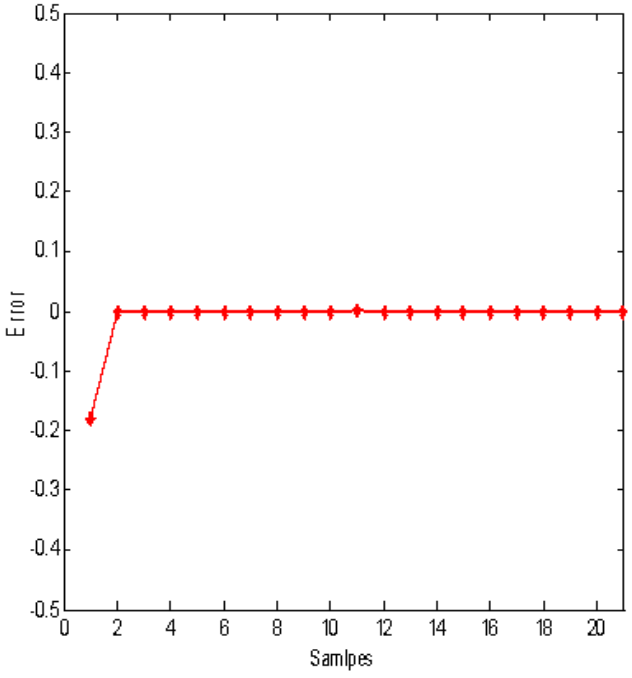

Fig.3.54 Test Error of phase C for fault on phase C

Figs. 3.53 and 3.54 show the RNN test output and test error of phase C when an inter-turn short circuit fault occurs on phase C inside the stator winding of an induction motor. From Fig. 3.53 it

is clear that the RNN is able to learn the test data. Fig.3.54 shows that the RNN is able to locate correctly the fault occurring on phase C. The testing error is 1.5000×10^{-3} as shown in Fig.3.54.

3.3.3 Fault Detection Performance using RBFNN

3.3.3.1 Training Results for RBFNN

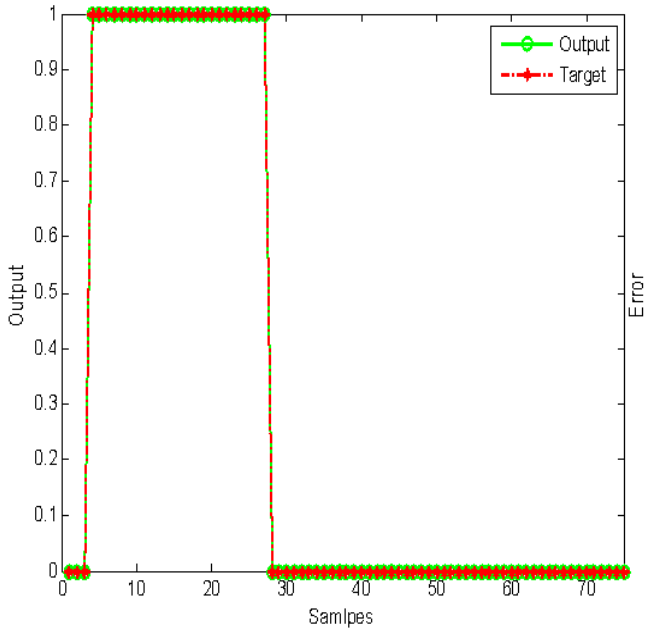

Fig.3.55 RBFNN Output for fault on phase A

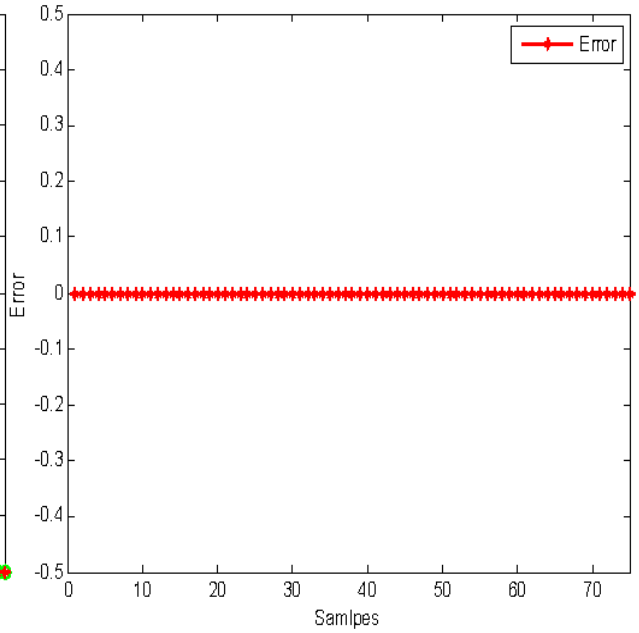

Fig.3.56 RBFNN Error for fault on phase A

Figs.3.55 and 3.56 show the RBFNN output and error when a stator inter-turn short circuit fault occurs on phase A of an induction motor respectively. Fig.3.55 shows that the output of the RBFNN from which the star one is the target value (either 0 or 1 for healthy and inter-turn faulty condition respectively) and the circle one is the output of the RBFNN. When a stator inter-turn fault occurs on phase A, then the output of that phase is one and others are zero. From Fig. 3.55 it is clear that the RBFNN has well learned the input data and correctly reproduced the desired output. Hence, the error which is the difference between the target value and the actual output is very small i.e 7.6403×10^{-7} as shown in Fig.3.56.

The RBFNN output and error when a stator inter-turn short circuit fault occurs on phase B of an induction motor respectively as shown in Figs.3.57 and 3.58. Fig.3.57 shows that the output of the RBFNN from which the star one is the target value (either 0 or 1 for healthy and inter-turn faulty condition respectively) and the circle one is the output of the RBFNN. From Fig. 3.57 it is

clear that the RBFNN has properly learned the input data. Hence, the error which is the difference between the target value and the actual output is 6.5409×10^{-7} as shown in Fig.3.58.

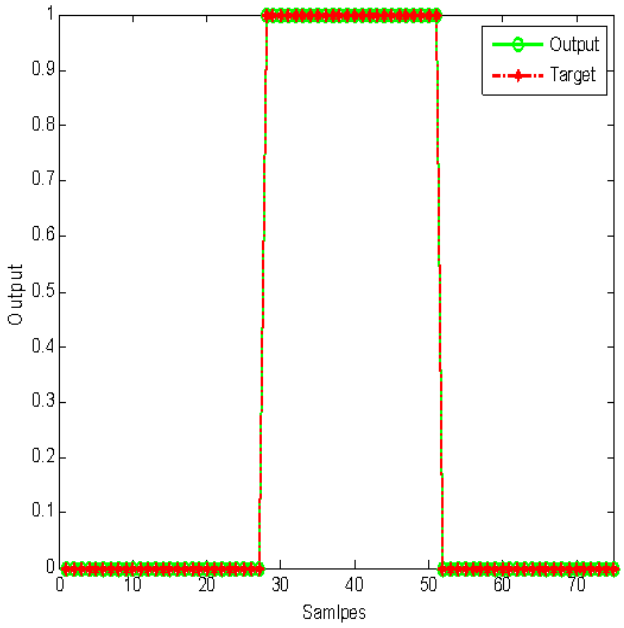

Fig.3.57 RBFNN Output for fault on phase B

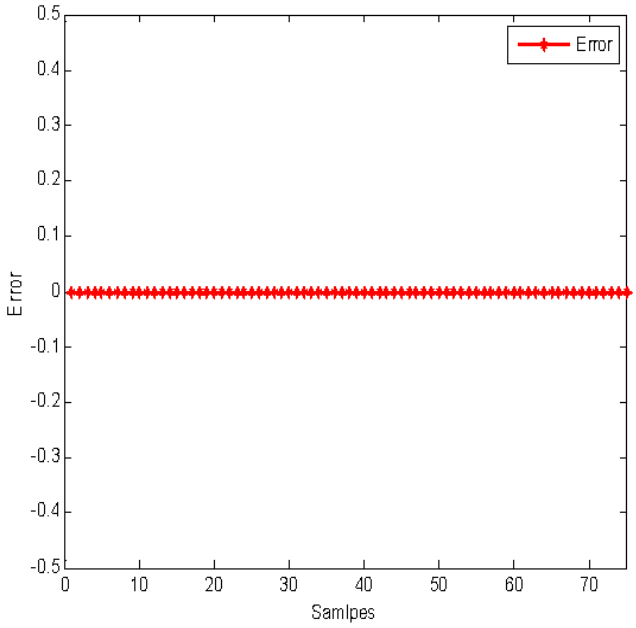

Fig.3.58 RBFNN Error for fault on phase B

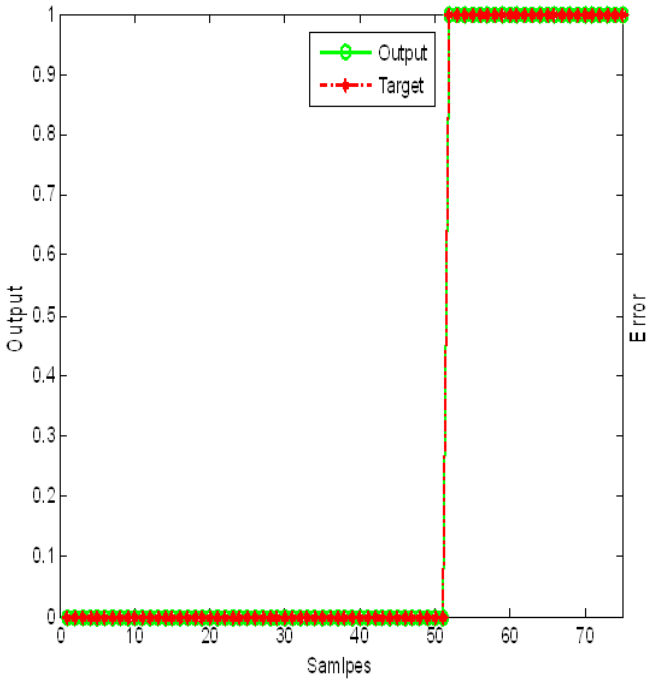

Fig.3.59 RBFNN Output for fault on phase C

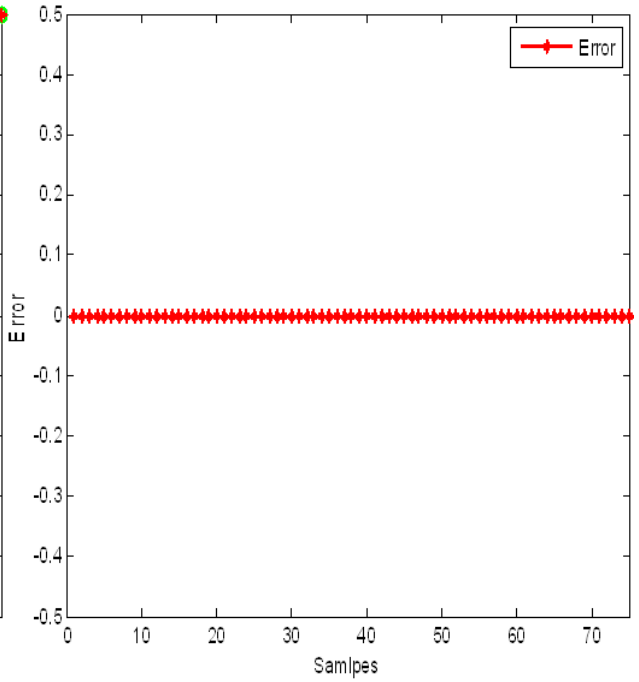

Fig.3.60 RBFNN Error for fault on phase C

Figs.3.59 and 3.60 show that the RBFNN output and error when a stator inter-turn short circuit fault occurs on phase C of an induction motor respectively. The target output (either 0 or 1 for

healthy and inter-turn faulty condition respectively) of the RBFNN i.e the star one and the circle one is the actual output of the RBFNN as shown in Fig. 3.59. When a stator inter-turn fault occurs on phase C then the output of that phase is one and others are zero. From Fig. 3.59 it is clear that the RBFNN has well learned the input data and correctly reproduced the desired output. The error which is the difference between the target value and the actual output is 1.7904×10^{-7} as shown in Fig.3.60.

3.3.3.2 Testing Results for RBFNN

Figs. 3.61 and 3.62 show the RBFNN test output and error of phase A when an inter-turn fault occurs on phase A inside the stator of an induction motor. From Fig. 3.61 the RBFNN test output is equal to zero for first three samples and is equal to one for the faulty condition from 4 to 21 samples with good accuracy. This shows that the RBFNN is able to locate correctly the fault occurring on phase A. The testing error is 5.2727×10^{-7} as shown in Fig.3.62.

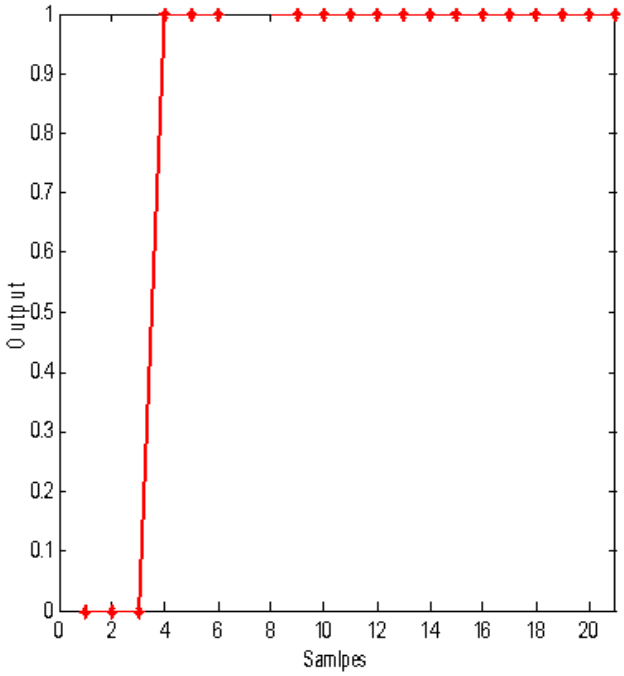

Fig.3.61 Test Output of phase A for fault on phase A

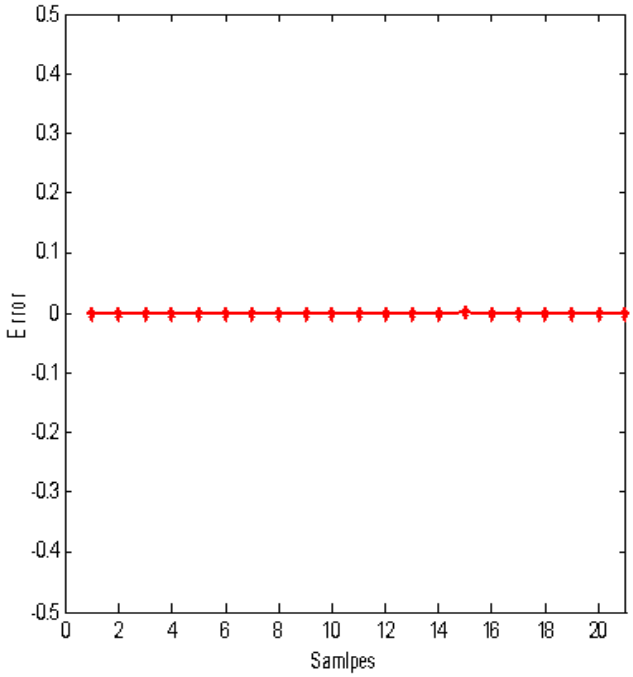

Fig.3.62 Test Error of phase A for fault on phase A

The RBFNN test output and error of phase B when an inter-turn short circuit fault occurs on phase A inside the stator of an induction motor as shown in Figs. 3.63 and 3.64. From Fig. 3.63 it is clear that the RBFNN well learn the test data with good accuracy. Hence the RBFNN is able to

locate correctly the stator inter-turn short circuit fault occurring on A phase. The testing error is very low i.e 4.0955×10^{-7} as shown in Fig.3.64.

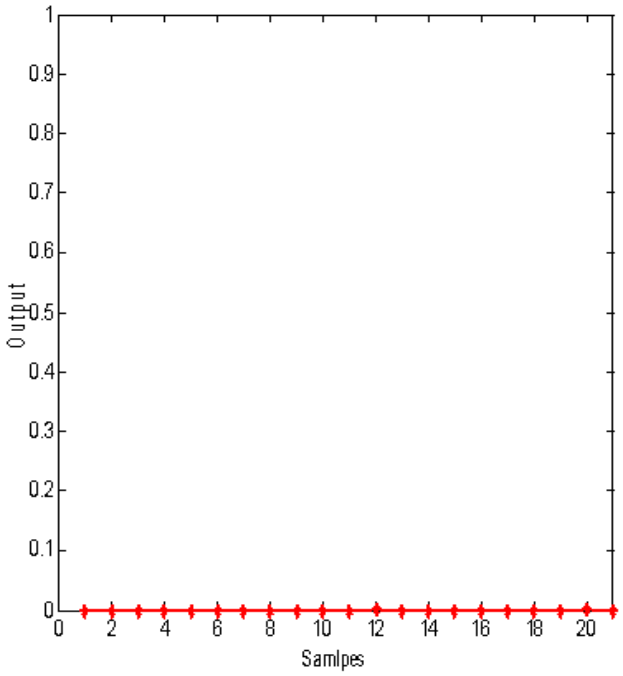

Fig.3.63 Test Output of phase B for fault on phase A

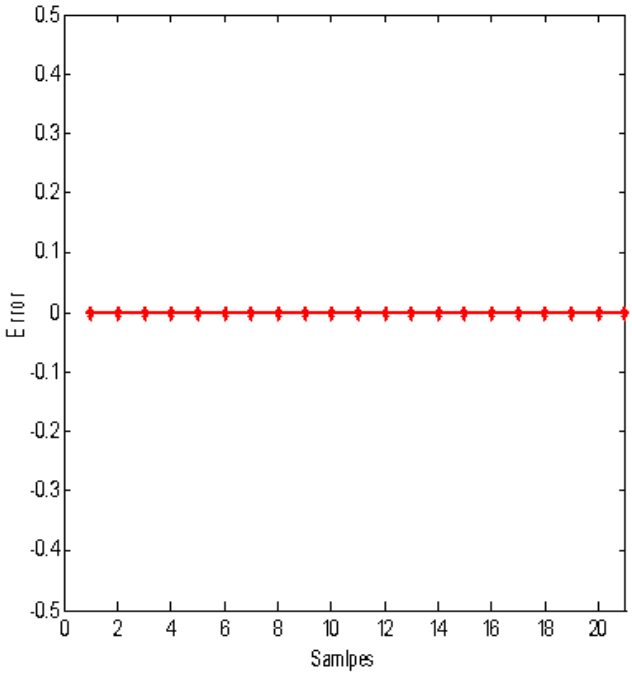

Fig.3.64 Test Error of phase B for fault on phase A

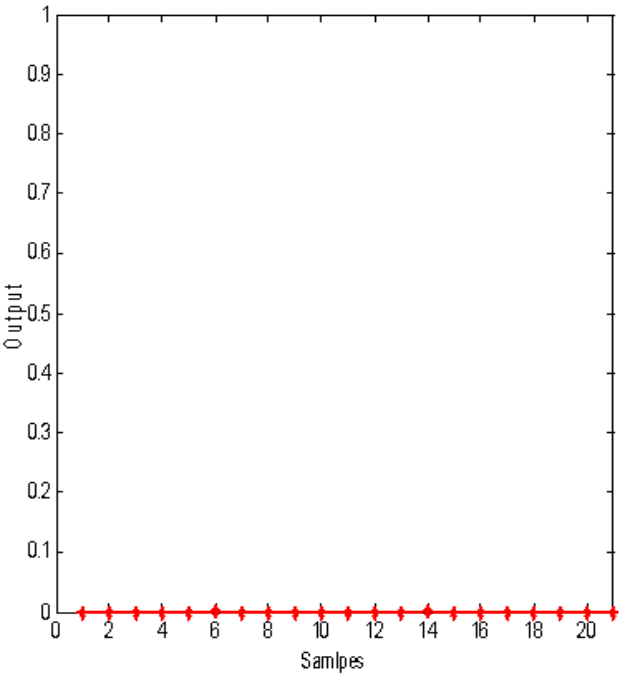

Fig.3.65 Test Output of phase C for fault on phase A

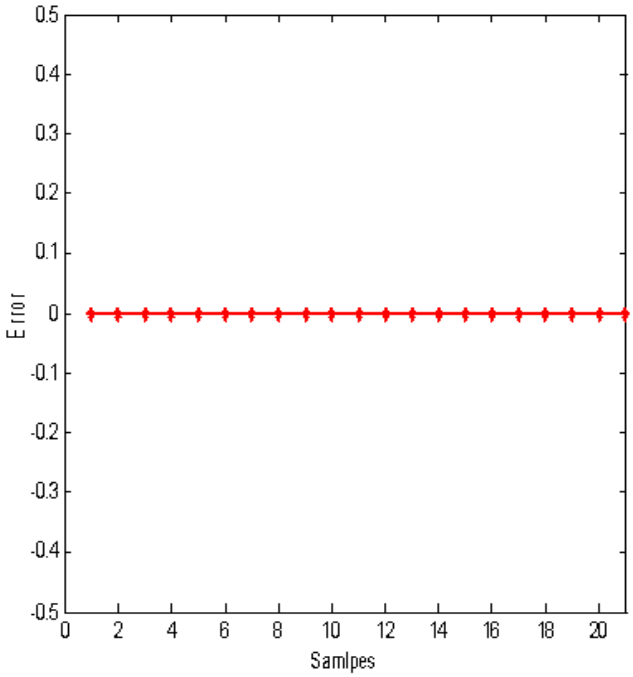

Fig.3.66 Test Error of phase C for fault on phase A

Figs. 3.65 and 3.66 show the RBFNN test output and test error of phase C when an inter-turn short circuit fault occurs on phase A inside the stator of an induction motor. Fig. 3.65 shows that the RBFNN well learn the test data and gives the test output with good accuracy. The testing error is 2.2727×10^{-7} as shown in Fig.3.66. Hence we conclude that the RBFNN is able to locate correctly the fault occurring on phase A.

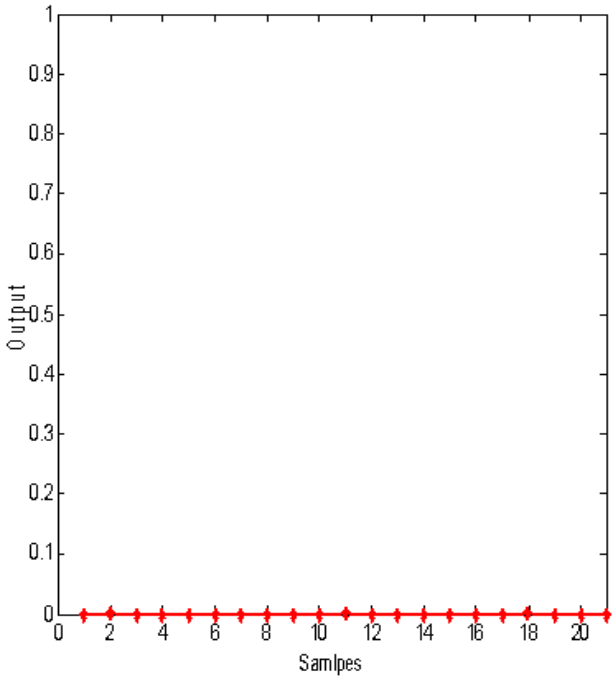

Fig.3.67 Test Output of phase A for fault on phase B

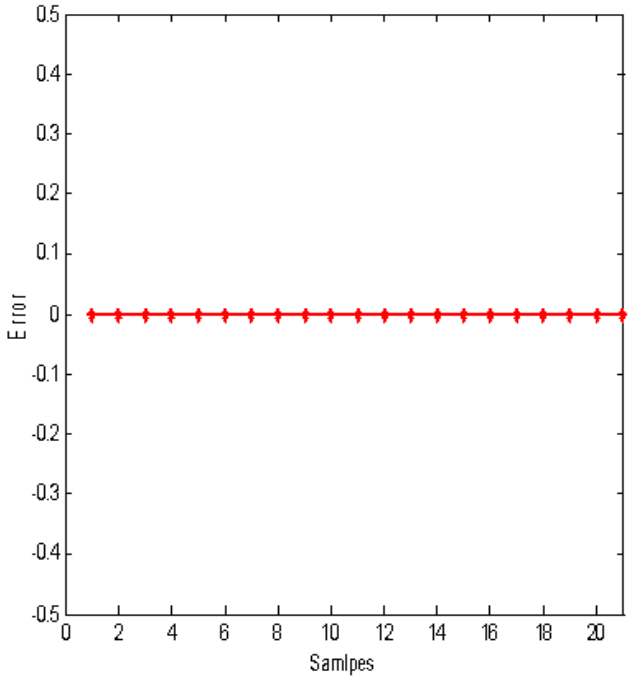

Fig.3.68 Test Error of phase A for fault on phase B

The RBFNN test output and test error of phase A when an inter-turn short circuit fault occurs on phase B inside the stator winding of an induction motor as shown in Figs. 3.67 and 3.68. From Fig. 3.67 it is clear that the RBFNN test output is equal to zero for all the samples with good accuracy. The testing error for this case is very low i.e 1.3182×10^{-8} as shown in Fig.3.68. Hence the RBFNN is able to locate correctly the inter-turn short circuit fault on phase B.

The RBFNN test output and error of phase B when an inter-turn short circuit fault occurs on phase B inside the stator of an induction motor as shown in Figs. 3.69 and 3.70. From Fig. 3.69 it is clear that the RBFNN has well learned the test data for all the samples with good accuracy. The testing error is i.e 1.8182×10^{-7} as shown in Fig.3.70.

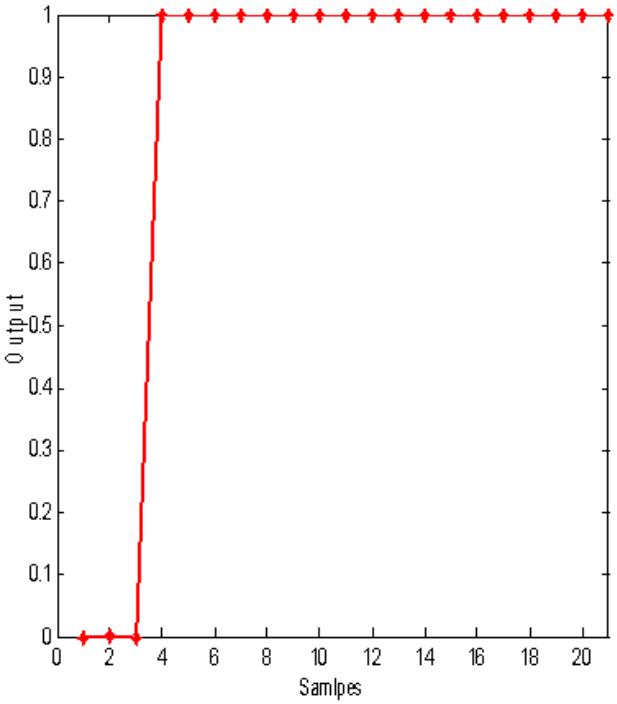

Fig.3.69 Test Output of phase B for fault on phase B

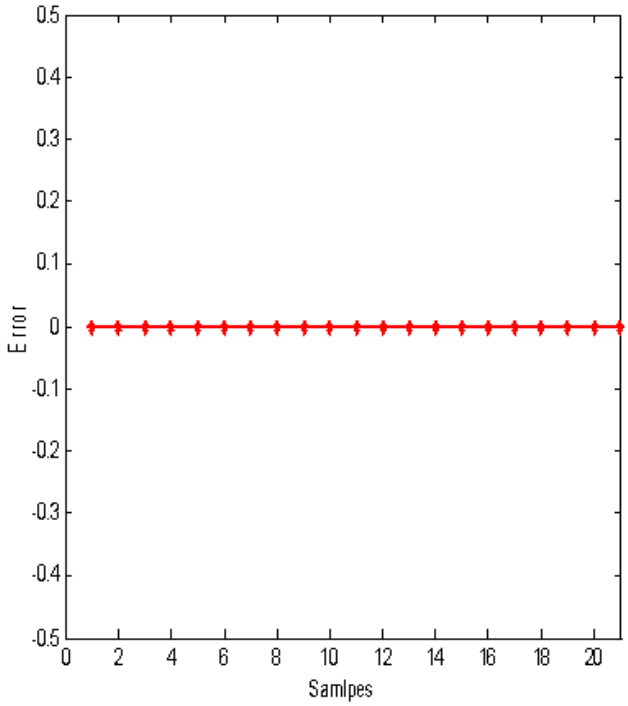

Fig.3.70 Test Error of phase B for fault on phase B

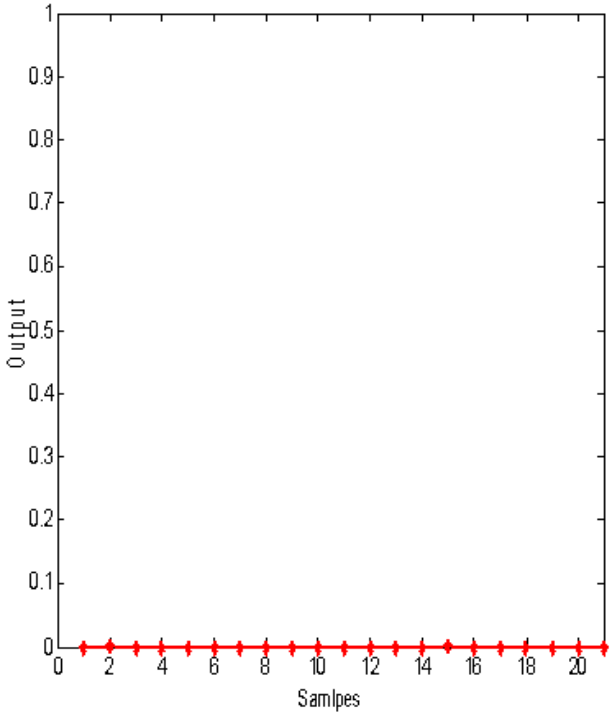

Fig.3.71 Test Output of phase C for fault on phase B

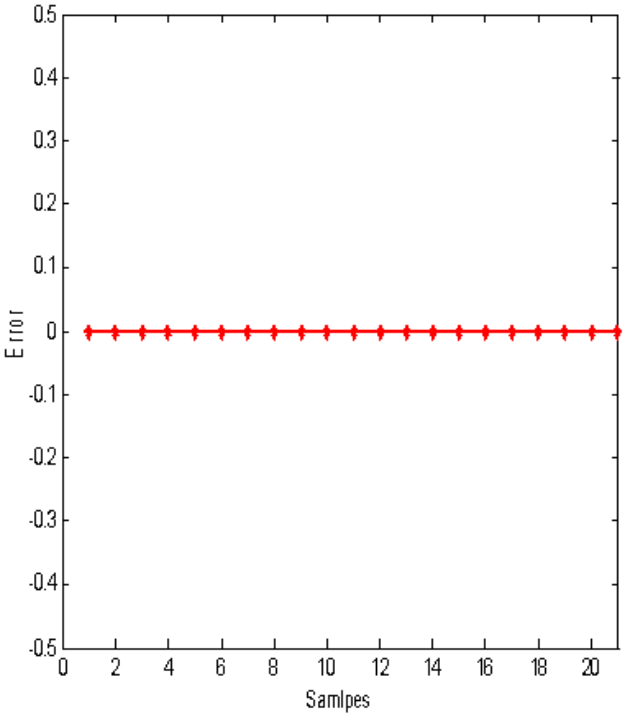

Fig.3.72 Test Error of phase C for fault on phase B

Figs. 3.71 and 3.72 show the RBFNN test output and error of phase C when an inter-turn fault occurs on phase B inside the stator of an induction motor. Fig. 3.71 shows the RBFNN well learn

the test data and gives the test output is equal to zero for all samples with good accuracy. Hence the RBFNN is able to locate correctly the stator inter-turn fault occurring on phase B. From Fig 3.72 the testing error is 3.6364×10^{-8}.

Figs. 3.73 and 3.74 show the RBFNN test output and test error of phase A when an inter-turn short circuit fault occurs on phase C inside the stator of an induction motor. Fig. 3.73 shows that the RBFNN well learn the test data and gives the test output with good accuracy. The testing error is 1.1364×10^{-7} as shown in Fig.3.74. Hence we conclude that the RBFNN is able to locate correctly the fault occurring on phase C.

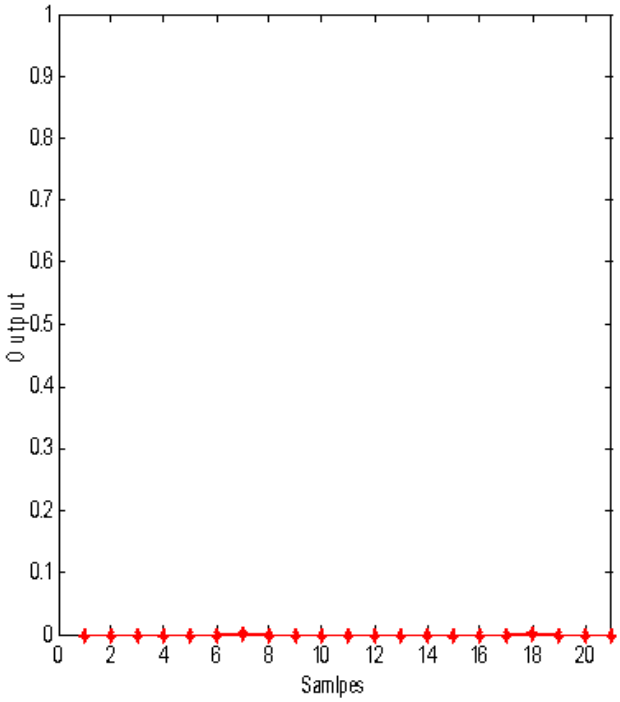

Fig.3.73 Test Output of phase A for fault on phase C

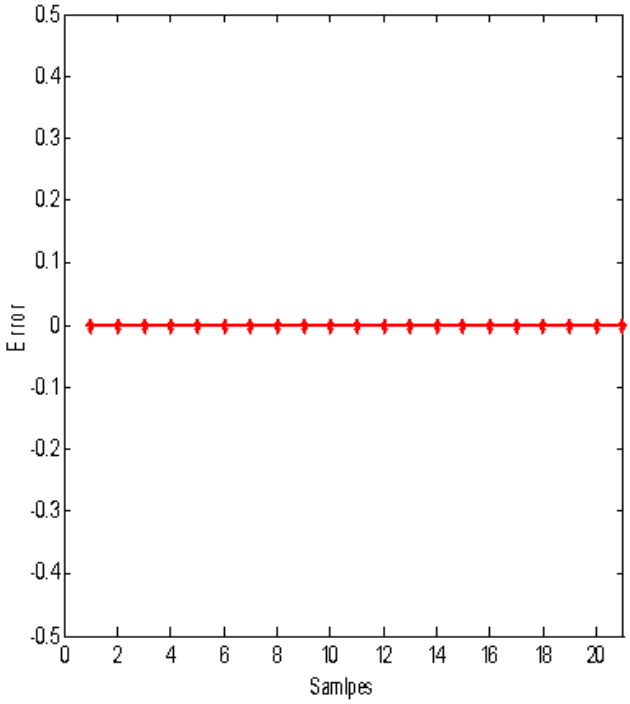

Fig.3.74 Test Error of phase A for fault on phase C

Figs. 3.75 and 3.76 show the RBFNN test output and test error of phase B when an inter-turn short circuit fault occurs on phase C inside the stator of an induction motor. The RBFNN well learn the test data and gives the test output with good accuracy as shown in Fig. 3.75. The testing error is very low i.e 1.8182×10^{-8} as shown in Fig.3.76. Hence we conclude that the RBFNN is able to locate correctly the stator inter-turn short circuit fault occurring on phase C.

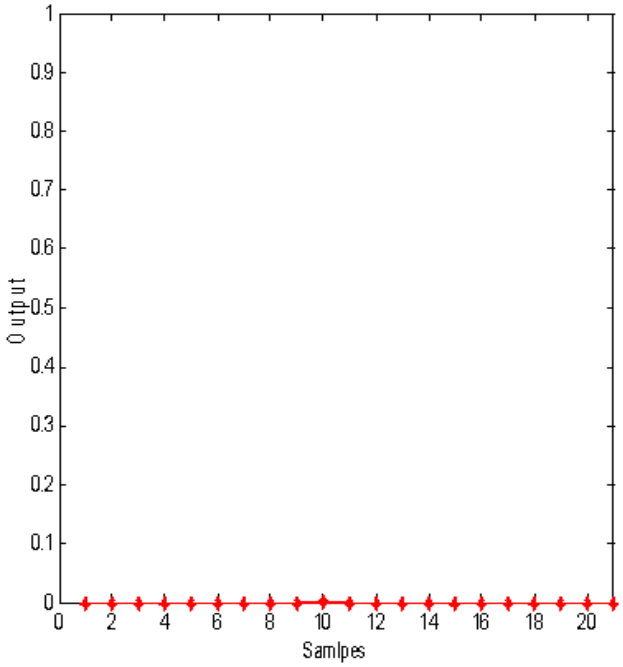

Fig.3.75 Test Output of phase B for fault on phase C

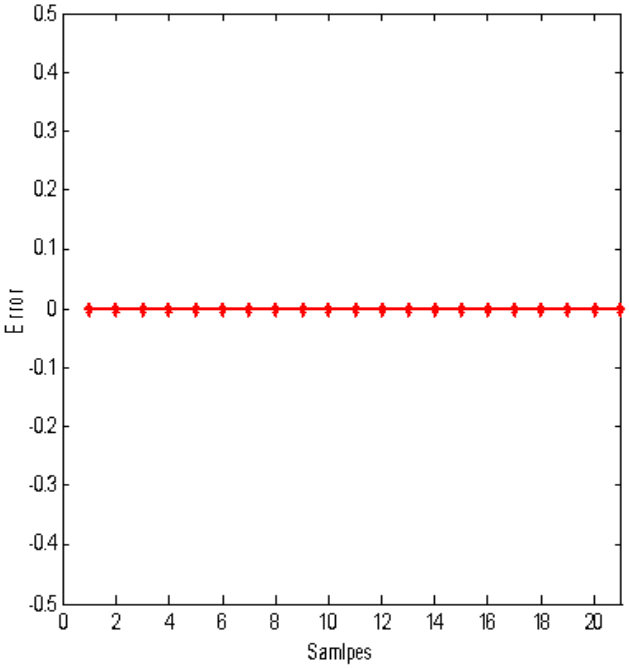

Fig.3.76 Test Error of phase B for fault on phase C

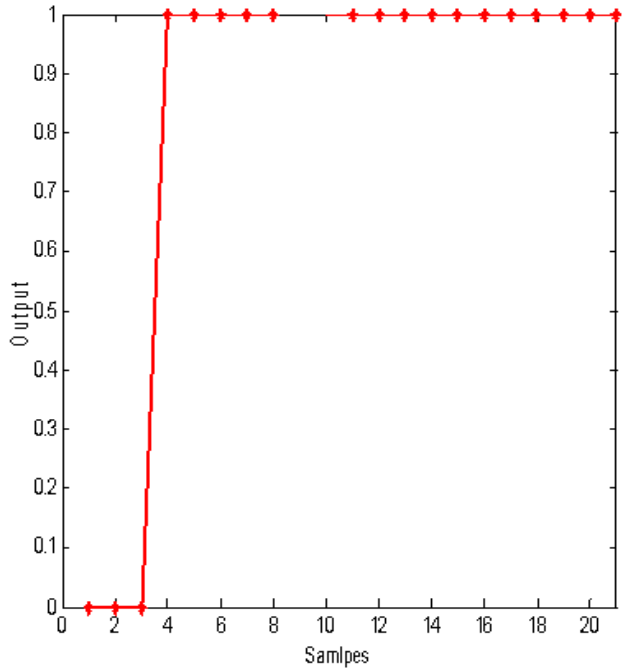

Fig.3.77 Test Output of phase C for fault on phase C

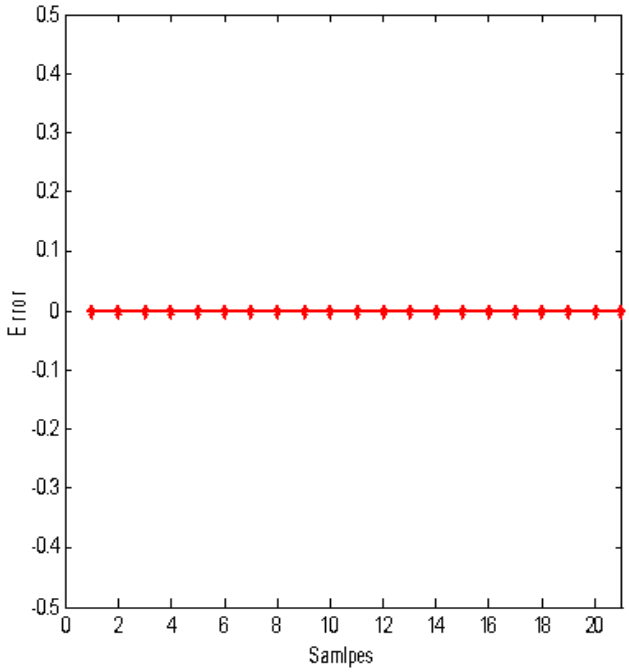

Fig.3.78Test Error of phase C for fault on phase C

Figs. 3.77 and 3.78 show the RBFNN test output and test error of phase C when an inter-turn short circuit fault occurs on phase C inside the stator winding of an induction motor. From Fig. 3.77 RBFNN test output is equal to zero for first three samples and is equal to one for the faulty

condition from 4 to 21 samples with good accuracy. Fig.3.77 shows that the MLPNN is able to locate correctly the fault occurring on phase C. The testing error is 1.8182×10^{-8} as shown in Fig.3.78.

3.3.4 Performance Evaluation using Proposed Approaches

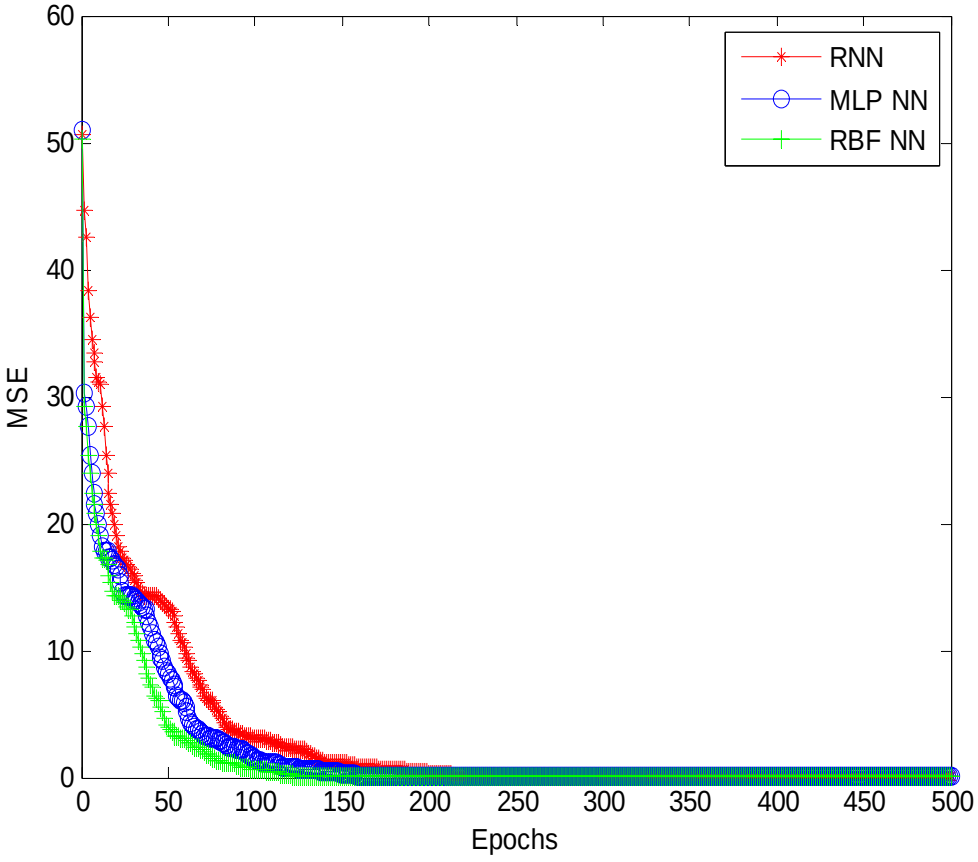

Fig.3.79 Comparison between the training performances of different NNs

The performance of the neural network fault diagnosis system is evaluated by its mean square error (MSE) Vs epoch curve shown in Fig. 3.79. We have compared the training performance of the MLPNN, RNN, and RBFNN. The RBFNN fault diagnosis scheme converges faster as compared with other two schemes. Also after learning for 500 epochs, the RBFNN scheme reaches the training error of 1.551×10^{-7} where as the training error for MLPNN and RNN reaches i.e equal to 1.33×10^{-6} and 5.948×10^{-5} respectively. Hence we conclude that RBFNN based fault detection scheme performs better as compared to the other two schemes for the

detection and location of stator inter-turn short circuit faults in the stator winding of an induction motor.

3.4 Chapter Summary

In this chapter, a number of soft computing techniques such as multilayer perceptron neural network (MLPNN), recurrent neural network (RNN), radial basis function neural network (RBFNN) have been applied for the detection and location of stator inter-turn short circuit fault in an induction motor. In this work, weight parameters of the multilayer perceptron neural network and radial basis function neural network are updated by using the gradient descent algorithm but the weight parameter in case of recurrent neural network is updated by using real time recurrent learning algorithm. In comparison between these proposed techniques, the radial basis function neural network (RBFNN) based technique provide better fault detection performance in terms of speed of convergence and fault identification capability. Further improvement in fault detection performance is suggested by proposing advanced techniques in subsequent chapters.

Chapter 4

Fault Detection Scheme using Neuro-Fuzzy Approach

4.1 Introduction

In the chapter 3, stator inter-turn fault detection based on different NNs such as multilayer perceptron neural network (MLPNN), recurrent neural network (RNN), and radial basis function neural network (RBFNN) was proposed. From which the RBFNN technique gives the best performance as compared to others. But it has been reported in many research work that hybrid methods such as adaptive neural fuzzy inference system (ANFIS) provide better result [51]. Hence in this chapter we have used the ANFIS technique for the detection of stator inter-turn short circuit fault of an induction motor.

ANFIS had gained popularity over other techniques due to its knowledge extraction feasibility, domain partitioning, rule structuring and modifications [52]. The artificial neural network (ANN) has the capability of solving the motor monitoring and fault detection problem using an inexpensive, reliable procedure. However, it does not provide heuristic reasoning about the fault detection process. On the other hand, fuzzy logic can easily provide heuristic reasoning, while being difficult to provide exact solutions. By merging the positive features of ANN and fuzzy logic, a simple noninvasive fault detection technique is developed [33]. By using a hybrid, supervised learning algorithm, ANFIS can construct an input-output mapping. The supervised learning (gradient descent) algorithm is used here to train the weights to minimize the errors.

In this chapter, application of ANFIS architecture takes into account the positive features of both the ANN and fuzzy logic technology for detection of stator winding inter-turn fault of an induction motor has been proposed. This system is a neural network structured upon fuzzy logic principles, which enables the neural fuzzy system to provide qualitative descriptions about the

motor condition and fault detection process. Here we have used the three phase shifts between the line currents and phase voltages of the induction motor as inputs to the ANFIS.

4.2 Brief Idea about ANFIS

This section introduces a brief idea about the architecture and learning procedure of the ANFIS which uses a feed-forward multilayer perceptron neural network (MLP) with supervised learning capability. An ANFIS, as its name implies, is a network structure consisting of nodes and directional links through which the nodes are connected. Moreover, part or all of the nodes are adaptive, which means their outputs of the ANFIS structure depend on the weights connected to the nodes, and the learning rule (gradient descent) specifies how these parameters should be changed to minimize a prescribed error measure.

4.2.1 ANFIS Architecture

For simplicity, we assume the fuzzy inference system under consideration has two inputs x and y and one output z. suppose that the rule base contains two fuzzy if then rules of Takagi and Sugeno's type [53].

Rule 1: if x is A_1 and y is B_1, then $f_1 = p_1x + q_1y + r_1$,

Rule 2: if x is A_2 and y is B_2, then $f_2 = p_2x + q_2y + r_2$.

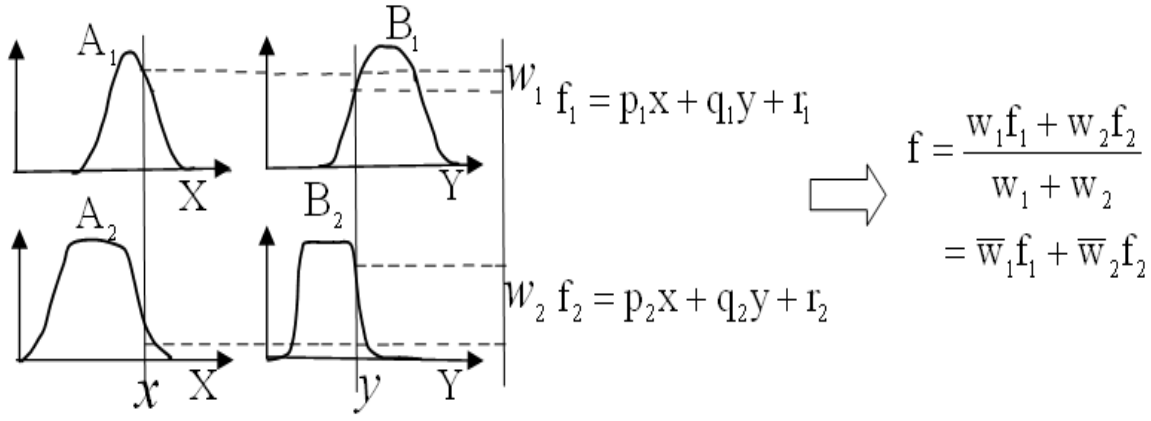

Fig.4.1 Type 3 fuzzy reasoning

Then the type-3 fuzzy reasoning is illustrated in Fig. 4.1, and the corresponding equivalent ANFIS architecture is shown in Fig. 4.2. The node functions in the same layer are of the same function family as described below:

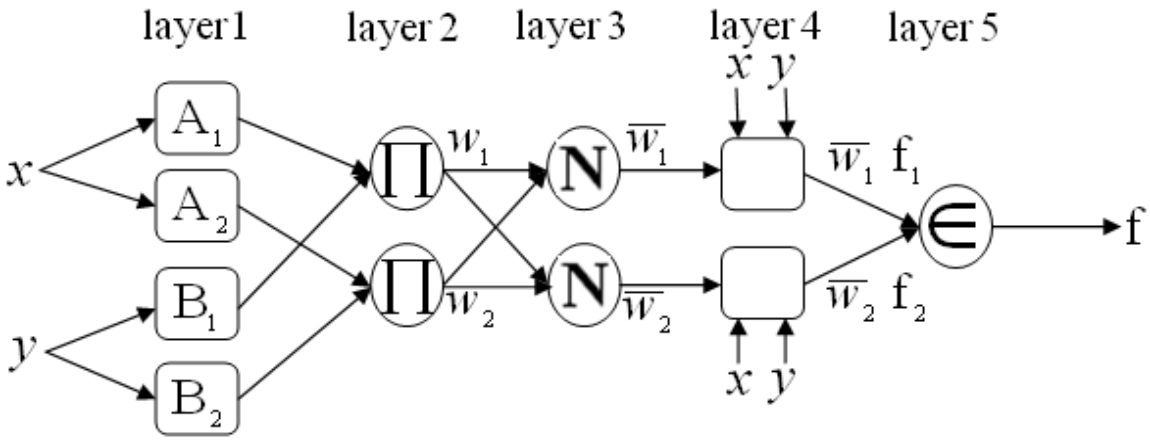

Fig.4.2 Equivalent ANFIS architecture

Layer 1: Every node I in this layer is a square node with a node function

$$O_i^1 = \mu_{Ai}(x) \qquad (4.1)$$

where

x = input to node i

A_i= linguistic label (small, large, etc) associated with this node function.

O_i^1 = Membership function of A_i and it specifies the degree to which the given x satisfies the quantifier A_i.

A bell-shaped membership function $\mu_{Ai}(x)$ with maximum equal to 1 and minimum equal to 0 is chosen for the ANFIS architecture

$$\mu_{Ai}(x) = \frac{1}{1+[(\frac{x-c_i}{a_i})^2]b_i} \qquad (4.2)$$

or

$$\mu_{Ai}(x) = \exp\{-(\frac{x-c_i}{a_i})^2\} \qquad (4.3)$$

where $\{a_i, b_i, c_i\}$ is the parameter set. As the values of these parameters change, the bell shaped functions vary accordingly, thus exhibiting various forms of membership functions on linguistic label A_i. In fact, any continuous and piecewise differentiable functions, such as commonly used Gaussian, trapezoidal or triangular shaped membership functions are also qualified candidates for node functions in this layer.

Layer 2: Every node in this layer is a circle node labeled Π which implies the incoming signals and sends the product out. For instance,

$$w_i = \mu_{Ai}(x) \times \mu_{Bi}(y) \tag{4.4}$$

where i = 1, 2.

Each node output presents the firing strength of a rule (in fact, other T-norms operators that perform generalized AND can be used as the node function in this layer).

Layer 3: Every node in this layer is a circle node labeled N. the i^{th} node calculates the ratio of the i^{th} rules firing strength to the sum of all rules firing strengths:

$$\overline{w}_i = \frac{w_i}{w_1 + w_2} \tag{4.5}$$

where i = 1, 2.

For convenience, outputs of this layer will be called normalized firing strengths.

Layer 4: Every node I in this layer is a square node with a node function

$$O_i^4 = \overline{w}_i f_i = \overline{w}_i (p_i x + q_i y + r_i) \tag{4.6}$$

where

$\overline{w}_i$ = Output of the layer 3

$\{p_i, q_i, r_i\}$ = the parameter set

Layer 5: The single node in this layer is a circle node labeled Σ that computes the overall output as the summation of all incoming signals i.e.

$$\text{Overall output} = O_1^5 = \sum_i \overline{w}_i f_i = \frac{\sum_i w_i f_i}{\sum_i w_i} \tag{4.7}$$

4.2.2 Fuzzy Inference Systems with Simplified Fuzzy if-then Rules

Though the reasoning mechanisms as shown in Fig. 4.3 are commonly used each of them have inherent draw backs. For type 1 reasoning, the membership functions on the consequence part are restricted to monotonic functions which are not compatible with linguistic terms such as "medium" whose member ship function should be bell-shaped. For type 2 reasoning, the de-fuzzification process is time consuming and systematic fine-tuning of the parameters are not easy. For type 3 reasoning, it is just hard to assign any appropriate linguistic to the consequence part which is a non-fuzzy function of the input variables. To cope with these disadvantages, simplified fuzzy if-then rules of the following form are introduced.

If x is big and y is small, then z is d.

Where d is a crisp value. Due to the fact that the output z is described by a crisp value (or equivalently, a singular membership function); this class of simplified fuzzy if-then rules can employ all three types of reasoning mechanisms. More specifically, the consequent part of this simplified fuzzy if-then rule is represented by a step function (at z=d) in type 2, and a constant output function in type 3, respectively. Thus the three reasoning mechanisms are unified under these simplified fuzzy if-then rules.

Most of all, with this simplified fuzzy if-then rule, it is possible to prove that under certain circumstances, the resulting fuzzy inference system has unlimited approximation power to match any nonlinear functions arbitrarily well on a compact set. We will proceed this in a descriptive way by applying the stone-weierstrass theorem [54, 55].

Suppose we have two fuzzy inference systems s and $\tilde{s}$: each has two rules and the output of each system can be expressed as

$$s : z = \frac{w_1 f_1 + w_2 f_2}{w_1 + w_2} \tag{4.8}$$

$$\tilde{s} : \tilde{z} = \frac{\tilde{w}_1 \tilde{f} + \tilde{w}_2 \tilde{f}_2}{\tilde{w}_1 + \tilde{w}_2} \tag{4.9}$$

where f_1, f_2, $\tilde{f}_1$ and $\tilde{f}_2$ are constant output of each rule. Then $az+b\tilde{z}$ and $z\tilde{z}$ can be calculated as follows,

$$az + b\tilde{z} = a\frac{w_1 f_1 + w_2 f_2}{w_1 + w_2} + b\frac{\tilde{w}_1\tilde{f}_1 + \tilde{w}_2\tilde{f}_2}{\tilde{w}_1 + \tilde{w}_2}$$

$$= \frac{w_1\tilde{w}_1(af_1 + b\tilde{f}_1) + w_1\tilde{w}_2(af_1 + b\tilde{f}_2)}{w_1\tilde{w}_1 + w_1\tilde{w}_2 + w_2\tilde{w}_1 + w_2\tilde{w}_2}$$

$$+ \frac{w_2\tilde{w}_1(af_2 + b\tilde{f}_1) + w_2\tilde{w}_2(af_2 + b\tilde{f}_2)}{w_1\tilde{w}_1 + w_1\tilde{w}_2 + w_2\tilde{w}_1 + w_2\tilde{w}_2}$$

$$z\tilde{z} = \frac{w_1\tilde{w}_1 f_1\tilde{f}_1 + w_1\tilde{w}_2 f_1\tilde{f}_2 + w_2\tilde{w}_1 f_2\tilde{f}_1 + w_2\tilde{w}_2 f_2\tilde{f}_2}{w_1\tilde{w}_1 + w_1\tilde{w}_2 + w_2\tilde{w}_1 + w_2\tilde{w}_2} \qquad (4.10)$$

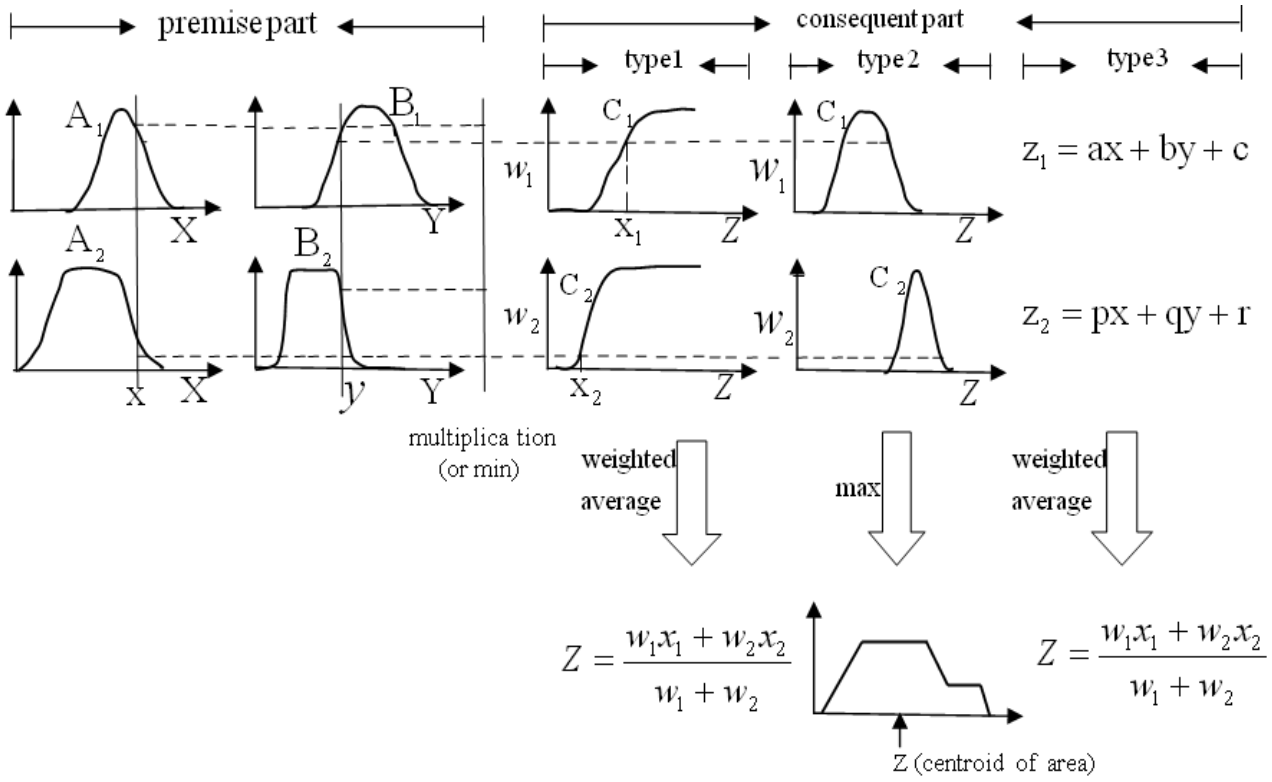

Fig.4.3 commonly used fuzzy if-then rules and fuzzy reasoning mechanism

which are of the same as (4.8) and (4.9), apparently the ANFIS architectures that compute $az+b\tilde{z}$ and $z\tilde{z}$ are of the same class of s and $\tilde{s}$ if and only if the class of membership functions are invariant under multiplication. This is loosely true if the class of membership functions is the

set of all bell-shaped functions, since the multiplication of two bell-shaped functions is almost always still bell-shaped. Another more highly defined class of membership functions satisfying these criteria, as pointed out by Wang [56, 57], is the scaled Gaussian membership function:

$$\mu_{Ai}(x) = a_i \exp[-(\frac{x - c_i}{a_i})^2] \qquad (4.11)$$

Therefore by choosing an appropriate class of membership functions, we can conclude that the ANFIS with simplified fuzzy if-then rules satisfy the criteria of the stone-weierstrass theorem. Consequently for any given $\varepsilon > 0$, and any real valued function g, there is a fuzzy inference system $s$such that $|g(\bar{x}) - s(\bar{x})| < \varepsilon$ for all $\bar{x}$ in the underlying compact set. Moreover, since the simplified ANFIS is a proper subset of all three types of ANFIS in Fig. 4.3, we can draw the conclusion that all the three types of ANFIS have unlimited approximation power to match any given data set.

4.3 Proposed ANFIS Approach for Induction Motor Fault Detection

The proposed work consists of detection and location of an inter-turn short circuit fault in the stator windings of a three phase induction motor by using the combination of the positive features of neural networks and fuzzy logic.

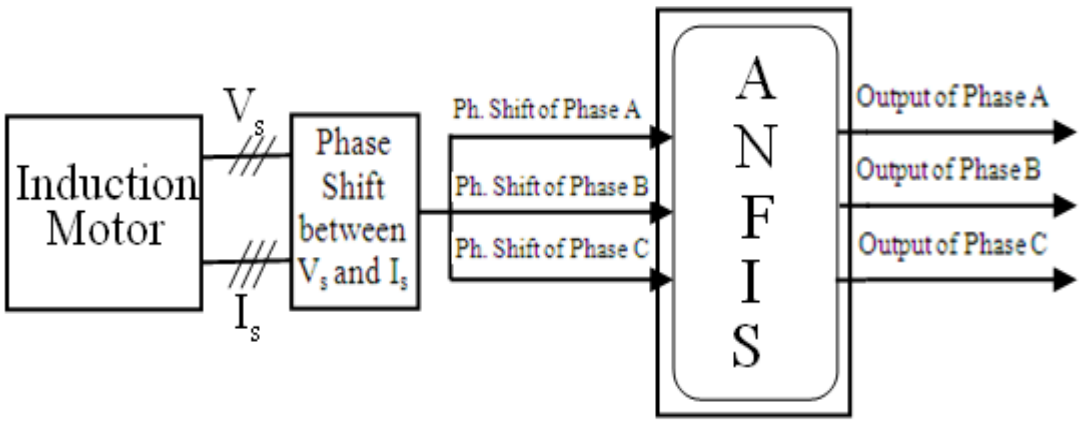

Fig.4.4 Block diagram of the fault location procedure

Fig. 4.4 shows the block diagram of the procedure to detect and locate inter-turn fault in the stator winding of an induction motor. The first step of in this procedure is the acquisition of the three line currents and phase voltages from the induction motor in order to extract the three phase

shift between the line currents and the phase voltages. The three phase shifts are fed to the ANFIS network.

ANFIS has to learn the relationships between the fault signature i.e the three phase shifts between the line currents and phase voltages under different load conditions (ANFIS inputs) and the corresponding operating condition (ANFIS outputs) to be able to locate correctly the faulty phase.

Fig. 4.4 shows the ANFIS has three inputs namely, the three phase shifts and three outputs corresponding to the three phases of the induction motor, where the fault can occur. If a short circuit is detected and located in one of the three phases, the corresponding ANFIS is set to 'one', otherwise it is 'zero'.

The design process of the ANFIS based fault diagnosis includes the following steps.

- Preparation of a suitable training data set for the ANFIS.
- Selection of a suitable ANFIS Structure.
- Training of the ANFIS.
- Evaluation of the test pattern.

4.3.1 Preparation of a Suitable Training Data Set for the ANFIS

A training data set constituted by input (Phase shift between the line currents and phase voltages) and output data sets has been applied to the neural network. The input data are collected through simulation as shown in Chapter 2 (Section 2.7).

The output data set is formed by the following desired output (T_i) which indicates the state of each phase.

$T_1 = 1$ for a short circuit at phase A; otherwise, $T_1 = 0$;

$T_2 = 1$ for a short circuit at phase B; otherwise, $T_2 = 0$;

$T_3 = 1$ for a short circuit at phase C; otherwise, $T_3 = 0$;

Therefore, the output states of the neural network are set to the following.

[0; 0; 0] no fault (healthy condition);

[1; 0; 0] fault occurred at phase A;

[0; 1; 0] fault occurred at phase B;

[0; 0; 1] fault occurred at phase C;

1.3.2 Selection of a Suitable ANFIS Structure

The neural-fuzzy architecture takes into account both ANN and fuzzy logic technologies. The system is a neural network structured upon fuzzy logic principles, which enables the neural-fuzzy system to provide qualitative descriptions about the motor condition and fault detection process. This knowledge is provided by the fuzzy parameters of membership functions and fuzzy rules. The fault detector based on ANFIS, which is a fuzzy inference system implemented on five layers feed-forward network.

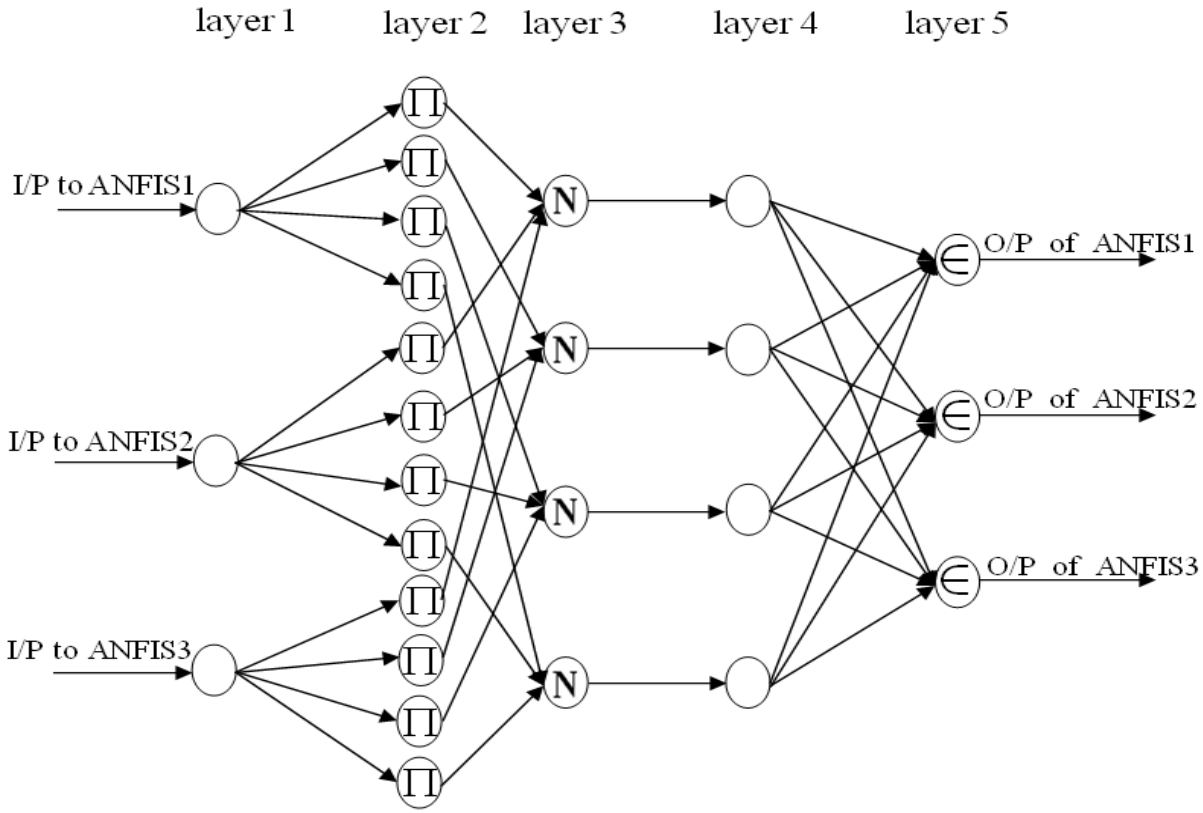

Fig.4.5 ANFIS fault detector

The ANFIS architecture enables a change in rule structure during the evaluation of fuzzy inference system. The ANFIS optimized itself in given the number of iterations by providing a change in rules, by discarding unnecessary rules, and by changing shapes of membership functions, this is called modifications. It is an inherent characteristic of ANFIS architecture. The use of least square estimation is due to the fact that the network output is linear function of the consequence parameters. Once the system is trained for specific data over a wide range, it can be applicable to similar types of motor use in plants, and thus there is no need to train the model for each and every motor.

4.3.3 Training of the ANFIS

Here we have written a suitable ANFIS program in the MATLAB environment which is used for fault detection purposes. The detection system is trained by using the simulated data as given in Chapter 2 (Section 2.7). The detector is developed with three input parameters (three phase shifts). The ANFIS motor fault detector is trained to learn inter-turn short circuit fault in the stator winding of an Induction motor. Fig. 4.5 shows the three inputs training data (three phase shifts) is applied for training the inter-turn short circuit fault in the stator winding of an induction motor. The four membership functions all Gaussian in nature are developed for each input.

Training data of all the three input parameters (three phase shifts) are applied to both the fault detector for obtaining the optimize architecture for the detection of inter-turn short circuit fault in the stator winding of an induction motor.

Figs.4.6 and 4.7 show the ANFIS output and error when a stator inter-turn short circuit fault occurs on phase A of an induction motor respectively. Fig.4.6 shows that the output of the ANFIS from which the star one is the target value (either 0 or 1 for healthy and inter-turn faulty condition respectively) and the circle one is the output of the ANFIS. When a stator inter-turn fault occurs on phase A, then the output of that phase is one and others are zero. From Fig. 4.6 it is clear that the ANFIS is well learned the input data and correctly reproduced the desired output. Hence, the error which is the difference between the target value and the actual output is very small i.e 8.3087×10^{-8} as shown in Fig.4.7.

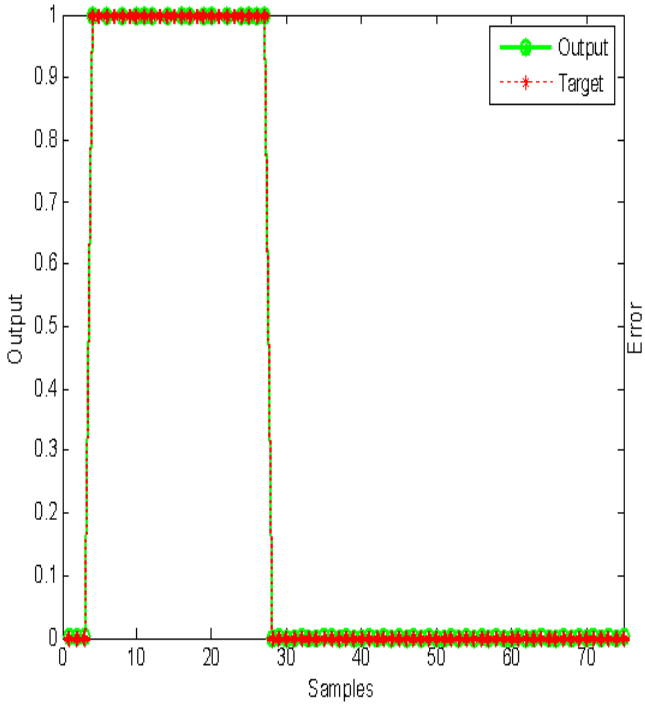

Fig. 4.6 ANFIS Output for fault on phase A

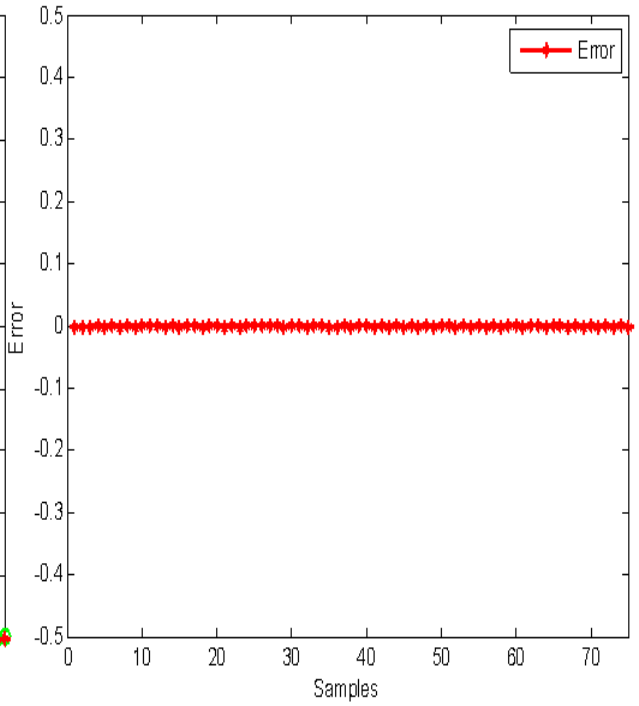

Fig. 4.7 ANFIS Error for fault on phase A

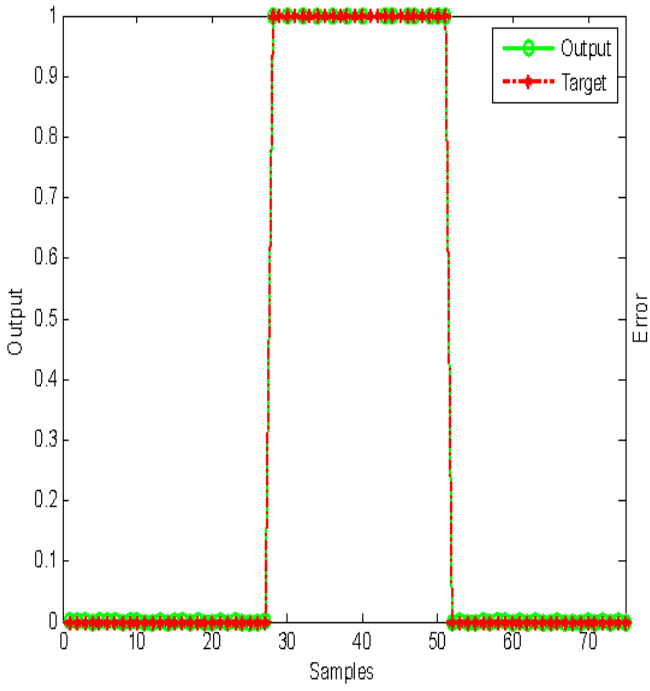

Fig. 4.8 ANFIS Output for fault on phase B

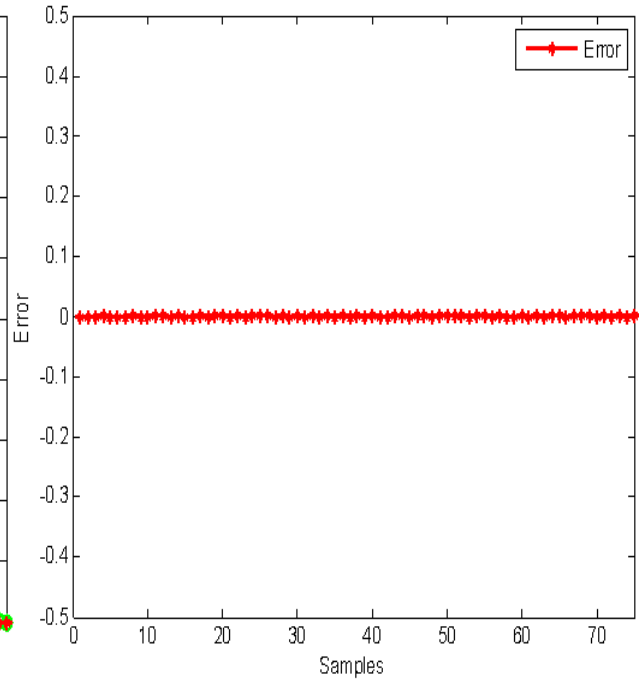

Fig. 4.9 ANFIS Error for fault on phase B

The ANFIS output and error when a stator inter-turn short circuit fault occurs on phase B of an induction motor respectively as shown in Figs.4.8 and 4.9. Fig.4.8 shows that the output of the ANFIS from which the star one is the target value (either 0 or 1 for healthy and inter-turn faulty

condition respectively) and the circle one is the output of the ANFIS. From Fig. 4.8 it is clear that the ANFIS is properly learned the input data. Hence, the error which is the difference between the target value and the actual output is 2.3047×10^{-8} as shown in Fig.4.9.

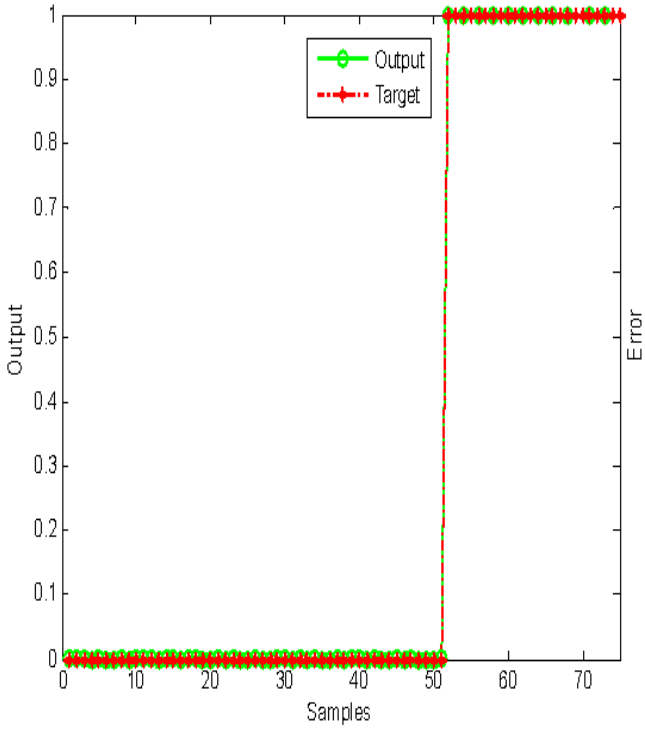

Fig. 4.10 ANFIS Output for fault on phase C

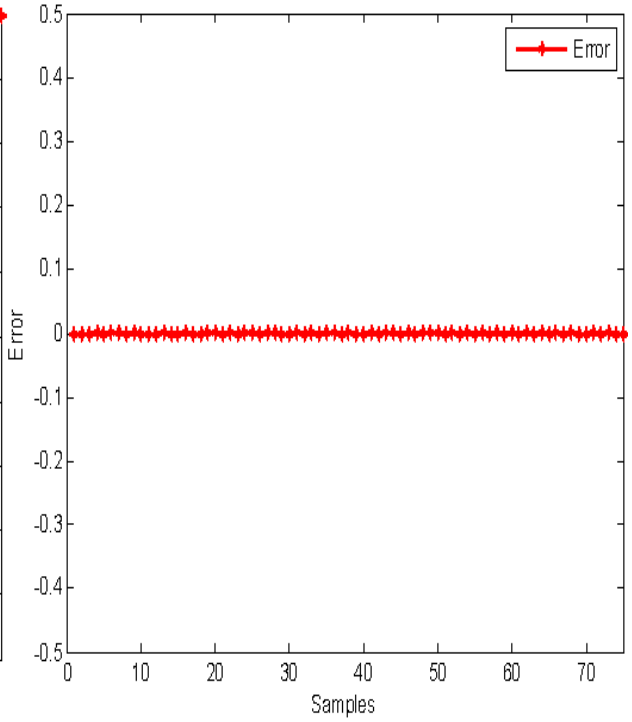

Fig. 4.11 ANFIS Error for fault on phase C

Figs.4.10 and 4.11 show that the ANFIS output and error when a stator inter-turn short circuit fault occurs on phase C of an induction motor respectively. The target output (either 0 or 1 for healthy and inter-turn faulty condition respectively) of the ANFIS i.e the star one and the circle one is the actual output of the ANFIS as shown in Fig. 4.10. When a stator inter-turn fault occurs on phase C then the output of that phase is one and others are zero. From Fig. 4.10 it is clear that the ANFIS is well learned the input data and correctly reproduced the desired output. The error which is the difference between the target value and the actual output is 3.9841×10^{-8} as shown in Fig.4.11.

The performance of the ANFIS based fault diagnosis is evaluated by its mean square error (MSE) Vs epoch curve as shown in Fig. 4.12. We have compared the training performance of the ANFIS and RBFNN. The ANFIS fault diagnosis scheme is converged faster as compared with RBFNN scheme. Also after learning for 500 epochs the ANFIS scheme reaches the training error of 8.558×10^{-9} where as the training error for RBFNN reaches i.e equal to 1.551×10^{-7}. Hence

we conclude that ANFIS based fault detection scheme gives better performance as compared with the RBFNN scheme for the detection and location of stator inter-turn short circuit fault in the stator winding of an induction motor.

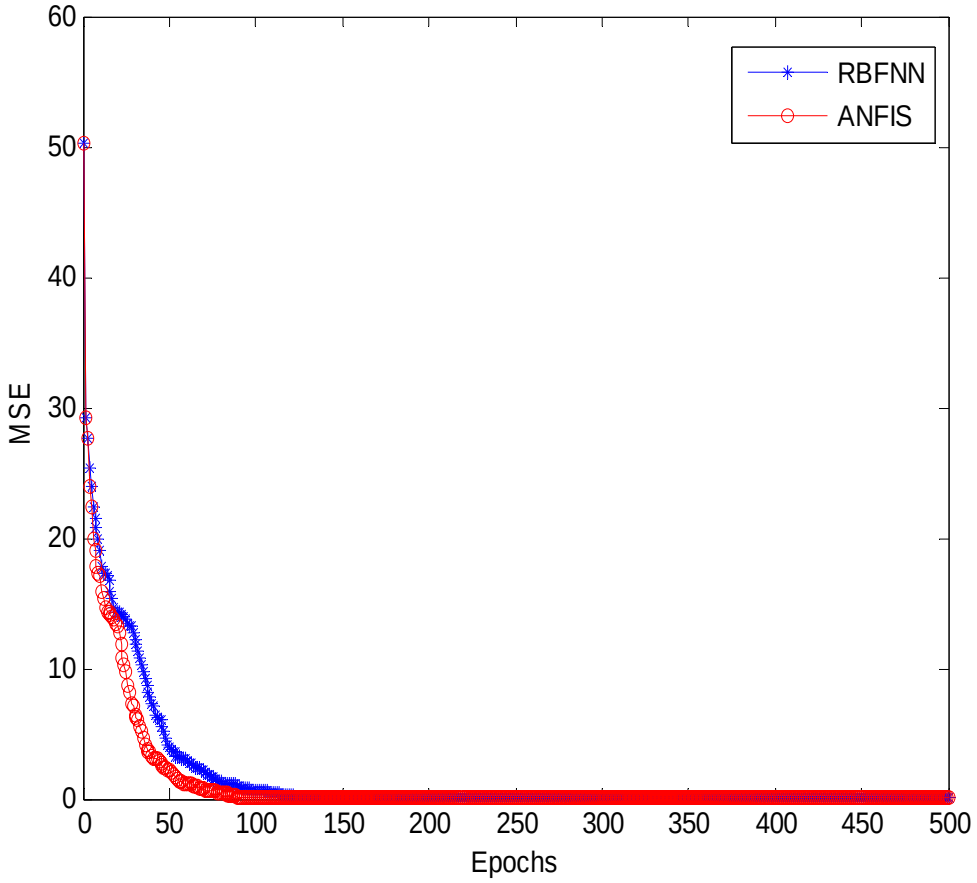

Fig. 4.12 Comparison between the Training Performance between ANFIS and RBFNN

4.3.4 Testing Results for ANFIS

The performance of ANFIS on the testing data set represents its generalization ability. The data set is divided into two. One set is used for training and the other for testing. In fact a generalized neural network will perform well for both training and testing data. The test procedure is conducted by a test data set that is different from the training data set to assess the generalization capacity of the adopted network.

The test data set are presented to the neural networks under three load torques (τ_1 = 3 N-m, τ_2 = 5 N-m, τ_3 = 7 N-m) and represent the following different operating cases of the induction motor: healthy (three points) and fault of an even number of shorted turns (2, 4, 6, 8, 10, and 12) on

each stator phase [18 (6 × 3) points]. Thus, a total of 21(18 + 3) testing samples has been collected testing the each phase stator inter-turn fault.

Figs. 4.13 and 4.14 show the ANFIS test output and error of phase A when an inter-turn fault occurs on phase A inside the stator of an induction motor. From Fig. 4.13 the ANFIS test output is equal to zero for first three samples and is equal to one for the faulty condition from 4 to 21 samples with good accuracy. This shows that the ANFIS is able to locate correctly the fault occurring on phase A. The testing error is 1.5045×10^{-7} as shown in Fig.4.14.

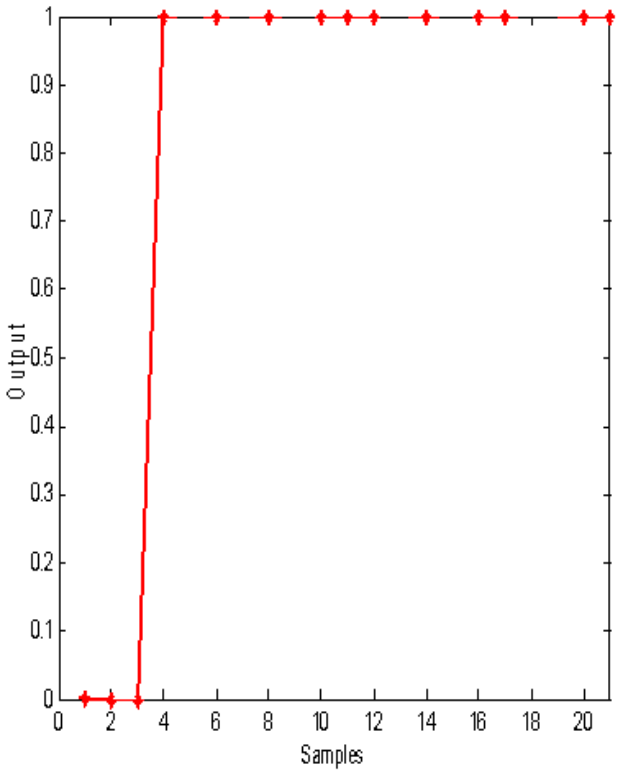

Fig.4.13 Test Output of phase A for fault on phase A

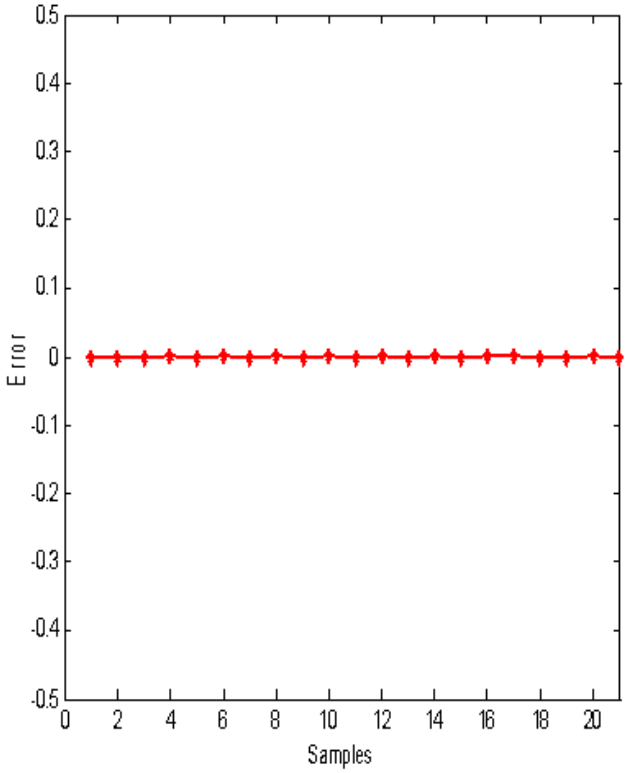

Fig.4.14 Test Error of phase A for fault on phase A

The ANFIS test output and error of phase B when an inter-turn short circuit fault occurs on phase A inside the stator of an induction motor as shown in Figs. 4.15 and 4.16. From Fig. 4.15 it is clear that the ANFIS well learn the test data with good accuracy. Hence the ANFIS is able to locate correctly the stator inter-turn short circuit fault occurring on A phase. The testing error is very low i.e 9.5000×10^{-8} as shown in Fig.4.16.

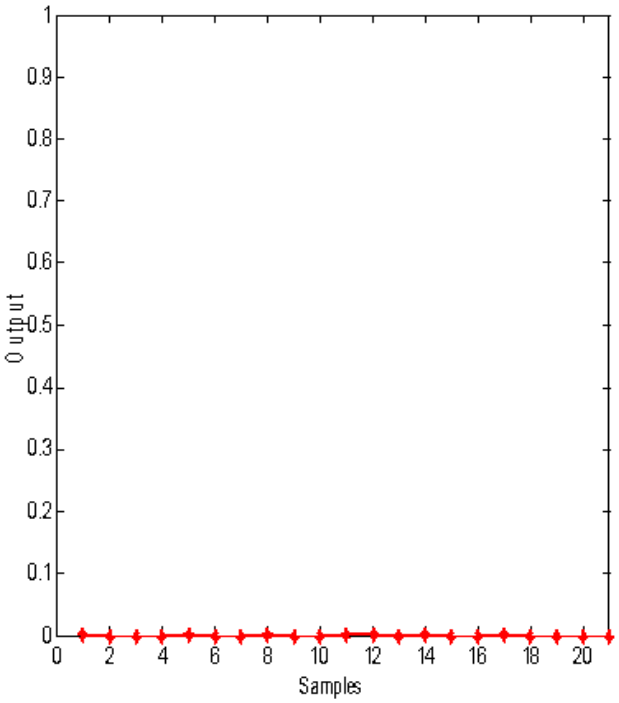

Fig.4.15 Test Output of phase B for fault on phase A

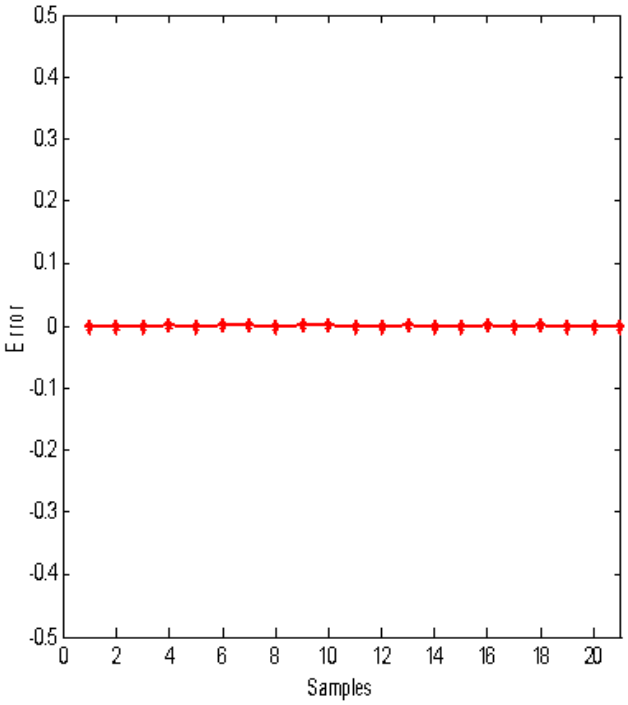

Fig.4.16 Test Error of phase B for fault on phase A

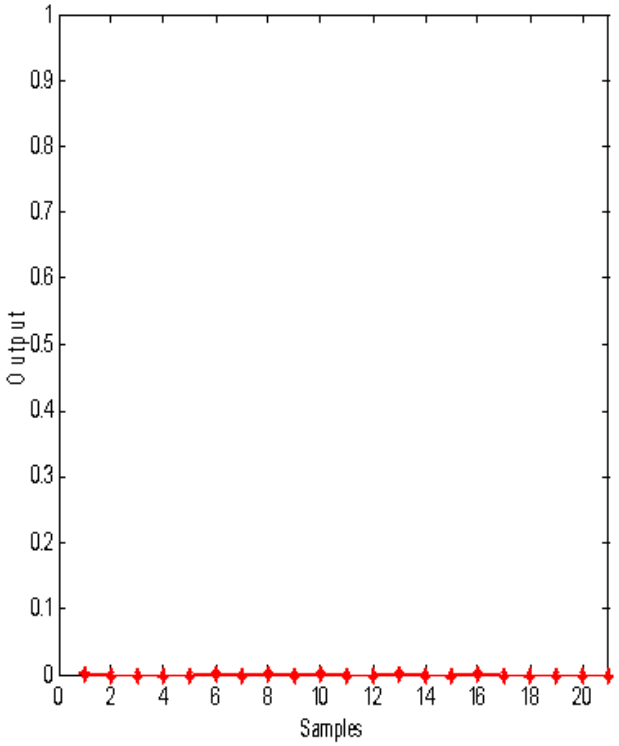

Fig.4.17 Test Output of phase C for fault on phase A

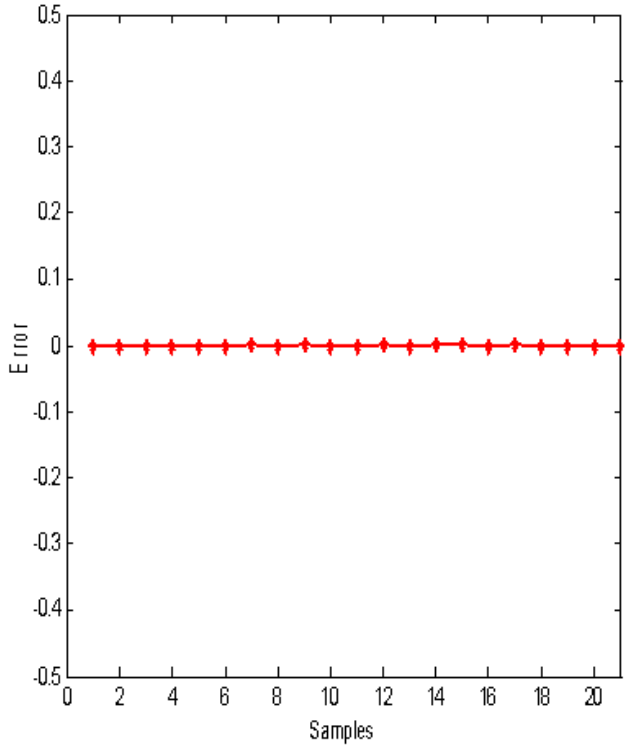

Fig.4.18 Test Error of phase C for fault on phase A

Figs. 4.17 and 4.18 show the ANFIS test output and test error of phase C when an inter-turn short circuit fault occurs on phase A inside the stator of an induction motor. Fig. 4.17 shows that

the ANFIS well learn the test data and gives the test output with good accuracy. The testing error is 4.0909×10^{-8} as shown in Fig.4.18. Hence we conclude that the ANFIS is able to locate correctly the fault occurring on phase A.

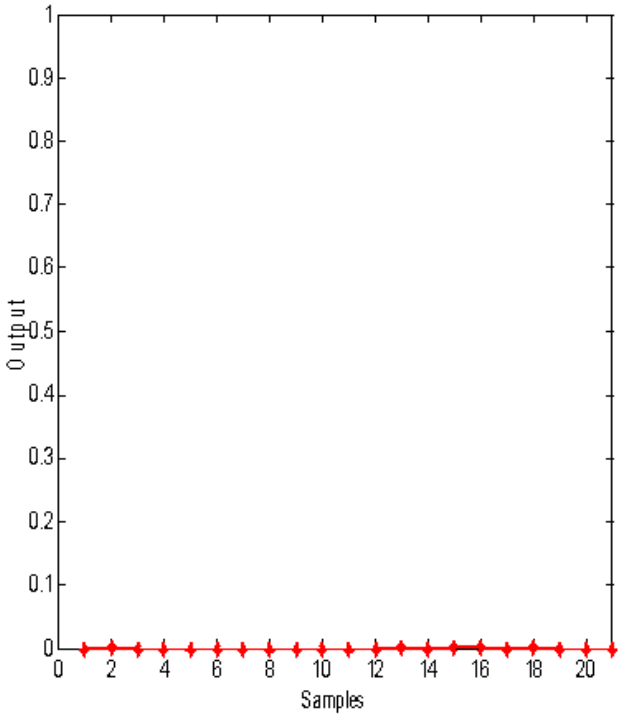

Fig.4.19 Test Output of phase A for fault on phase B

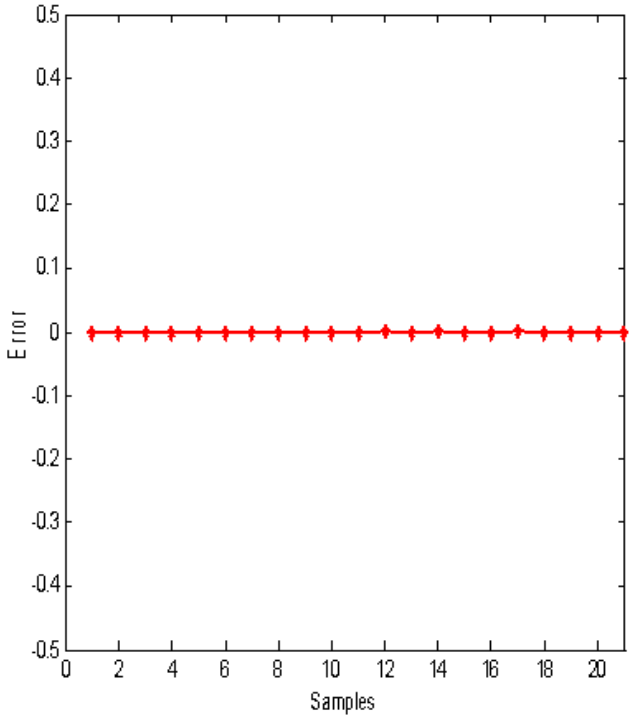

Fig.4.20 Test Error of phase A for fault on phase B

The ANFIS test output and test error of phase A when an inter-turn short circuit fault occurs on phase B inside the stator winding of an induction motor as shown in Figs. 4.19 and 4.20. From Fig. 4.19 it is clear that the ANFIS test output is equal to zero for all the samples with good accuracy. The testing error for this case is very low i.e 3.8636×10^{-8} as shown in Fig.4.20. Hence the ANFIS is able to locate correctly the inter-turn short circuit fault on phase B.

The ANFIS test output and error of phase B when an inter-turn short circuit fault occurs on phase B inside the stator of an induction motor as shown in Figs. 4.21and 4.22. From Fig. 4.21 it is clear that the ANFIS is well learned the test data for all the samples with good accuracy. The testing error is i.e 3.3636×10^{-8} as shown in Fig.4.22.

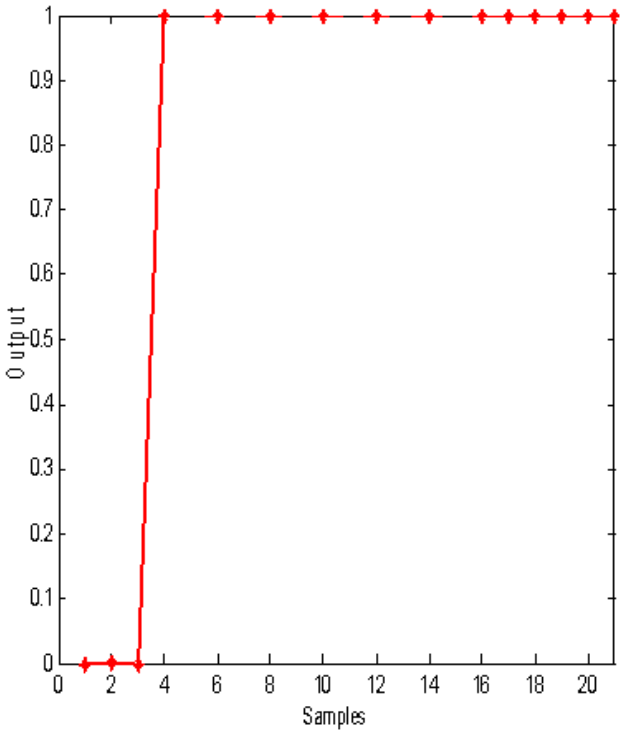

Fig.4.21 Test Output of phase B for fault on phase B

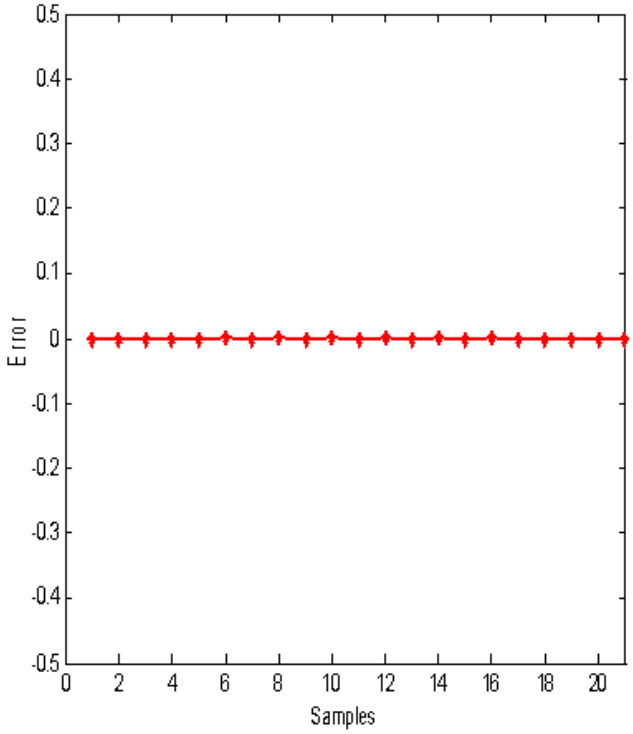

Fig.4.22 Test Error of phase B for fault on phase B

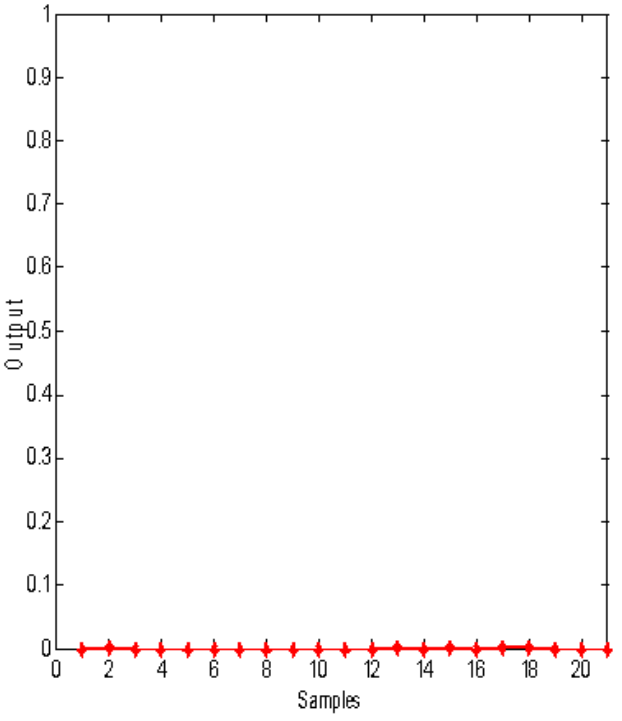

Fig.4.23 Test Output of phase C for fault on phase B

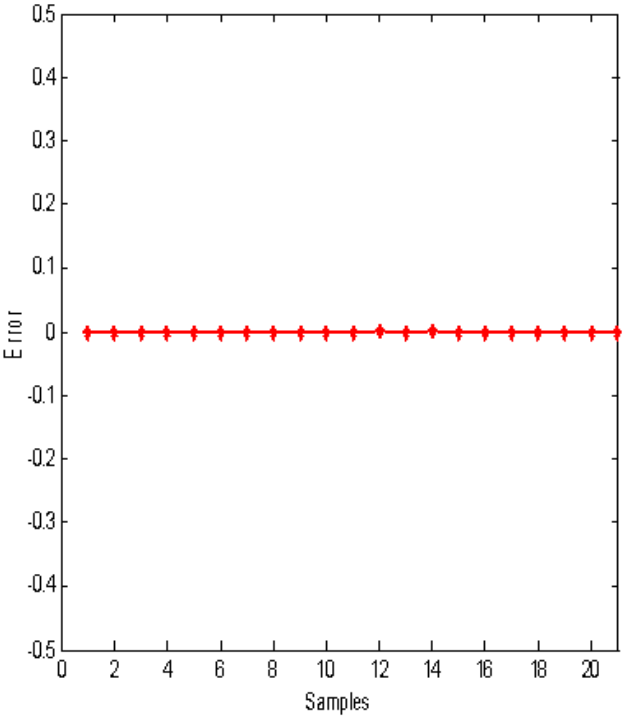

Fig.4.24 Test Error of phase C for fault on phase B

Figs. 4.23 and 4.24 show the ANFIS test output and error of phase C when an inter-turn fault occurs on phase B inside the stator of an induction motor. Fig. 4.23 shows the ANFIS is well

learned the test data and gives the test output is equal to zero for all samples with good accuracy. Hence the ANFIS is able to locate correctly the stator inter-turn fault occurring on phase B. From Fig 4.24 the testing error is 3.1818×10^{-8}.

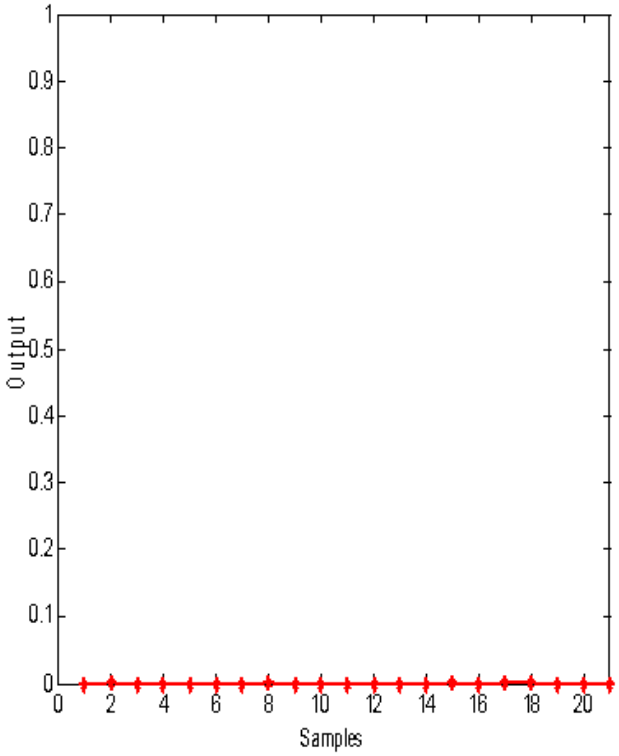

Fig.4.25 Test Output of phase A for fault on phase C

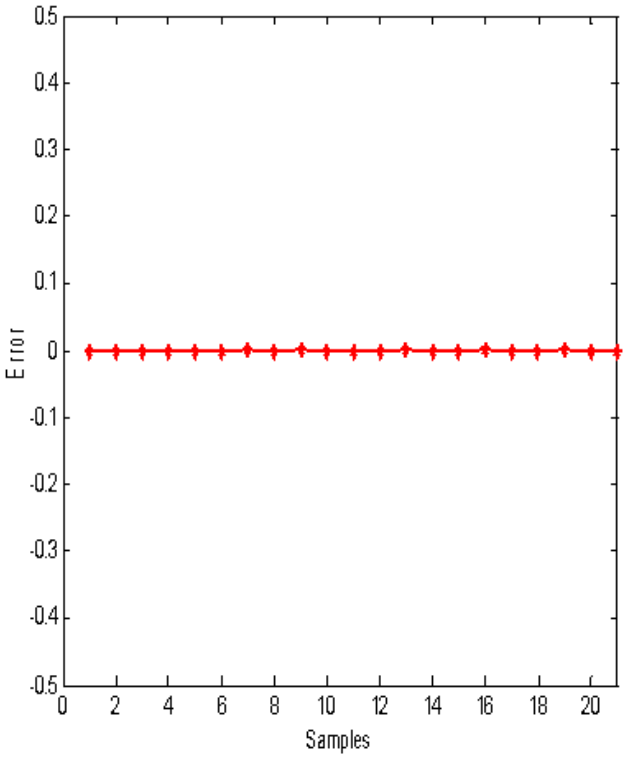

Fig.4.26 Test Error of phase A for fault on phase C

Figs. 4.25 and 4.26 show the ANFIS test output and test error of phase A when an inter-turn short circuit fault occurs on phase C inside the stator of an induction motor. Fig. 4.25 shows that the ANFIS well learn the test data and gives the test output with good accuracy. The testing error is 1.3182×10^{-7} as shown in Fig.4.26. Hence we conclude that the ANFIS is able to locate correctly the fault occurring on phase C.

Figs. 4.27 and 4.28 show the ANFIS test output and test error of phase B when an inter-turn short circuit fault occurs on phase C inside the stator of an induction motor. The ANFIS well learn the test data and gives the test output with good accuracy as shown in Fig. 4.27. The testing error is very low i.e 6.7273×10^{-8} as shown in Fig.4.28. Hence we conclude that the ANFIS is able to locate correctly the stator inter-turn short circuit fault occurring on phase C.

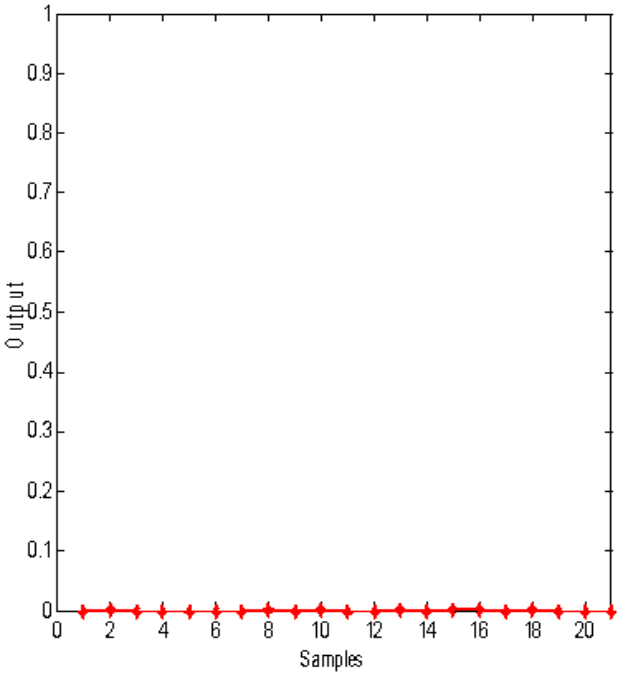

Fig.4.27 Test Output of phase B for fault on phase C

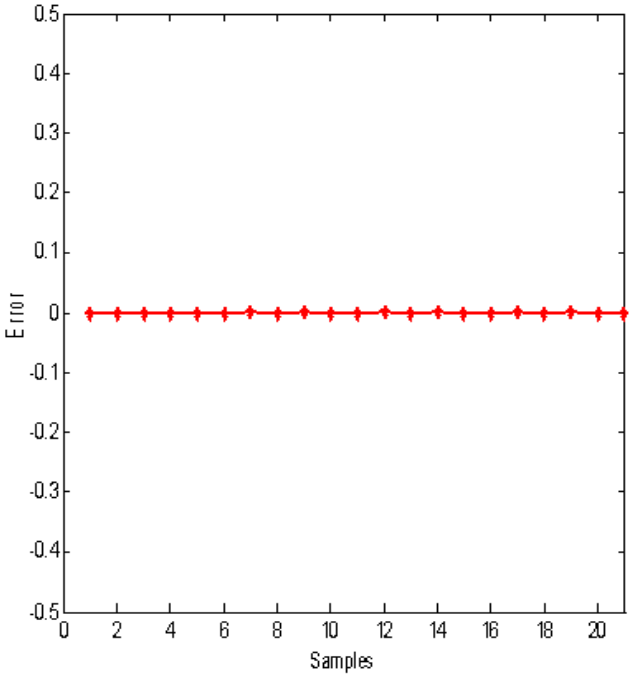

Fig.4.28 Test Error of phase B for fault on phase C

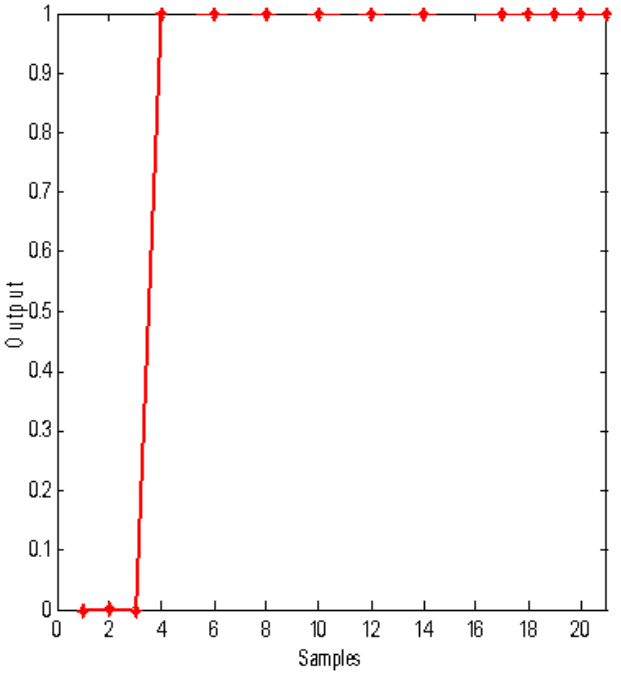

Fig.4.29 Test Output of phase C for fault on phase C

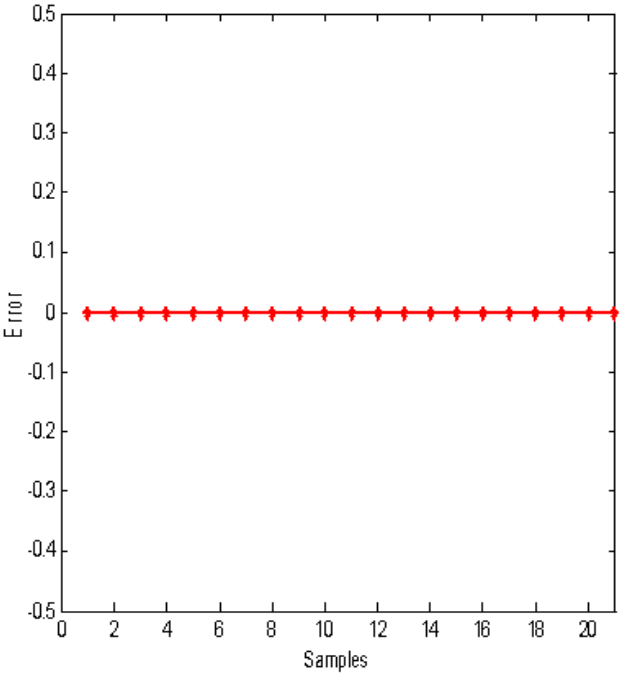

Fig.4.30 Test Error of phase C for fault on phase C

Figs. 4.29 and 4.30 show the ANFIS test output and test error of phase C when an inter-turn short circuit fault occurs on phase C inside the stator winding of an induction motor. From Fig. 4.29 ANFIS test output is equal to zero for first three samples and is equal to one for the faulty

condition from 4 to 21 samples with good accuracy. Fig.4.29 shows that the MLPNN is able to locate correctly the fault occurring on phase C. The testing error is 0 as shown in Fig.4.30.

TABLE IV
COMPARISON BETWEEN TRAINING ERRORS

Training Errors	MLPNN	RNN	RBFNN	ANFIS
Fault on Phase A	7.1701×10^{-6}	2.7000×10^{-3}	7.6403×10^{-7}	8.3087×10^{-8}
Fault on Phase B	1.4800×10^{-2}	5.6651×10^{-4}	6.5409×10^{-7}	2.3047×10^{-8}
Fault on Phase C	9.0743×10^{-7}	4.6000×10^{-3}	1.7904×10^{-7}	3.9841×10^{-8}
MSE	1.3300×10^{-6}	5.9480×10^{-5}	1.5510×10^{-7}	8.5580×10^{-9}

TABLE V
COMPARISON BETWEEN TESTING ERRORS

Testing Errors	MLPNN	RNN	RBFNN	ANFIS
Error of Phase A for Fault on Phase A	2.8400×10^{-5}	2.1089×10^{-4}	5.2727×10^{-7}	1.5045×10^{-7}
Error of Phase B for Fault on Phase A	2.8297×10^{-5}	2.1083×10^{-4}	4.0955×10^{-7}	9.5000×10^{-8}
Error of Phase C for Fault on Phase A	3.1063×10^{-5}	2.1083×10^{-4}	2.2727×10^{-7}	4.0909×10^{-8}
Error of Phase A for Fault on Phase B	4.9091×10^{-8}	1.8000×10^{-3}	1.3182×10^{-8}	3.8636×10^{-8}
Error of Phase B for Fault on Phase B	1.1900×10^{-2}	1.8000×10^{-3}	1.8182×10^{-7}	3.3636×10^{-8}
Error of Phase C for Fault on Phase B	7.0909×10^{-8}	1.8000×10^{-3}	3.6364×10^{-8}	3.1818×10^{-8}
Error of Phase A for Fault on Phase C	1.9227×10^{-7}	1.5000×10^{-3}	1.1364×10^{-7}	1.3182×10^{-7}
Error of Phase B for Fault on Phase C	4.5455×10^{-8}	1.5000×10^{-3}	1.8182×10^{-8}	6.7273×10^{-8}
Error of Phase C for Fault on Phase C	2.9314×10^{-6}	1.5000×10^{-3}	1.8182×10^{-8}	0.0000

From table IV and V, we got that both the training and testing errors in case of using an adaptive neural fuzzy inference system is less as compared to the other soft computing techniques. Hence it proves that the ANFIS based technique is better and it can detect and locate the inter-turn short circuit faults in the stator winding of an induction motor accurately.

4.4 Chapter Summary

In this chapter, an application of adaptive neural fuzzy inference system (ANFIS) technique to locate the stator inter-turn fault of an induction motor has been presented. The diagnostic process is carried out through monitoring simultaneously the values of the three phase shifts between the line currents and the phase voltage by the adaptive neural fuzzy inference system (ANFIS).

The training performance in case of using ANFIS technique is better as compared with RBFNN technique as shown in Fig. 4.12. The training MSE converged faster towards zero in case of ANFIS technique as compared with RBFNN technique. Both training and testing results of using ANFIS technique are less as compared with RBFNN technique. Hence it proves that the ANFIS based technique can diagnosis the inter-turn short circuit faults in the stator winding of an induction motor accurately.

Chapter 5

Fault Detection Scheme using Discrete Wavelet Analysis

5.1 Introduction

Wavelet Transform (WT) is a powerful signal analysis tool that has been used successfully in many areas for more than a decade. It is the transform of a signal from one form to another form. It does not change the information content present in the signal. The multi-resolution analysis (MRA) is one of the most active branches of the wavelet transform (WT) theory. The multi-resolution analysis (MRA) provides an effective way to examine the features of a signal at different frequency bands. This feature may be essential for pattern recognition. Hence it is well suited for the fault identification and classification problems in an induction motor.

The wavelet transform provides a time-frequency representation of the signal. The short time Fourier transform (STFT) gives a constant resolution at all frequencies, while the wavelet transform uses multi-resolution technique by which different frequencies are analyzed with different resolutions. The wavelet transform was developed to overcome the short coming of the short time Fourier transform (STFT), which can also be used to analyze the non-stationary signals.

Recently, the applications of wavelet transforms in induction motor fault detection have been reported in [58, 59, and 60]. In [58] the discrete wavelet transform technique is applied to the diagnosis of the cage motor condition using transient stator currents. The approach is based on the identification of characteristic patterns introduced by fault components in the wavelet signals obtained from the discrete wavelet transform of transient stator currents. A diagnosis of rotor asymmetries in induction motors based on the transient extraction of fault components using filtering techniques have been proposed in [59]. A new algorithm for transient motor current signature analysis using wavelets has been presented in [60]. In this chapter, the inter-turn fault

detection in the stator winding of an induction motor using wavelet technique has been proposed. The results obtained for both healthy and faulty condition are presented.

5.2 Discrete Wavelet Transform

Wavelets are functions [61], that satisfy the requirement of both time and frequency localization. Wavelets are localized in both time (through translation) and frequency (through dilation). Wavelet can produce multiple resolutions in both time and frequency domain. The signal can be accurately reproduced with the wavelet analysis using relatively small number of components [62]. The analyzing wavelets are called the 'mother wavelets' and its dilated and translated versions are called the 'daughter wavelets'.

5.2.1 Motivation of using Discrete Wavelet Transform

The wavelet multi-resolution analysis (MRA) is a new and powerful method of signal analysis well suited to fault generated signals [63]. The windowing of wavelet transform is adjusted automatically for low and high frequencies, i.e. it uses short time intervals for high frequency components and long time intervals for low frequency components and thereby, each frequency components gets treated in the same manner without requiring any reinterpretation of the results. This gives the wavelet transform much greater compact support for the analysis of the signals with localized transient components. The time frequency localization means that more energetic wavelet coefficients are localized. This is useful for feature extraction. Therefore, it is well suited for the fault location problem in the electrical machines.

The Fourier transform has been the main frequency domain analysis tool in many applications [64]. However, it cannot provide accurate time-frequency information of a signal, because any time-local information in the original signal, such as an abrupt change, is spread out over the whole frequency axis after transformation, due to the infinite length of its basis function. This problem is partly solved by the short time Fourier transform (STFT) [65], where the basis function is localized by multiplying with a time window centered at a different instant. STFT can describe the frequency components of a signal at a specified time. Nevertheless, as a single window is used for all frequencies, the resolution of the STFT cannot vary for different frequencies. Compared with STFT, the window length is variable in the wavelet transform (WT),

which is especially described in many applications. The continuous wavelet transform (CWT) of a signal x (t) is defined as

$$CWT(x,a,b) = \frac{1}{\sqrt{|a|}} \int_{-\infty}^{+\infty} x(t)\psi(\frac{t-b}{a})dt \qquad (5.1)$$

where

ψ = the wavelet function.

a = scaling (dilation) constant.

b = translation (time shift) constant.

In general, the mother wavelet is compactly supported in both time-domain and frequency-domain which together with dilation and translation operations, provides variable time-frequency resolution ability for different frequencies.

The wavelet is simply a sampled version of the continuous wavelet transform, and the information it provides is highly redundant as far as the reconstruction of the signal is concerned. This redundancy on the other hand requires a significant amount of computation time. To overcome these problem discrete wavelets provides sufficient information both for analysis and synthesis of the original signal with a significant reduction in the computation time. For a signal x(t), wavelet transform of sampled waveforms can be obtained by implementing the DWT, which is given by

$$DWT(x,a,b) = \frac{1}{\sqrt{a_0^m}} \sum_k x(k)\psi(\frac{t-ka_0^m}{a_0^m}) \qquad (5.2)$$

where the parameters a and b in (5.1) are replaced by a_0^m and ka_0^m, k and m being integer variables. Associated with the wavelet is a scaling function $\varphi(t)$. The scaling function along with the wavelet function creates an MRA of the signal.

The scaling function of one level can be represented as a sum of a scaling function of the next finer level.

$$\varphi(t) = \sum_{n=-\infty}^{\infty} h(n)\sqrt{2}\varphi(2t-n) \tag{5.3}$$

The wavelet function is also related to the scaling function by

$$\psi(t) = \sum_{n=-\infty}^{\infty} h_1(n)\sqrt{2}\varphi(2t-n) \tag{5.4}$$

where h(k) and $h_1(k)$ represents the scaling and wavelet functions respectively, and are related as

$$h_1(k) = (-1)^k h(1-k) \tag{5.5}$$

We can make use of the scaling function to represent the signal as

$$y(t) = \sum_{k=-\infty}^{\infty} C_{j0}(k)2^{j0/2}\varphi(2^{j0}t-k) + \sum_{k=-\infty}^{\infty}\sum_{j=j0}^{\infty} d_j(k)2^{j/2}\psi(2^j t-k) \tag{5.6}$$

where j0 represents the coarsest scale spanned by the scaling function.

The scaling and wavelet coefficients of the signal y (t) can be evaluated by using a filter bank of quadrature mirror filter

$$C_j(k) = \sum_{m=-\infty}^{\infty} C_{j+1}(m)h(m-2k) \tag{5.7}$$

$$d_j(k) = \sum_{m=-\infty}^{\infty} C_{j+1}(m)h_1(m-2k) \tag{5.8}$$

Equations (5.7) and (5.8) show that the coefficients at a coarser level can be attained by passing the coefficients at the finer level to their respective filters followed by a decimation of two. This will result in the number of samples at the finer level. For a signal that is sampled at a frequency higher than the Nyquist frequency, the samples are used as $C_{j+1}(m)$.

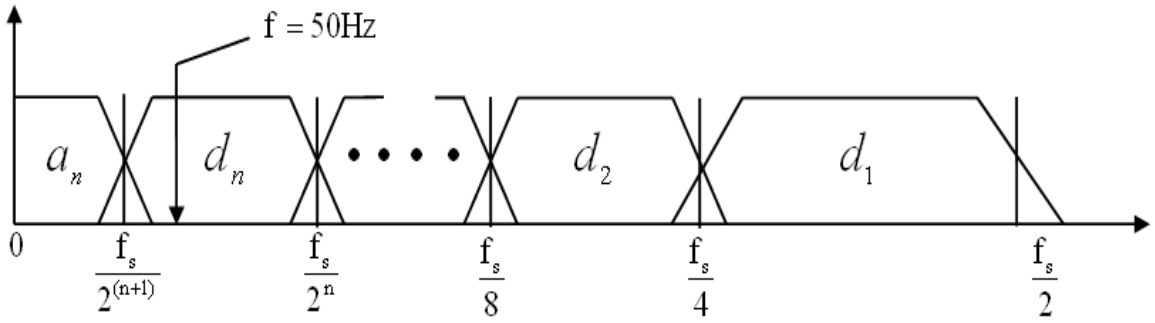

Fig.5.1 Filtering Process performed by the DWT

The main idea that underlies the application of discrete wavelet transform (DWT) is the involvements of the successive pairs of high and low pass filters at each scaling stage of wavelet transform. Providing a certain sampled signal, discrete wavelet transform (DWT) decomposes it into several wavelet signals (an approximation signal a_n and n detail signal d_k) [66, 67]. A certain frequency band is associated with each wavelet signal. The wavelet signal reflects the time evaluation of the frequency components of the original signal, which are contained within its associated frequency band [68].

More concretely, if f_s (in samples per second) is a sampling rate used for capturing the signal, then the d_k contains the information concerning the signal components with frequencies included in the interval

$$f(d_k) \in [2^{-(k+1)}.f_s, 2^{-k}.f_s]Hz \tag{5.9}$$

The approximation signal a_n includes the low-frequency components of the signal belonging to the interval.

$$f(a_n) \in [0, 2^{-(n+1)}.f_s]Hz \tag{5.10}$$

Therefore, discrete wavelet transform (DWT) carries out the filtering process shown in Fig.5.1. Note that the filtering is not ideal, a fact leading to a certain overlap between the adjacent frequencies bands [69, 70]. This causes some distortion if a certain frequency component of the signal is close to the limit of a band.

5.3 DWT Based Fault Identification

Fig.5.2 shows a scheme with the steps that should be followed in order to apply the discrete wavelet transform (DWT) based methodology for the diagnosis of inter-turn short circuit faults in the stator winding of an induction motor.

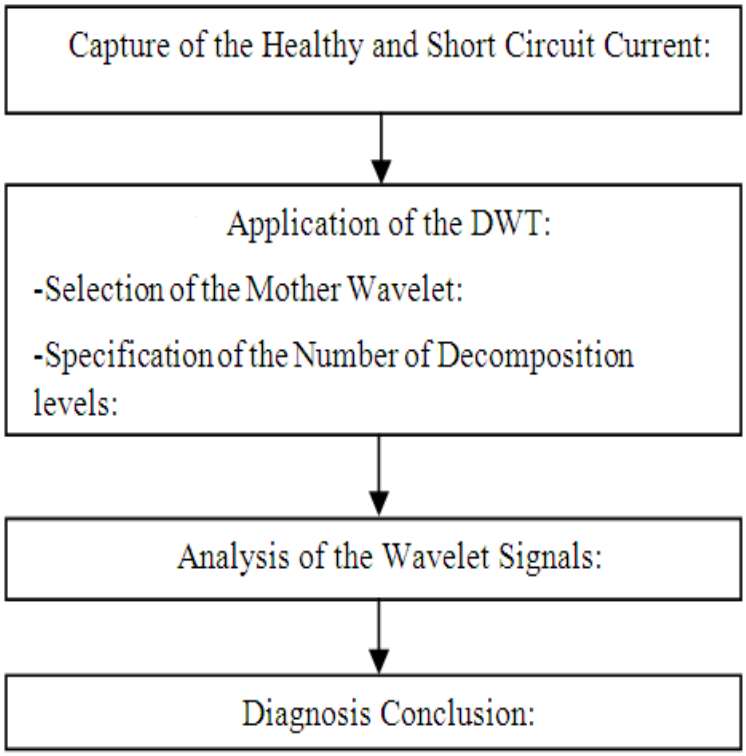

Fig.5.2. Flowchart for the DWT-based diagnosis methodology

5.3.1 Capture of the Phase Currents under Healthy and Faulty Condition

The first step to be carried out for the discrete wavelet based fault diagnosis consists of the capture of the currents both under healthy as well as inter-turn short circuit condition of an induction motor. It must be considered, when capturing the current signal that the sampling frequency f_s play an important role. Taking into account the Nyquist criterian, a very high sampling frequency is not mandatory for the application of the method [69], since most of the important fault components are usually in the low-frequency region. Sampling frequencies of 2 or 5K samples f_s enables good resolution analyses.

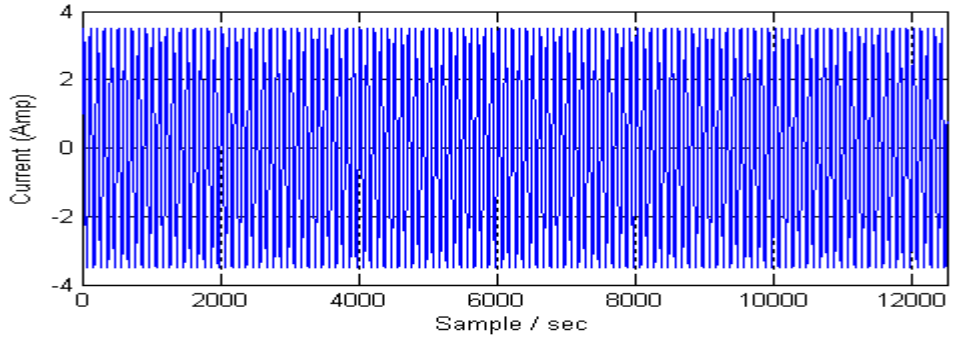

Fig.5.3 Stator Phase current in case of healthy condition

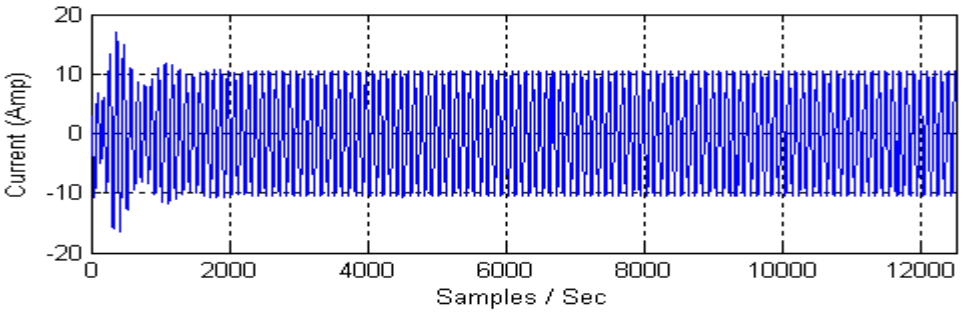

Fig. 5.4 Stator A phase current in case of faulty condition

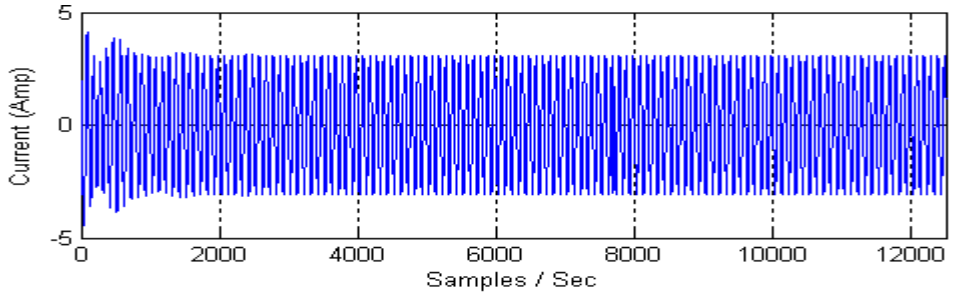

Fig.5.5 Stator B phase current in case of faulty condition

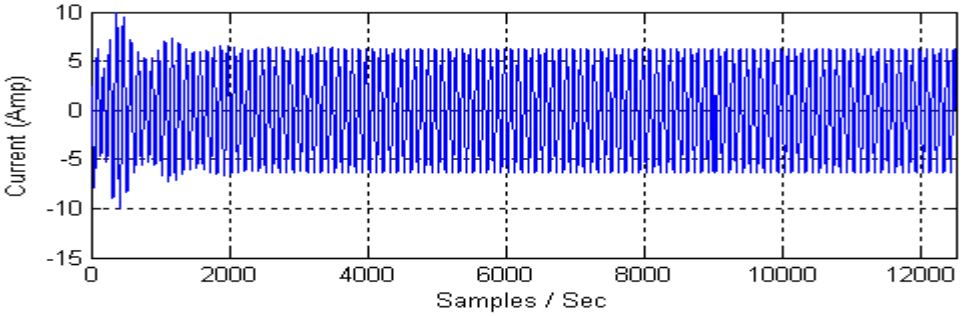

Fig.5.6 Stator C phase current in case of faulty condition

It may be noted that, due to the non-ideal filtering carried out by the wavelet signals (Fig.5.1), it is advisable not to set the limits of the band of the wavelet signal containing the fundamental frequency f very close to this frequency. Otherwise, this component could partially be filtered

within the adjacent bands, masking the evolution of other components within these bands due to its much higher amplitude. Typically, sampling frequencies being dyadic multiples of around 40 Hz (for instance, 5000 samples/s) are recommended for the application in the fault diagnosis of an induction motor.

5.3.2 Application of the DWT

Before the application of the discrete wavelet transform (DWT), first we have to select the type of mother wavelet and the number of decomposition levels.

5.3.2.1 Selection of the Mother Wavelet

An important step is the selection of the mother wavelet to carry out the analysis. The selected mother wavelet is related to the coefficients of the filters used in the filtering process inherent to the DWT [67, 68]. There are several wavelet families with different mathematical properties have been developed [67]. These wavelets are Infinite supported wavelets (Gaussian, Mexican Hat, Morlet, Meyer, etc.) and wavelets with compact support (orthogonal wavelets such as Daubechies or Coiflet, and biorthogonal wavelets) etc [67]. In the field of fault diagnosis of an induction motor, some families have shown better results for particular applications.

However, it has to be remarked that, in the case of compactly supported wavelets, once the wavelet family is selected, it is advisable to carry out the DWT using a high-order mother wavelet; this is a wavelet with an associated filter with a large number of coefficients. If a low-order wavelet is used, the frequency response gets worse, and the overlap between adjacent frequency bands as shown in Fig.5.1 increases. Daubechies wavelet with orders higher than 20 has shown satisfactory results. In our case we have used Daubechies-44 as the mother wavelets used for the DWT analyses.

5.3.2.2 Specification of the Number of Decomposition Levels

The number of decomposition levels is determined by the low-frequency components to be traced. The extracted frequency band becomes lower if the number of decomposition levels of the DWT becomes higher as shown in Table.VI. So, the evolution of these components will be reflected through the high-level signals resulting from the analysis.

TABLE VI
FREQUENCY BANDS FOR THE WAVELET SIGNAL

Level	Signal	Frequency Band for f_s=5000 samples/sec
d_1	Detail Signal	1250-2500Hz
d_2		625-1250Hz
d_3		312.5-625Hz
d_4		156.25-312.5Hz
d_5		78.12-156.25Hz
d_6		39.06-78.12Hz
a_6	Approximation Signal	0-39.06Hz

Typically, for the extraction of the frequency components caused by rotor asymmetries or even eccentricities, the number of decomposition levels should be equal or higher than that of the detail signal containing the fundamental frequency. This number of decomposition levels (n_f) is by given by [61].

$$n_f = \text{integer}\left[\frac{\log(f_s/f)}{\log(2)}\right] \tag{5.11}$$

For instance, considering f_s = 5000 samples/s and f = 50 Hz, the application of (8) leads to n_f = 6.

According to equations (5.9) and (5.10), the frequency bands associated with each wavelet signal are the ones shown in Table VI. Once the mother wavelet and the number of decomposition levels have been selected, it is possible to carry out the DWT of the analyzed signal.

5.3.3 Analysis of the Wavelet Signals

The next step to be carried out consists of the study of the wavelet signals resulting from the DWT. Two different and complementary types of analyses should be carried out, i.e., a qualitative analysis and a quantitative analysis.

1) Qualitative Analysis: The aim of the qualitative analysis is to detect the presence of characteristic patterns caused by the evolution of the stator inter-turn fault components during the inter-turn short circuit fault through the oscillations appearing in the wavelet signals. More specifically, this step comprises three phases described as follows.

i) Physical analysis in order to determine the theoretical transient evolution of the fault-related components to be detected. The evolution will be justified in both amplitude and frequency. As an example, Figs. 5.3, 5.4, 5.5, and 5.6 show the stator phase currents in healthy as well as faulty three phase currents, respectively.

ii) Determination of the frequency bands through which the fault-related component evolves. Each wavelet signal reproduces the evolution of the theoretical signal in the corresponding frequency band associated with that wavelet signal. Therefore, knowing the frequency bands through which the component evolves, one can detect the presence of the fault-related component through the oscillations appearing in the wavelet signals covering those bands. These oscillations will be arranged in a characteristic way, according to the evolution in amplitude and frequency of the fault component during the transient.

iii) Determination of the type of fault, depending on the characteristic pattern arising from the oscillations in the wavelet signals.

2) Quantitative Analysis: Once the condition of the machine has preliminarily been diagnosed, using the qualitative identification of characteristic patterns, it is advisable to compute the quantification parameters defined for the corresponding fault in order to assess the degree of failure in the machine.

These parameters can also be used for generating alert signals in non-supervised monitorized systems. Although alerts based on quantitative parameters are not as reliable as the identification of a characteristic pattern, they have the advantage of being much easier to be implemented.

In Section 5.5, some non-dimensional parameters will be introduced and computed for the cases qualitatively analyzed in the Section 5.4.

5.3.4 Diagnosis Conclusion

Once the qualitative patterns associated with a particular fault have been detected and the failure severity has been quantified, the diagnosis conclusion can be reached.

5.4 Results and Discussions

In this section, discrete wavelet transform is applied for diagnosing induction machine under healthy as well as stator inter-turn faulty operating condition. A detailed interpretation of the signals resulting from DWT is provided for each case. The tests were performed in the laboratory using a squirrel cage motor with four poles, 552 turns per phase winding on the stator, rated 1.5 kW, 415 V, 50 Hz as discussed in chapter 2. The phase currents were used as the diagnostic signal.

5.4.1 Diagnosis of a Healthy Induction Motor

Fig 5.7 shows the sampled healthy phase current (signal s, at the top) and the signals resulting from the DWT i.e approximation signal (a_6), and detail signals (d_6… d_1). These graphs are explained below.

i) The approximation signal a_6 does not show any relevant pattern once the initial oscillation due to electromagnetic transient is extinguished. This means that there are no significant low-frequency components (below 39.06 Hz) within the signal.

ii) The detail signal d_6 practically reproduces the analyzed healthy current. This is because, for the sampling frequency used, the frequency band corresponding to this signal is [39.06, 78.12] Hz (see Table VI) and so includes the fundamental component of the current, which is more than 30 times greater than the rest of the components.

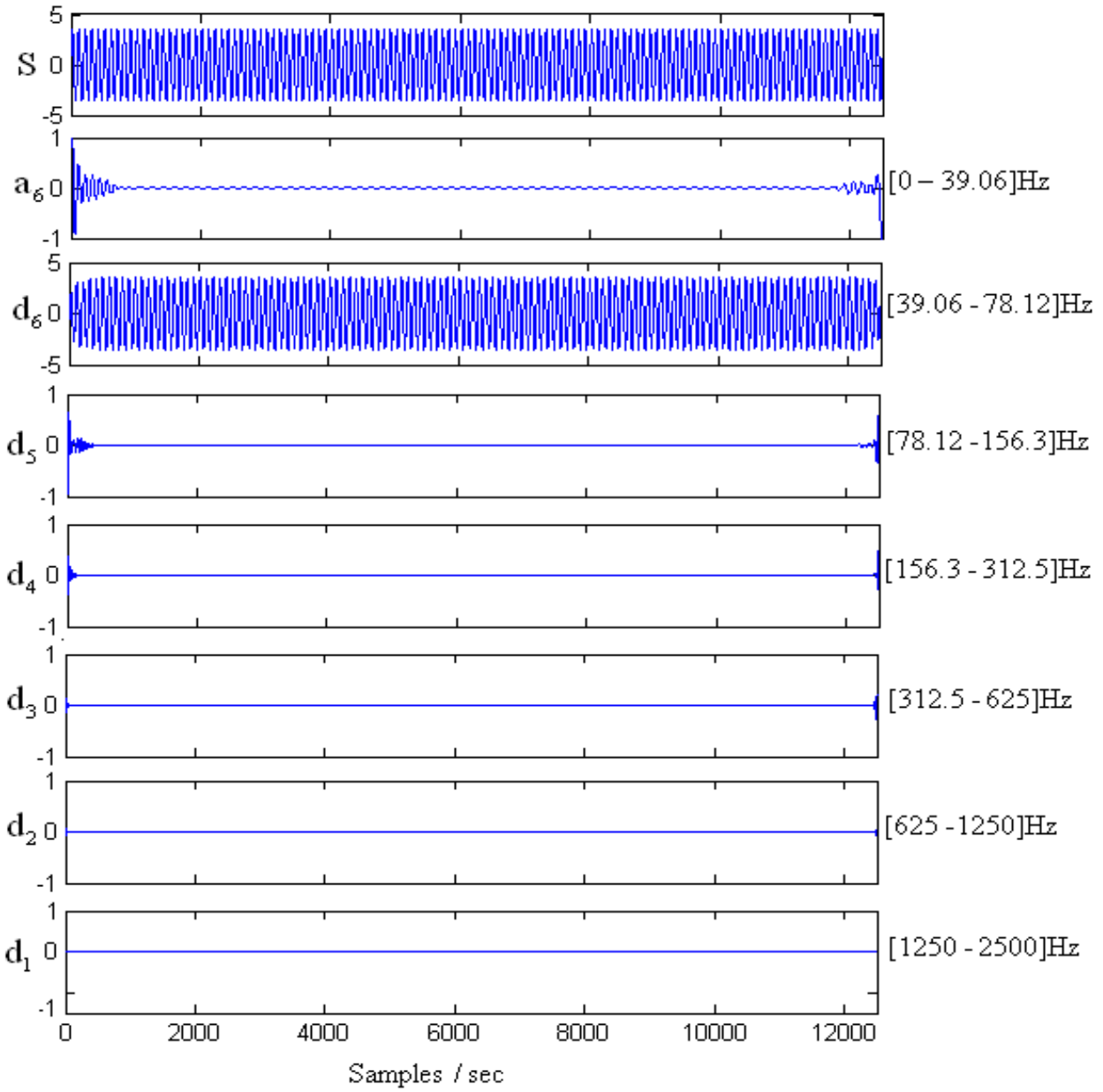

Fig.5.7 DWT of stator phase current of a healthy Induction Motor

iii) The detail pattern signal d_5 is produced by a component with frequency increasing with time. In the detail pattern d_5 at 525 samples per second (t = 0.105 sec) its frequency becomes higher than 78.12 Hz and the component penetrates within the detail pattern signal d_5. For the detail signal pattern d_4, d_3, d_2 and d_1 which contains very high frequency signals as shown in Fig. 5.7. From which it can be seen that no oscillations are there after the initial electromagnetic transient. This is due to the fact that the machine is healthy and therefore, no significant patterns exist after the transient condition.

5.4.2 Diagnosis of a Faulty Induction Motor

The previous test was repeated but using a machine in which the stator winding turns are shorted artificially in the different phases of an induction motor. Figs. 5.8, 5.9 and 5.10 show the sampled stator inter-turn faulty current (signal s, at the top) and the signals resulting from the DWT i.e approximation signal (a_6), and detail signals (d_6… d_1).

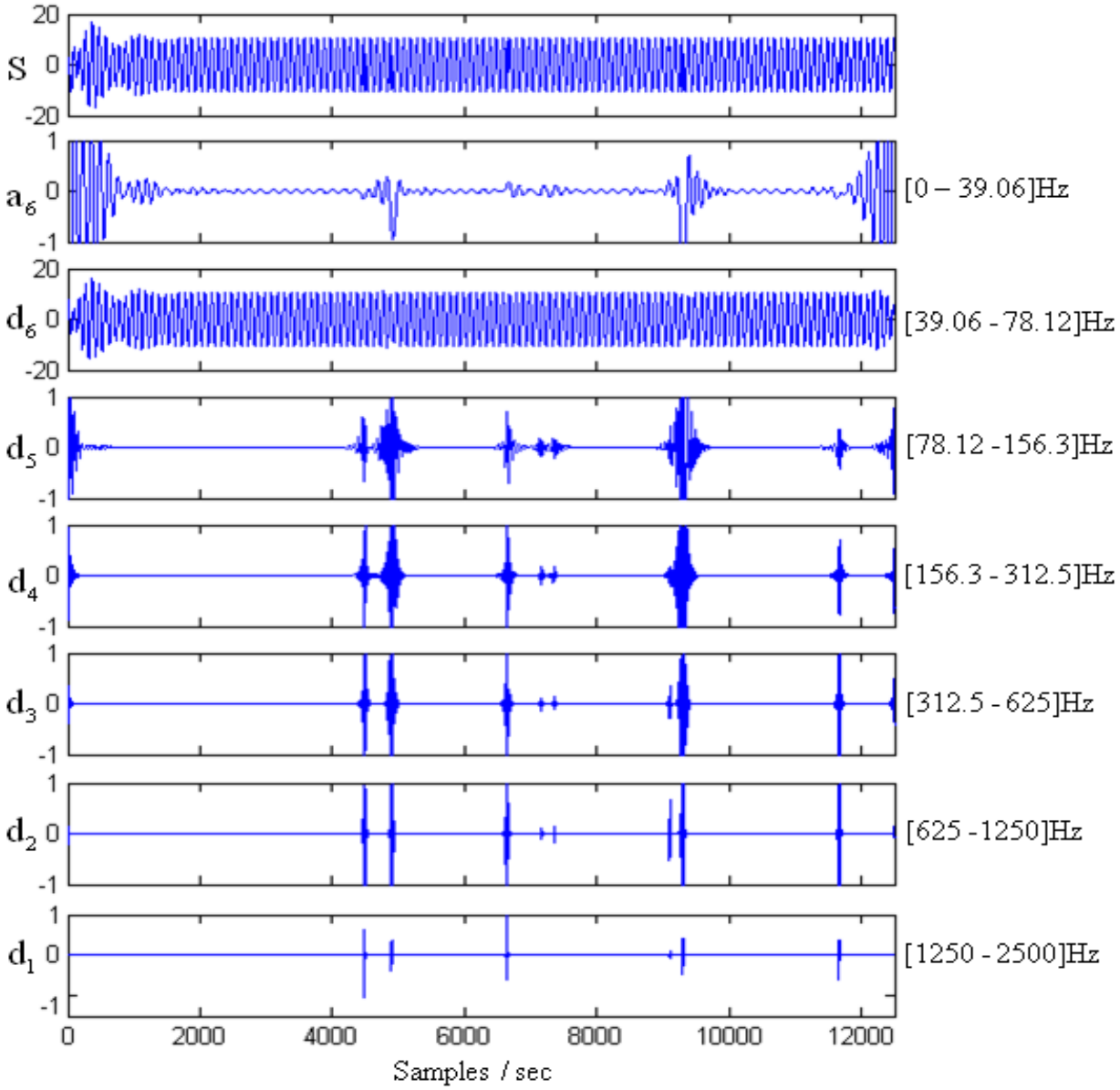

Fig.5.8 DWT of stator A phase current of a Faulty Induction Motor

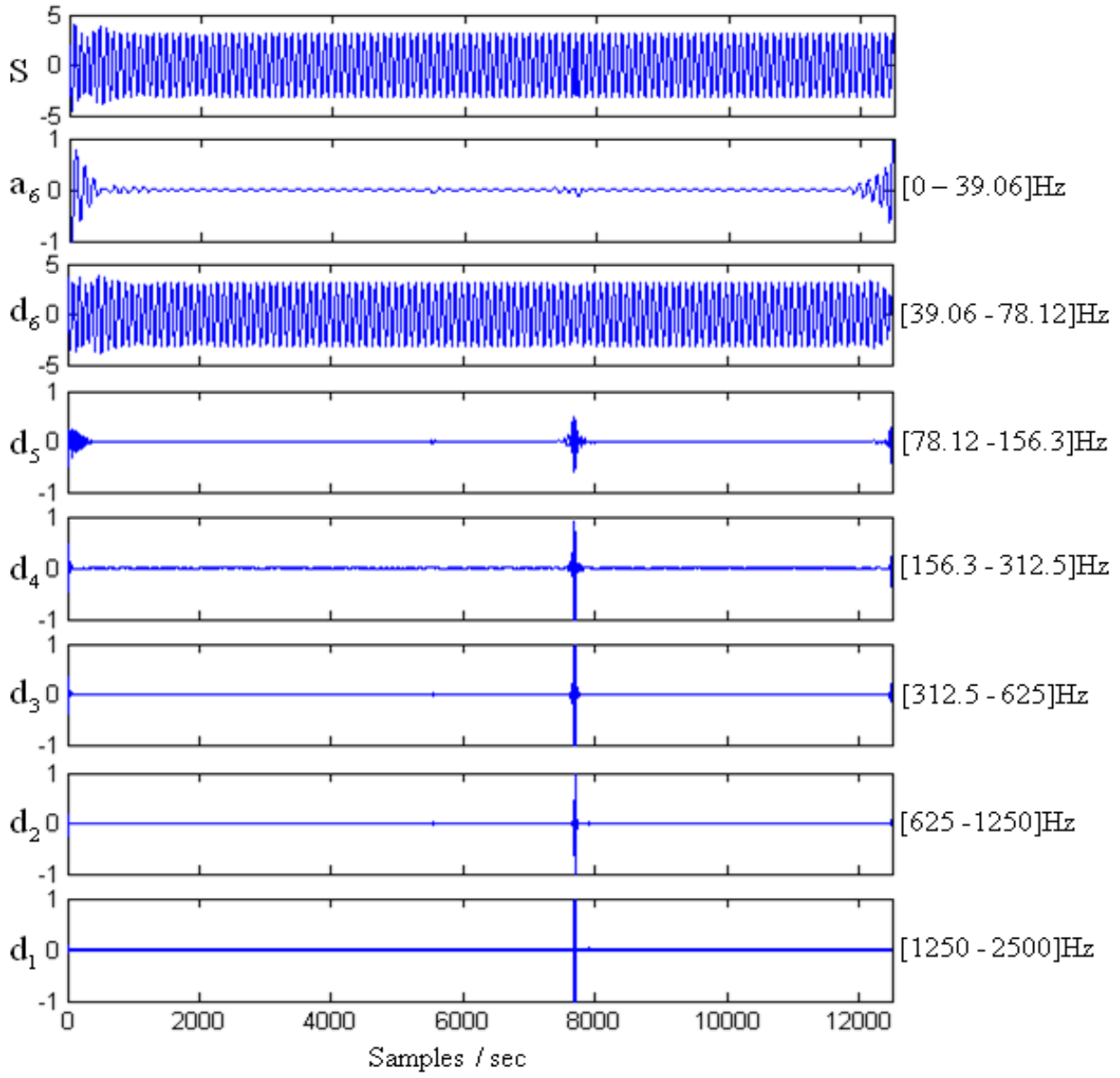

Fig.5.9. DWT of stator B phase current of a Faulty Induction Motor

i) From Figs. 5.7, 5.8, 5.9 and 5.10, it is clearly observed that the inter-turn fault can detected through the alteration of the approximation signal a_6, we get a clearly disturbance was occurred after the initial electromagnetic transient was extinguished.

ii) The detail signal d_6 practically reproduces the analyzed induction motor stator inter-turn short circuit fault current. This is because, for the sampling frequency used, the frequency band corresponding to this signal is [39.06, 78.12] Hz (see Table VI) and so includes the fundamental component of the current, which is more than 30 times greater than the rest of the components.

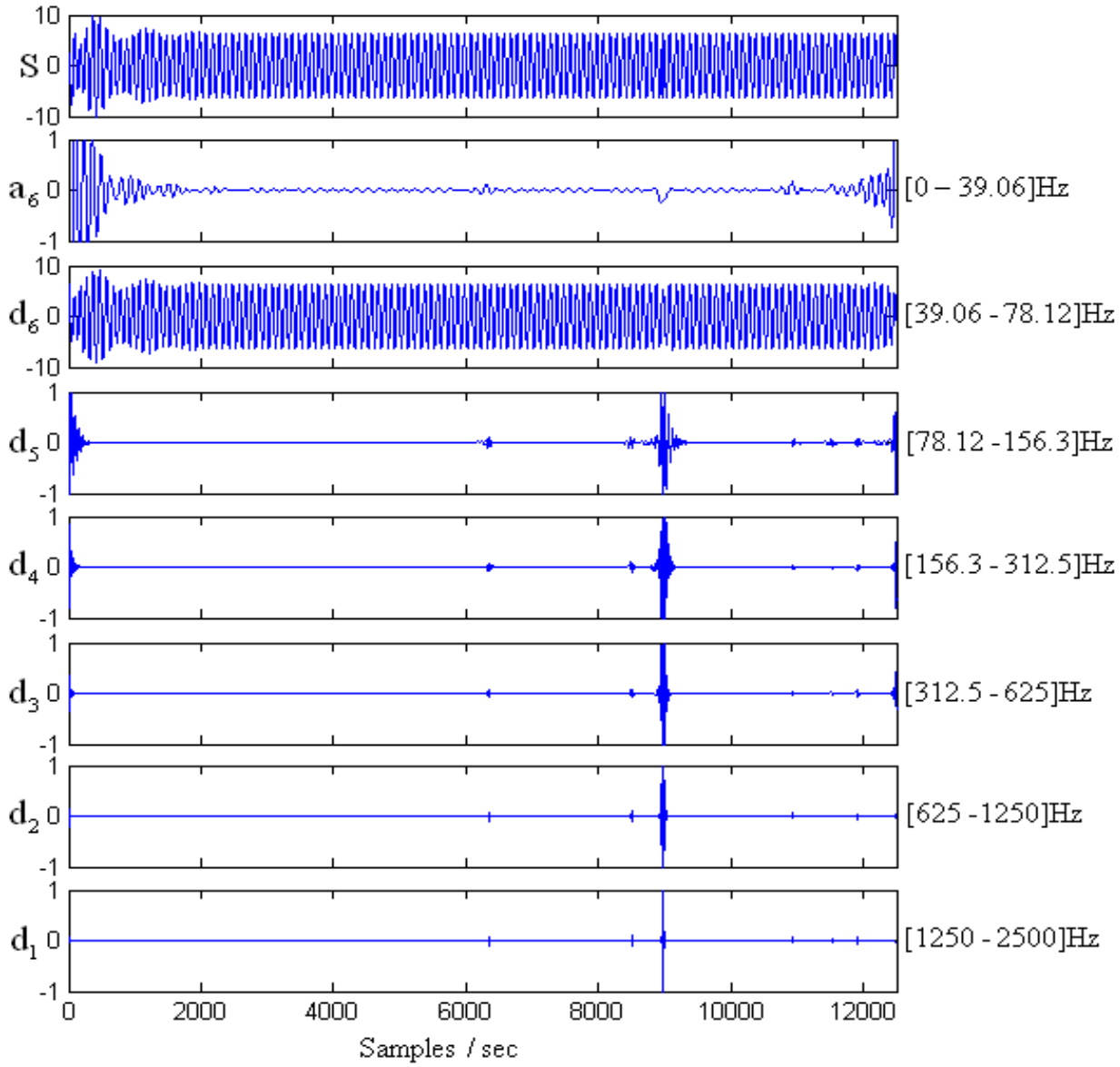

Fig.5.10 DWT of stator C phase current of a Faulty Induction Motor

iii) From the detail signals d_5, d_4, d_3, d_2, and d_1 a clear oscillation was observed after the initial transient. This oscillation is produced by a component with frequency increasing with time. Comparing Figs. 5.7, 5.8, 5.9 and 5.10, it is clearly show that, in case of Fig. 5.7 no significant oscillation is appeared after the initial transient due to the healthy condition but from the Figs. 5.8, 5.9, and 5.10 a clear significant oscillation is appeared after the initial transient due to inter-turn short circuit fault in the stator winding of an induction motor. This is due to the fact that the machine is under inter-turn faulty condition and therefore, some significant inter-turn fault components exist.

5.5 Quantification of the Degree of Severity of Fault

The qualitative analysis described in section 5.4, it is shown that in faulty conditions the oscillations reflecting the evolution of fault components appear in one or several wavelet signals. These oscillations lead to increase in the energy of the involved wavelet signals which can be used as a basis for defining the parameters for the quantification of the severity of the fault.

A general expression for calculating the non-dimensional parameters based on the increments of the energy of a wavelet signal is given as

$$\gamma_{nf}\,(\text{in decibels}) = 10\log\left[\frac{\sum_{j=Nb}^{Ns} i_j^2}{\sum_{j=Nb}^{Ns}\left[A_{nf}(j)\right]^2}\right] \qquad (5.12)$$

where i_j is the value of the j^{th} sample of the current signal, $A_{nf}(j)$ is the j^{th} element of the order n_f approximation signal. N_s are the number of samples of the signals until a steady state region is reached, and N_b is selected in such a way that the oscillations appearing in the wavelet signal due to the electromagnetic transient phenomena are avoided. The parameters calculated by using equation (5.12) represent the ratio between the energy of the tasted short circuit current and the energy of the wavelet signal used for the quantification within referred time interval, expressed in decibel.

In this case, for the calculation of the fault parameter γ_{nf}, where $N_f = d_5$ is selected, because the approximation with level 5 is the signal used for carrying out the diagnosis. The value of N_b and Ns are selected according to the evolution of the signals in healthy state (Fig.5.7).

The value of N_b= 525(0.105 sec) samples have been selected since at this time the initial oscillation caused by the electromagnetic switch on transient are practically extinguished in d_5. The selected value of N_s=12068(2.4136 sec.) corresponds to the end of the oscillations due to the fault. Table VII shows the fault parameters for both the healthy and faulty machine. So we conclude from the Table VII that the proposed parameters suffer significant reductions when an inter-turn short circuit fault occurs in the stator windings of an induction motor.

TABLE VII
CALCULATED QUANTIFICATION PARAMETERS

Test	Inter-turn Short Circuit fault
Wavelet Signal	d_5
N_b	525
N_s	12068
Healthy Machine	41.66 dB
Faulty Machine (A phase)	27.618 dB
Faulty Machine (B phase)	36.40 dB
Faulty Machine (C phase)	33.10 dB

5.6 Chapter Summary

In this chapter, the discrete wavelet transform technique is applied to locate the stator inter-turn fault of an induction motor. This technique is based on the analysis of stator phase currents under both healthy and inter-turn faulty condition. By using the discrete wavelet transform analysis employing daubechies-44 as the mother wavelet, the approximation signals and detail signals of the fault patterns of the machine are generated. From those generated detail signals the severity of the fault condition can be determined.

From the results presented and analysis made in section 5.4, it is obvious that the machines subjected to inter-turn short circuit fault can be diagnosed through the characteristic patterns caused by inter-turn short circuit fault components in the DWT analysis by using the stator phase currents. Oscillations after the initial transient are not observed in case of healthy condition, but some oscillations after the initial transient are notified in case of inter-turn faulty condition. In this work by using the fault current patterns we are also able to find out the quantification of the degree of severity of the stator inter-turn fault in an induction motor. Thus the simulation study, analysis and results presented in this work prove the efficacy of discrete wavelet transform technique in induction motor fault diagnosis.

Chapter 6

Conclusions and Suggestions for Future Work

6.1 Summary of the thesis work

The thesis has mainly investigated on detection and location of an inter-turn short circuit fault in the stator winding of an induction motor. In this work, a number of neuro computing paradigms such as multilayer perceptron neural network (MLPNN), recurrent neural network (RNN), radial basis function neural network (RBFNN), and adaptive neural fuzzy inference system (ANFIS) have been used.

An experimental setup is developed for the generation of induction motor parameters such as stator resistance, rotor resistance, stator inductance, rotor inductance, and magnetizing inductance both under healthy and stator inter-turn short circuit fault conditions. For the generation of those parameters, we have conducted several tests (no-load test, DC test, and block rotor test) under both healthy and shorting the stator winding for every two turns sequentially, beginning with the start point of turn '1' and ending with the end point of turn '45' of the induction motor. To limit the circular loop current, a variable resistor is connected between the taps of the shorted portion of the winding turns. Those induction motor parameters are used in the model equation [36] to generate the currents in the different phases under both conditions. By using the model equation, the data (phase shift between the line currents and phase voltages) have been generated under both conditions at different load torques i.e τ_1 = 3 N-m, τ_2 = 5 N-m, τ_3 = 7 N-m which will be useful in subsequent chapters for studying stator inter-turn fault conditions.

A number of soft computing techniques such as multilayer perceptron neural network (MLPNN), recurrent neural network (RNN), radial basis function neural network (RBFNN) have been applied for the detection and location of stator inter-turn short circuit fault in an induction motor. In this work, weight parameters of the multilayer perceptron neural network and radial basis function neural network are updated by using the gradient descent algorithm but the weight parameter in case of recurrent neural network is updated by using real time recurrent learning algorithm. In terms of identification error, it is observed that the radial basis function neural network (RBFNN) based technique offer improved identification performance compared with multilayer perceptron neural network (MLPNN), and recurrent neural network (RNN) based techniques.

Adaptive neural fuzzy inference system (ANFIS) had gained popularity over other soft computing techniques due to its knowledge extraction feasibility, domain partitioning, rule structuring, and modifications. Hence we have developed ANFIS based technique for the detection and location of stator inter-turn short circuit fault of an induction motor. The identification results are compared in terms of identification capability. It is observed that the adaptive neural fuzzy inference system (ANFIS) based technique offer improved identification performance as compared with radial basis function neural network (RBFNN) based technique.

A discrete wavelet transform based technique has been proposed for the detection and location of an inter-turn short circuit fault in the stator winding of an induction motor. This technique is based on the analysis of stator phase currents under both healthy and inter-turn faulty conditions. In this work, Daubechies-44 is used as the mother wavelet. Using only the neural networks and adaptive neural fuzzy inference system technique one can find out the phase where the fault occurs but cannot find the severity of this fault. Thus this method is not only suitable to detect and locate the stator winding inter-turn fault but also to find out the severity of this fault in the different phases of an induction motor.

The objectives of the thesis proposed in 1.4 have been thus met and the limitations of existing multilayer perceptron neural network based stator inter-turn fault detection scheme of an induction motor have been overcome.

6.2 Thesis Contributions

The following are the contributions of the thesis.

- Development of an experimental setup for the generation of induction motor parameters under both healthy and inter-turn faulty conditions.
- Application of different soft computing techniques based fault diagnosis schemes of induction motor such as multilayer perceptron neural network (MLPNN), recurrent neural network (RNN), radial basis function neural network (RBFNN), and adaptive neural fuzzy inference system (ANFIS).
- Proposing discrete wavelet transform approach to detect and locate stator inter-turn short circuit fault together with identification of the severity of this fault in the stator winding of an induction motor.

6.2 Future scope of work

In the present work, several soft computing techniques have been presented for the detection and location of stator inter-turn short circuit fault in the stator winding of an induction motor.

- Discrete wavelet transform approach is successfully used to detect and locate stator inter-turn short circuit fault together with identification the severity of this fault in the stator winding of an induction motor. The same approach can be extended to identify the other faults such as bearing fault, rotor broken bar fault, and eccentricity related fault of an induction motor.
- Neural network ensembles are receiving increasing attention in the field of research such as control, fault diagnosis, decision making, identification, robotics etc. due to their learning and generalization abilities, nonlinear mapping, and parallelism of computation. However, for solving fault detection problems the neural networks may get stuck on a local minimum of the error surface, and the network convergence rate is generally slow. A suitable approach for overcoming these disadvantages is the use of wavelet functions in the network structure. Wavelet function is a waveform that has limited duration and an average value of zero. A wavelet neural network has a nonlinear regression structure that

uses localized basis functions in the hidden layer to achieve the input-output mapping. The integration of the localization properties of wavelets and the learning abilities of neural network results in the advantages of wavelet neural network over neural network for the detection and location of an inter-turn short circuit fault in the stator winding of an induction motor.

Bibliography

[1] P.F. Albrecht, J.C. Appiarius, R.M. McCoy, E.L. Owen, D.K. Sharma, Assessment of the Reliability of Motors in Utility Applications – Updated, IEEE Trans. Energy Convers. vol.: EC-1, issue 1, pp.39-46, 1986.

[2] A. H. Bonnett, G. C. Soukup, "Cause and Analysis of Stator and Rotor Failures in Three-Phase Squirrel-Cage Induction Motors," IEEE Trans. Ind. Appl., vol. 28, no. 4, pp. 921–937, 1992.

[3] S. Rajakarunakaran, P. Venkumar, K. Devaraj, and K. S. P. Rao, "Artificial Neural Network Approach for Fault Detection in Rotary System," Appl. Soft Comput., vol. 8, no. 1, pp. 740–748, 2008.

[4] P. V. J. Rodriguez, A. Arkkio, "Detection of Stator Winding Fault in Induction Motor Using Fuzzy Logic," Appl. Soft Comput., vol. 8, no.2, pp. 1112-1120, 2008.

[5] V.Uraikul, C.W.Chan, and P.Tontiwachwuthikul, "Artificial Intelligence for Monitoring and Supervisory Control of Process Systems," Eng. Appl. Artif. Intelligent, vol. 20, issue 2, pp.115–131, 2007.

[6] A. Siddique and G. S. Yadava, "A Review of Stator Fault Monitoring Techniques of Induction Motors," IEEE Trans. Energy Convers., vol. 20, no. 1, pp. 106–114, 2005.

[7] P. J. Tavner, A. F. Anderson, "Core Faults in Large Generators', IEE Proceedings on Electric Power Applications, Vol. 152, Issue 6, pp. 1427-1439, 2005.

[8] J. Ramirez-Nino, A. Pascacio, "Detecting Interturn Short Circuits in Rotor Windings," IEEE Comp. Appl. in Power, vol. 14, issue 4, pp. 39 - 42, 2001.

[9] N. Paterson, "The Analysis and Detection of Faults in Three Phase Induction Machines Using Finite Element Techniques," Doctoral Thesis, Robert Gordon University, Wetherby British Library, Aberdeen, 1998, UK, 180 p.

[10] Electric Power Research Institute, "Improved Motors for Utility Applications," Publication EL-2678, Vol. 1, 1763-1, final report, October, 1982.

[11] S. Barker, "Avoiding Premature Bearing Failure With Inverter Fed Induction Motors," Power Engineering Journal, Vol. 14, Issue 4, pp. 182-189, 2000.

[12] I. Kerszenbaum, “Shaft Currents in Electric Machines Fed by Solid-State Drives,” IEEE Conference on Industrial and Commercial Power Systems, Pittsburgh-PA, USA, May 4-7, pp. 71-79, 1992.

[13] P. Vas, “Parameter Estimation, Condition Monitoring, and Diagnosis of Electrical Machines’, Oxford, Clarendon, 1993, ISBN: 0198593759, 378 p.

[14] W. T. Thomson, R. J. Gilmore, “Motor Current Signature Analysis to Detect Faults in Induction Motor Drives–Fundamentals, Data Interpretation, and Industrial Case Histories,” Proceedings of the 32nd Turbo machinery Symposium, Houston, TX, USA, Sept. 8-11, pp. 145-156, 2003.

[15] S. Nandi, H. A. Toliyat, “Detection of Rotor Slot and Other Eccentricity Related Harmonics in a Three Phase Induction Motor With Different Rotor Cages,” Conference Proceedings of International Conference on Power Electronic Drives and Energy Systems for Industrial Growth–PEDES ’98, Perth, Australia, Nov. 30-Dec. 3, Vol. 1, pp. 135-140, 1998.

[16] A. Barbour, W. T. Thomson, “Finite Element Study of Rotor Slot Designs With Respect to the Current Monitoring for Detecting Static Airgap Eccentricity in Squirrel-Cage Induction Motor,” The 1997 IEEE Industry Applications Society Conference: The 32nd IAS Annual Meeting, New Orleans, Louisiana, Oct. 5-8, pp. 112-119, 1997.

[17] R. Isermann, “Model Based Fault Detection and Diagnosis—Status and Applications,” Annu. Rev. Control, vol. 29, no. 1, pp. 71–85, 2005.

[18] M. Arkan, D. Kostic-Perovic, P. J. Unsworth, “Modelling and Simulation of Induction Motors with Inter-Turn Faults for Diagnostics,” Electric Power Systems Research, vol. 75, pp. 57-66, 2005.

[19] M. Sahraoui, A. Ghoggal, S. E. Zouzou A. Aboubou, H. Razik “Modelling and Detection of Inter-Turn Short Circuits in Stator Windings of Induction Motor,” IEEE Trans. Energy Convers. vol.EC 1, issue 1, pp. 4981-4986, 2006.

[20] S. Bachir, S. Tnani, J. C. Trigeassou, and G. Champenois, “Diagnosis by Parameter Estimation of Stator and Rotor Faults Occurring in Induction Machines,” IEEE Trans. Ind. Electron., vol. 53, issue 3, pp. 963–973, 2006.

[21] F. L. Stanislaw, A .H. M. Sadrul Ula, A. M. Trzynadlowski, “Instantanious Power as a Medium for the Signature Analysis of Induction Motors,” IEEE Trans. Ind. Appl., vol. 32, no. 4, pp. 904-909, 1996.

[22] G. G. Yen, K. C. Lin, “Wavelet Packet Feature Extraction for Vibration Monitoring,” IEEE Trans. Ind. Electron., vol. 47, no. 3, pp. 650–667, 2000.

[23] W. Thomson and M. Fenger, “Current Signature Analysis to Detect Induction Motor Faults,” IEEE Ind. Appl. Mag., vol. 7, no. 4, pp. 26–34, 2001.

[24] K. Kim, A. G. Parlos, and R. M. Bharadwaj, “Sensorless Fault Diagnosis of Induction Motors,” IEEE Trans. Ind. Electron., vol. 50, no. 5, pp. 1038–1051, 2003.

[25] H. Douglas, P. Pillay, and A.K Ziarani, “A New Algorithm for Transient Motor Current Signature Analysis Using Wavelets,” IEEE Trans. Ind. Appl., vol. 40, no. 5, pp. 1361–1368, 2004.

[26] J-H Jung, J-J Lee, and B-H Kwon, “Online Diagnosis of Induction Motors Using MCSA,” IEEE Trans. Ind. Electron., vol. 53, no. 6, pp. 1842–1852, 2006.

[27] A. M. D. Silva, R. J. Povinelli and N. A. O. Demerdash, “Induction Machine Broken Bar and Stator Short-Circuit Fault Diagnostics Based on Three-Phase Stator Current Envelope,” IEEE Trans. Ind. Electron., vol. 55, issue.3, pp. 1310-1318, 2008.

[28] M. Riera- Guasp, J. A. Antonino-Daviu, M. Pineda-Sanchez, R. Puche-Panadero, J. Perez-Cruz, “ A General Approach for the Transient Detection of Slip-Dependent Fault Components Based on the Discrete Wavelet Transform,” IEEE Trans. Ind. Electron., vol. 55, no. 12, pp. 4167–4180, 2008.

[29] H. Nejjari, M. H. Benbouzid, “Monitoring and Diagnosis of Induction Motors Electrical Faults using a Current Park’s Vector Pattern Learning Approach,” IEEE Trans. Ind. Appl., vol. 36, no. 3, 2000.

[30] F. Filippetti, G. Franceschini, and C. Tassoni, “Recent Developments of Induction Motor Drives Fault Diagnosis Using AI Techniques,” IEEE Trans. Ind. Electron., vol. 47, no.5, pp. 994–1003, 2000.

[31] M. A. Awadallah, and M. M. Morcos, “ANFIS- Based Diagnosis and Location of Stator Inter-turn Faults in PM Brushless DC Motors,” IEEE Trans. Energy Conv., vol. 19, no. 4, pp. 795-796, 2004.

[32] W. W. Tan, H. Huo, “ A Generic Neuro-Fuzzy Model-Based Approach for Detecting Faults in Induction Motors,” IEEE Trans. Ind. Electron., vol. 52, no. 5, pp. 1420-1427, 2005.

[33] M. S. Ballal, Z. J. Khan, H. M. Suryawanshi, R. L. Sonolikar, “Adaptive Neural Fuzzy Inference System for the Detection of Inter-Turn Insulation and Bearing

Wear Faults in Induction Motor," IEEE Trans. Ind. Electron., vol. 54, no. 1, pp. 250–258, 2007.

[34] P. V. J. Rodriguez, A. Arkkio, "Detection of Stator Winding Fault in Induction Motor Using Fuzzy Logic," Appl. Soft Comput., vol. 8, no. 2, pp. 1112–1120, 2008.

[35] R. H. Abiyev, O. Kaynak, " Fuzzy Wavelet Neural Networks for Identification and Control of Dynamic Plants- A Novel Structure and a Comparative Study," IEEE Trans. Ind. Electron., vol. 55, no. 8, pp. 3133–3140, 2008.

[36] M. B. K. Bouzid, G. Champenois, N. M. Bellaaj, L. Signac, and K. Jelassi, "An Effective Neural Approach for the Automatic Location of Stator Inter-Turn Faults in Induction Motor," IEEE Trans. Ind. Electron., vol. 55, no. 12, pp. 4277-4289, 2008.

[37] N. Neale, Condition Monitoring Methods and their Interpretation. A guide to the condition monitoring of machines (pp 50-89). London: department of trade and industry press (1980).

[38] V. Wowk, Machinery Monitoring. Machinery Vibration- Measurement and Analysis (pp. 17-18). New York: McGraw-Hill Inc.

[39] A. H. Bonnet and G. C Soukup, "Cause and Analysis of Stator and Rotor Failure in Three Phase Squirrel Cage Induction Motor," IEEE Trans. on Ind. Appl. vol. 28, no. 4, 1998.

[40] G. C. Stone, B. K. Gupta and M. Kurtz, D. K. Sharma, "Investigation of Turn Insulation Failure Mechanism in Large AC Motors," IEEE Trans. on Power Apparatus and Systems, vol. pas-103, issue 9, pp. 2588-2595, 1984.

[41] B. K. Gupta, and I. M. Culbert, "Assessment of Insulation Condition in Rotating Machine Stators," IEEE Trans. Energy Conv., vol. 7, no. 3, pp. 500-508, 1992.

[42] P.G. McLaren and M.H. Abdel-Rahman, "Modelling of large AC Motor Coils for Steep Fronted Surge Studies," IEEE Trans. on Ind. Appl., vol. 24, no 3, pp. 422-426, 1988.

[43] F. Filippetti, G. Franceschini, and C. Tassoni, "A survey of AI Techniques approach for Induction Machines On-Line Diagnostics," in proc.PEMC'96, vol. 2, Budapest, Hunghary, pp. 314-418, 1996.

[44] S. Rajakarunakaran, P. Venkumar, K. Devaraj, and K. S. P. Rao, "Artificial Neural Network approach for Fault Detection in Rotary System," Appl. Soft Comput., vol. 8, no. 1, pp. 740-748, 2008.

[45] H. C. Cho, J. Knowles, M. S. Fadali, and K. S. Lee, "Fault Detection and Isolation of Induction Motors Using Recurrent Neural Networks and Dynamic Bayesian Modeling," IEEE Trans. on Control Systems Tech., vol. 18, no. 2, pp. 430-437, 2010.

[46] Z. R. Yang, "A Novel Radial Basis Function Neural Network for Discriminant Analysis," IEEE Trans. on Neural Networks, vol. 7, no. 3, pp. 604-612, 2006.

[47] M. Y. Chow and S. O. Yee, "Using Neural Networks to Detect Incipient Faults in Induction Motors," J. Neural Netw. Comput., vol. 2, no. 3, pp. 26-32, 1991.

[48] M. Y. Chow, R. N. Sharpe, and J. C. Humg,"On the Application and Design of Artificial Neural Networks for Motor Fault Detection," IEEE Trans. Ind. Electron., vol. 40, no. 2, pp. 181-196, 1993.

[49] X. Boqiary, L. Heming, and S. Liling, "Feature Signal Extraction of Inter-Turn Short Circuit Fault in Stator Windings of Induction Motors," In Proc. IEEE ICIT, Bangkok, Thailand, vol. 1, pp. 97-100, 2002.

[50] S. J. Hong and G. S. May, "Neural- Network- Based Sensor Fusion of Optical Emission and Mass Spectroscopy Data for Real-Time Fault Detection in Reactive ion Etching," IEEE Trans. Ind. Electron., vol. 52, no. 4, pp. 1063-1072, 2005.

[51] M. A. Awadallah, and M. M. Morcos, "ANFIS- Based Diagnosis and Location of Stator Inter-turn Faults in PM Brushless DC Motors," IEEE Trans. Energy Conv., vol. 19, no. 4, pp. 795-796, 2004.

[52] S. Altug, M. Y. Chow, and H. J. Trussell, "Fuzzy Inference System Implemented on Neural Architectures for Motor Fault Detection and Diagnosis," IEEE Trans. Ind. Electron., vol. 46, no. 6, pp. 1069-1079, 1999.

[53] T. Takagi and M. Sugeno, "Derivation of Fuzzy Control Rules from Human Operator's Control Actions," In Proc. IFAC Symp., Fuzzy Inform., Knowledge Representation and Decision Analysis, pp. 55-60, 1983.

[54] L. V. Kantorovich and G. P. Akilov, Functional Analysis, second edition. Oxford, UK, Pergamon, 1982.

[55] H. L. Royden, Real Analysis, seconded. New York: Macmillan, 1968.

[56] L.X. Wang, "Fuzzy Systems are Universal Approximators," in Proc. IEEE Int. Conf. Fuzzy Systems, San Diego, CA, 1992.

[57] L. X. Wang and J. M. Mendel, “Fuzzy Basis Function, Universal Approximation, and Orthogonal Least Squares Learning,” IEEE Trans. Neural Networks, vol. 3 no. 5, pp. 807-814, 1992.

[58] M. Riera- Guasp, J. A. Antonino-Daviu, M. Pineda-Sanchez, R. Puche-Panadero, J. Perez-Cruz, “ A General Approach for the Transient Detection of Slip-Dependent Fault Components Based on the Discrete Wavelet Transform,” IEEE Trans. Ind. Electron., vol. 55, no. 12, pp. 4167–4180, 2008.

[59] M. Riera-Guasp, J. Antonino-Daviu, J. Rusek, J. Roger-Folch, “Diagnosis of Rotor Asymmetries in Induction Motors Based on the Transient Extraction of Fault Components Using Filtering Techniques,” Electric Power Systems Research, vol. 79, issue 8, pp. 1181-1191, 2009.

[60] H. Douglas, P. Pillay, and A.K Ziarani, “A New Algorithm for Transient Motor Current Signature Analysis Using Wavelets,” IEEE Trans. Ind. Appl., vol. 40, no. 5, pp. 1361–1368, 2004.

[61] H. T. Yang, W. Y. Chang, C. L. Huang, “A New Neural Network Approach to On-Line Fault Section Estimation Using Information of Protective Relays and Circuit Breakers,” IEEE Trans. on power delivery, vol. 9, no.1, pp. 220-230, 1994.

[62] S. Mallat, “A Theory for Multi-Resolution Signal Decomposition: the Wavelet Decomposition,” IEEE Trans. on pattern analysis and machine intelligence, vol. 11, no.7, pp. 674-693, 1989.

[63] C. Chui, An Introduction to Wavelets, Academic press, New York, 1992.

[64] M. E. H. Benbouzid, “A Review of Induction Motors Signature Analysis as a Medium for Faults Detection,” IEEE Trans. Ind. Elect., vol. 47, no. 5, pp. 984-993, 2000.

[65] M. Portnoff, “Time-Frequency Representation of Digital Signals and Systems Based on Short-Time Fourier Analysis. IEEE Transactions on Acoustics, Speech, and Signal Processing, vol. 28, issue 1, pp. 55-69, 1980.

[66] J. Antonino-Daviu, M. Riera-Guasp, J. Roger-Folch, and M. P. Molina, “Validation of a New Method for the Diagnosis of Rotor Bar Failures via Wavelet Transformation in Industrial Induction Machines,” IEEE Trans. Ind. Appl., vol. 42, no. 4, pp. 990–996, 2006.

[67] C. S. Burrus, R. A. Gopinath, and H. Guo, Introduction to Wavelets and Wavelet Transforms. A Primer, Englewood Cliffs, NJ: Prentice- Hall, 1998.

[68] R. Polikar, the Wavelet Tutorial (Online). Available: http://engineering. rowan.edu/polikar/WAVELETS/WTtutorial.html.

[69] J. Antonino-Daviu, M. Riera-Guasp, J. Roger-Folch, F. Martínez- Giménez, and A. Peris, "Application and Optimization of the Discrete Wavelet Transform for the Detection of Broken Rotor Bars in Induction Machines," Appl. Comput. Harmon. Analysis, vol. 2, Issue 2, pp. 268–279, 2006.

[70] T. Tarasiuk, "Hybrid Wavelet-Fourier Spectrum Analysis," IEEE Trans. Power Del., vol. 19, no. 3, pp. 957–964, 2004.

[71] M. Riera-Guasp, J. Antonino-Daviu, J. Roger-Folch, and M. P. Molina, "The use of the Wavelet Approximation Signal as a Tool for the Diagnosis and Quantification of Rotor Bar Failures," IEEE Trans. Ind. Appl., vol. 44, no. 3, pp. 716–726, 2008.

Dissemination of the Research Work

In Journal

[1] R.Dash and B.Subudhi, “Stator Inter-Turn fault Detection of an Induction Motor using Neuro-Fuzzy Techniques”, International journal on Archives of Control Sciences, Vol. 20, no. 3, pp. 253-266, 2010.

In Conferences

[1] R.Dash, B.Subudhi, S.Das, “induction motor stator inter-turn fault detection using wavelet transform technique”, 5th IEEE International Conference on Industrial and Information Systems (ICIIS - 2010) NIT Surathkal, Jul 29- Aug 01, 2010.

[2] R.Dash, B.Subudhi, S.Das, “A comparison between MLP NN and RBF NN techniques for the detection of stator inter-turn fault of an induction motor”, Accepted in IEEE International Conference on Industrial Electronics, Control and Robotics (IECR - 2010) NIT Rourkela.